nature energy

Article https://doi.org/10.1038/s41560-022-01188-2

Energy- and carbon-efficient CO_2/CO electrolysis to multicarbon products via asymmetric ion migration–adsorption

Table of Contents

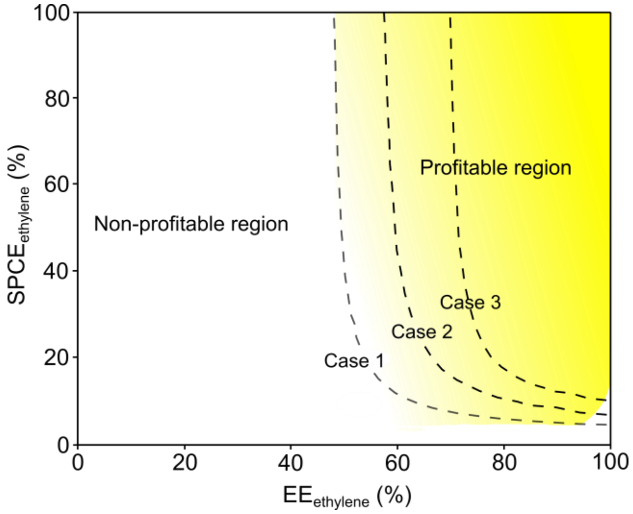

Supplementary Fig. 1 | Technoeconomic assessment for the idealized case of 100% FE in CO-to-ethylene conversion. The energy assessment was performed using a techno-economic (TEA) model as well as assumptions similar to those reported in refs. [1,2]. The dashed lines represent the EE$_{ethylene}$ and SPCE$_{ethylene}$ combinations in CO-to-ethylene conversion. The energy intensity target of 80 GJ ton^{-1} includes both CO_2-to-CO and CO-to-ethylene steps, and corresponds to a total process efficiency of ~55% given the lower heating value of ethylene (45 GJ ton^{-1}). The three cases shown correspond to the 80 GJ ton^{-1} target as could be achieved with the CO_2-to-CO step in a SOEC requiring 20 GJ ton^{-1} (Case 1), 30 GJ ton^{-1} (Case 2), and 40 GJ ton^{-1} (Case 3) (all values per ton of ethylene). Energy intensities given for SOEC (CO_2-to-CO conversion) are for 2 tons of CO produced, which is the amount required to produce 1 ton of ethylene here (Supplementary Note 1 and Supplementary Tables 1–3). A constant operating current density of 200 mA cm^{-2} and a constant ethylene FE of 100% were applied. The other performance metrics (i.e., cell potentials) and energy breakdown are provided in Supplementary Tables 1–3.

Supplementary Note 1 | Assessment of energy and carbon efficiency in a CORR system with 100% FE toward ethylene. Assessment of the CORR system for the idealized case of 100% ethylene FE was made using a techno-economic assessment (TEA) model similar to those reported in refs. [1,2]. Here, we briefly describe the TEA model used for all energy cost calculations. Energy intensities were calculated using the same base model described here. However, performance metrics including current density, full cell potential, SPCE, and Faradaic efficiency vary depending on the operating conditions and the systems. These are summarized in Supplementary Tables 1–3. The energy intensity of 80 GJ ton^{-1} (CO_2-to-ethylene) corresponds to a total process efficiency of ~55% and a lower heating value of ethylene (45 GJ ton^{-1}). Meeting this target requires low energy intensities for both steps (CO_2-to-CO and CO_2-to-ethylene). The first step is based on a solid oxide electrolyzer (SOEC) technology with three energy intensity cases: 20 GJ ton^{-1} (Case 1), 30 GJ ton^{-1} (Case 2), and 40 GJ ton^{-1} (Case 3) (all values per ton of ethylene). Energy intensities for SOEC (CO_2-to-CO conversion) are given for 2 tons of CO produced, which is the amount required to produce 1 ton of ethylene here, as unreacted CO is separated and recycled. The model considers ethylene as the only product and employs pressure swing adsorption (PSA) gas separation module at the cathode outlet for the separation of product ethylene from unreacted CO. The CO recovered from this separation is returned to the cathode inlet for utilization. The model considers 100 L of electrolyte per m^2 of electrolyser, which was inspired by the ratios used in lab-scale experiments. The total electrolyte required for the plant was assumed to be used for 1 year without replacement. Details on each cost component and sample calculations are provided in Supplementary Note 2. A constant operating current density of 200 mA cm^{-2} and a constant ethylene FE of 100% were considered. In order to match the energy intensities associated with the dashed lines in Supplementary Fig. 1 with $SPCE_{ethylene}$ lower than 10%, highly optimistic $EE_{ethylene}$ ($EE_{ethylene}$ of >90%) values in Supplementary Fig. 1 were modeled by inputting cell potentials closer to theoretical values (i.e. ~1.05 V). In practice, such a low SPCE would be incompatible with meeting 80 GJ ton^{-1} target. The dashed lines in Supplementary Fig. 1 represent the $EE_{ethylene}$ and $SPCE_{ethylene}$ combinations that would be required to meet the overall energy intensity target of 80 GJ ton^{-1}. Cases with higher SOEC input energy costs (Cases 2 and 3), demand greater performance of the CORR step. All cases demand a combination of high SPCE and EE that is beyond the state of the art.

Supplementary Note 2 | Example calculation for the CORR system. This section provides the details of equations used to determine the energy requirements for ethylene in a zero-gap, catholyte-free MEA electrolyser using input performance metrics from Supplementary Table 1 (a $\text{SPCE}_{\text{ethylene}}$ of 50%; a $\text{FE}_{\text{ethylene}}$ of 100%, a full-cell potential of 1.74 V).

Electrolyser electricity. We start by finding the production rate of ethylene in moles per second, assuming a constant plant production rate of 100 tons. Herein, we made the calculations on the basis of ethylene – the major C_2 product of the system.

We start by finding the rate of production in moles per second by considering a constant production rate of 100 tons.

$$Production\ rate\ \left[\frac{mol}{s}\right] = \frac{Production\ \left[\frac{g}{day}\right]}{molecular\ weight_{ethylene}\ \left[\frac{g}{mol}\right] \times 86400\ \left[\frac{s}{day}\right]} \tag{1a}$$

$$Production\ rate\ \left[\frac{mol}{s}\right] = \frac{100 \times \frac{10^6 g}{day}}{\frac{28g}{mol} \times \frac{86400s}{day}} = 41.336\,\frac{mol}{s} \tag{1b}$$

Next, we determine the current required to produce ethylene at this rate, considering an unity ethylene FE of 100%:

$$Total\ current\ required\ [A] = \frac{production\ rate\ \left[\frac{mol}{s}\right] \times electrons\ transferred \times Faraday's\ Constant}{FE_{ethylene}[decimal]} \tag{2a}$$

$$Total\ current\ needed\ [A] = \frac{41.336\,\frac{mol}{s} \times 8 \times 96485\,\frac{sA}{mol}}{1} = 31\ 906\ 431\ A \tag{2b}$$

Next, we multiply by the full cell voltage (1.74 V) to obtain the consumed power:

$$Power\ Consumed\ [W] = Total\ current\ needed\ [A] \times Cell\ voltage\ [V] = 31\ 906\ 431\ A \times 1.74\ V = 55\ 517\ kW \tag{3}$$

Next, we multiply by 24 h to find the energy required to run the plant for one day and achieve 100 tons:

$$Electricity\ Energy\ Requirement\ \left[\frac{GJ}{ton^{-1}}\right] = \frac{Power\ Consumed\ [W] \times 24[\text{h}]}{daily\ production\ [ton]} = \frac{55\ 517\ \text{k}W \times 24\ \text{h} \times 0.0036\ \text{GJ/kWh}}{100\ ton} = \mathbf{47.97}\ \frac{\boldsymbol{GJ}}{\boldsymbol{ton}} \tag{4}$$

Cathode separation. Separation of gases from the cathodic product stream is considered to be made using a pressure swing adsorption (PSA) separation unit. Our calculations for these are based on a model describing the capital and operating costs of a PSA system for biogas upgrading. The model considers ethylene as the only gas product of CORR (ethylene FE of 100%). The model uses a reference cost of $1 989 043 for a 1000 m^3 h^{-1} flow rate capacity with a scaling factor of 0.7 and an energy consumption of 0.25 kWh m^{-3}. We take the energy requirements as:

$$PSA\ Operating\ Energy\ \left[\frac{\mathrm{kWh}}{ton\ product}\right] = 0.25\ \frac{kWh}{m^3} \times flow\ rate \left[\frac{m^3}{h}\right] \times 24\,\frac{h}{day} \qquad (5a)$$

Before using these equations, we first find the total flow rate at the cathode output. Accordingly, we determine the flow rate of ethylene under standard conditions. This is given by:

$$Output\ ethylene\ flow\ rate\ \left[\frac{m^3}{h}\right] = \frac{100 \times 10^6\ g \times 8.314\, Jmol^{-1}K^{-1} \times 298K}{28\,\frac{g}{mol} \times 101\ 300\ Pa \times 24\,\frac{h}{day}} = 3640\ \frac{m^3}{h} \qquad (6)$$

Next, we determine the flow rate of CO at the outlet of the cathode by using single pass conversion and assuming constant pressure. It is worthwhile to note that this single pass conversion does not account for CO lost to carbonate and only relates the amount of CO that is reduced to any product to the CO that passes through the cathode stream, unreacted. Assuming a single-pass conversion of 31%, we have:

$$Output\ CO\ flow\ rate\ \left[\frac{m^3}{h}\right] =$$

$$ethylene\ flow\ rate\ \left[\frac{m^3}{h}\right] \times molar\ ratio\ \left[\frac{CO}{ethylene}\right] \times \left(\frac{100 - single\ pass\ conversion[\%]}{single\ pass\ conersion[\%]}\right) \qquad (7a)$$

$$Output\ CO\ flow\ rate\ \left[\frac{m^3}{h}\right] = 3640\,\frac{m^3}{h} \times 2 \times \frac{100-50}{50} = 7280\ \frac{m^3}{h} \qquad (7b)$$

Since we are assuming that H_2 is the only other product at the cathode product stream, we can define the current toward H_2 as:

$$Current\ towards\ H_2[A] = Total\ current\ needed[A] \times \frac{100 - FE_{product}[\%]}{100} \qquad (8a)$$

$$Current\ towards\ H_2[A] = 33\ 235\ 866\ A \times \frac{100-100}{100} = 0\ A \qquad (8b)$$

The H_2 production rate can be written as:

$$H_2\ production\ \left[\frac{mol}{h}\right] = \frac{Current\ towards\ H_2[A] \times 3600\,\frac{s}{h}}{2\,\frac{electrons}{H_2\ product} \times Faraday's\ Constant} \qquad (9a)$$

$$H_2\ production\ \left[\frac{mol}{h}\right] = \frac{0\ A \times 3600\,\frac{s}{hour}}{2\,\frac{electrons}{H_2\ product} \times 96485\,\frac{sA}{mol}} = 0\ \frac{mol}{h} \tag{9b}$$

Assuming an ideal gas with standard conditions, we can find the flow rate of H_2:

$$flow\ rate_{H2}\left[\frac{m^3}{h}\right] = \frac{H_2\ production\left[\frac{mol}{h}\right] \times 8.314\,\frac{J}{mol \times K} \times 298K}{101.3 \times 10^3 Pa} \tag{10a}$$

$$flow\ rate_{H2}\left[\frac{m^3}{h}\right] = \frac{0\,\frac{mol}{h} \times 8.314\,\frac{J}{mol \times K} \times 298K}{101.3 \times 10^3 Pa} = 0\ \frac{m^3}{h} \tag{10b}$$

Now, we can find the total cathode output flow rate by summing the flow rate of ethylene, CO, and H_2 using:

$$flow\ rate\ \left[\frac{m^3}{h}\right] = (3640 + 7280 + 0)\frac{m^3}{h} = 10\ 920\,\frac{m^3}{h} \tag{11}$$

With the final output flow rate, we calculate the required energy per ton of ethylene produced using Supplementary Equation 5a:

$$PSA\ Energy\ \left[\frac{\text{GJ}}{ton\ \text{ethylene}}\right] = 0.25\ \frac{kWh}{m^3} \times 10\ 920\,\frac{m^3}{h} \times 24\,\frac{h}{day} \times \frac{0.0036\ GJ\ kWh^{-1}}{100\ ton\ ethylene}$$
$$= \mathbf{2.4}\ \frac{\textbf{GJ}}{\boldsymbol{ton}\ \textbf{ethylene}} \tag{12}$$

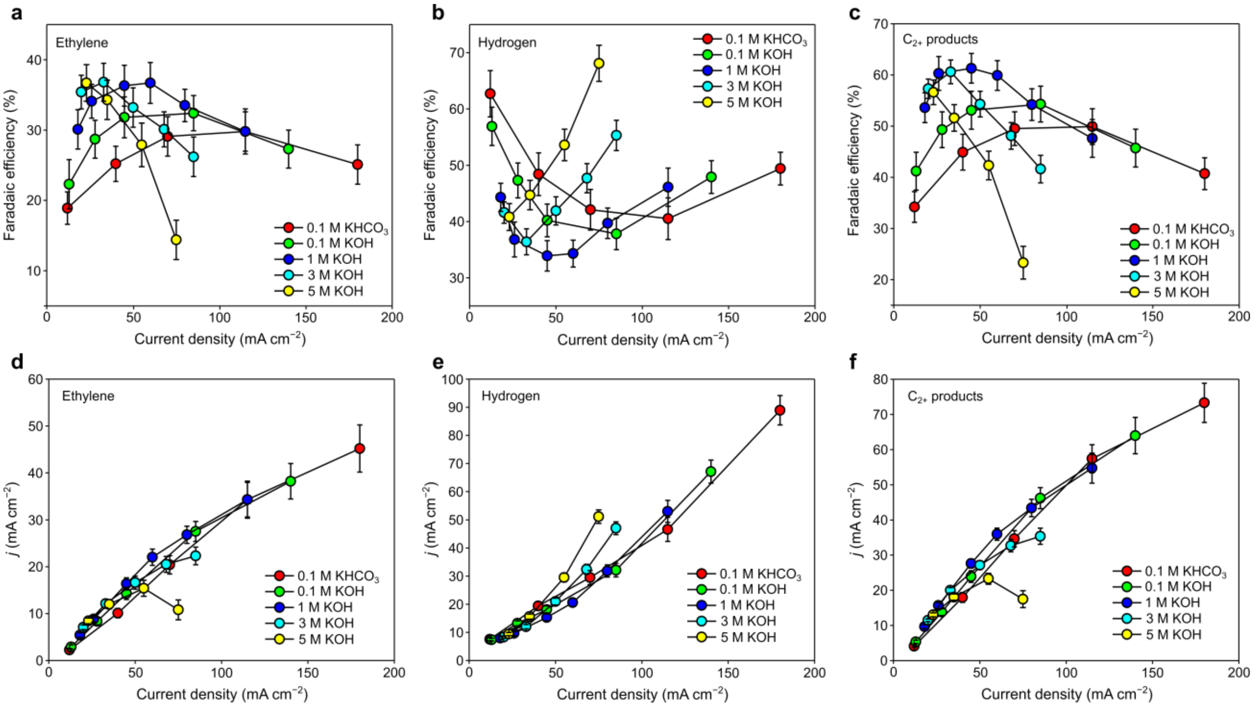

Supplementary Fig. 2 | CORR performance of Cu/PTFE catalyst in an anion exchange membrane (AEM) based membrane electrode assembly (MEA) using anolytes of various KOH concentrations (0.1 M $KHCO_3$ (pH 8.4), 0.1 M KOH (pH 13.0), 1 M KOH (pH 13.9), 3 M KOH (pH 14.4), and 5 M KOH (pH 14.7)) under low CO availability. a, Ethylene Faradaic efficiency versus current density. Error bars represent the standard deviation of three independent measurements. Data are presented as mean values ± standard deviation. **b,** Hydrogen Faradaic efficiency versus current density. Error bars represent the standard deviation of three independent measurements. Data are presented as mean values ± standard deviation. **c,** C_{2+} Faradaic efficiency versus current density. Error bars represent the standard deviation of three independent measurements. Data are presented as mean values ± standard deviation. **d,** Ethylene partial current density versus current density. Error bars represent the standard deviation of three independent measurements. Data are presented as mean values ± standard deviation. **e,** Hydrogen partial current density versus current density. Error bars represent the standard deviation of three independent measurements. Data are presented as mean values ± standard deviation. **f,** C_{2+} partial current density versus current density. Error bars represent the standard deviation of three independent measurements. Data are presented as mean values ± standard deviation. Operating conditions: anolyte flow rate 20 mL min^{-1}; CO flow rate: ~1 sccm cm^{-2}; and cell temperature and pressure: atmospheric conditions.

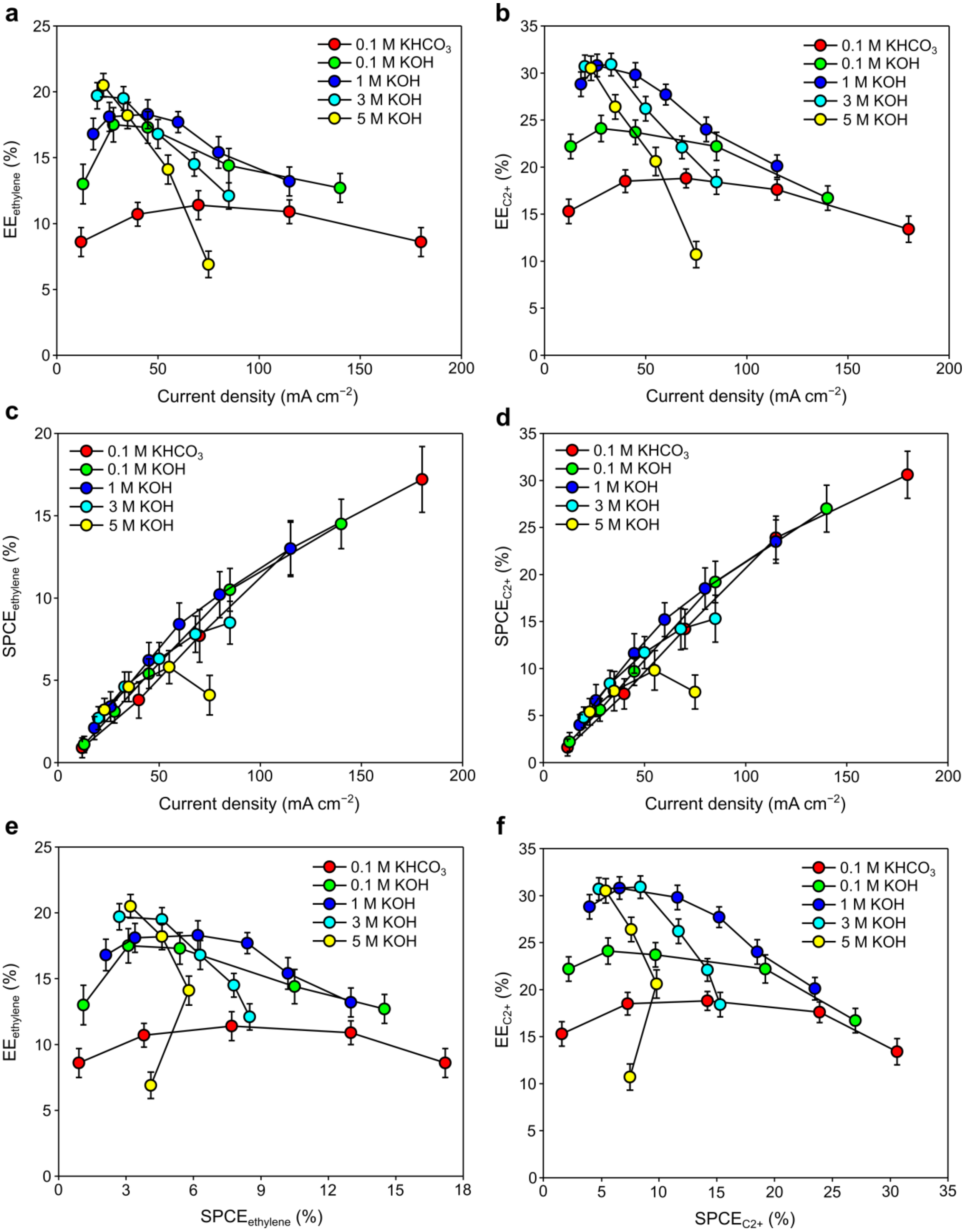

Supplementary Fig. 3 | CORR performance of Cu/PTFE catalyst in an anion exchange

membrane (AEM) based membrane electrode assembly (MEA) using anolytes of various KOH concentrations (0.1 M KOH (pH 13.0), 1 M KOH (pH 13.9), 3 M KOH (pH 14.4), and 5 M KOH (pH 14.7)) under low CO availability. a, CO-to-ethylene energy efficiency (EE) versus current density. Error bars represent the standard deviation of three independent measurements. Data are presented as mean values ± standard deviation. **b,** CO-to-C_{2+} energy efficiency (EE) versus current density. Error bars represent the standard deviation of three independent measurements. Data are presented as mean values ± standard deviation. **c,** CO-to-ethylene single-pass carbon efficiency (SPCE) versus current density. Error bars represent the standard deviation of three independent measurements. Data are presented as mean values ± standard deviation. **d,** CO-to-C_{2+} single-pass carbon efficiency (SPCE) versus current density. Error bars represent the standard deviation of three independent measurements. Data are presented as mean values ± standard deviation. **e,** CO-to-ethylene energy efficiency (EE) versus CO-to-ethylene single-pass carbon efficiency (SPCE). Error bars represent the standard deviation of three independent measurements. Data are presented as mean values ± standard deviation. **f,** CO-to-C_{2+} energy efficiency (EE) versus CO-to-C_{2+} single-pass carbon efficiency (SPCE). Error bars represent the standard deviation of three independent measurements. Data are presented as mean values ± standard deviation. Operating conditions: anolyte flow rate 20 mL min^{-1}; CO flow rate: ~1 sccm cm^{-2}; and cell temperature and pressure: atmospheric conditions.

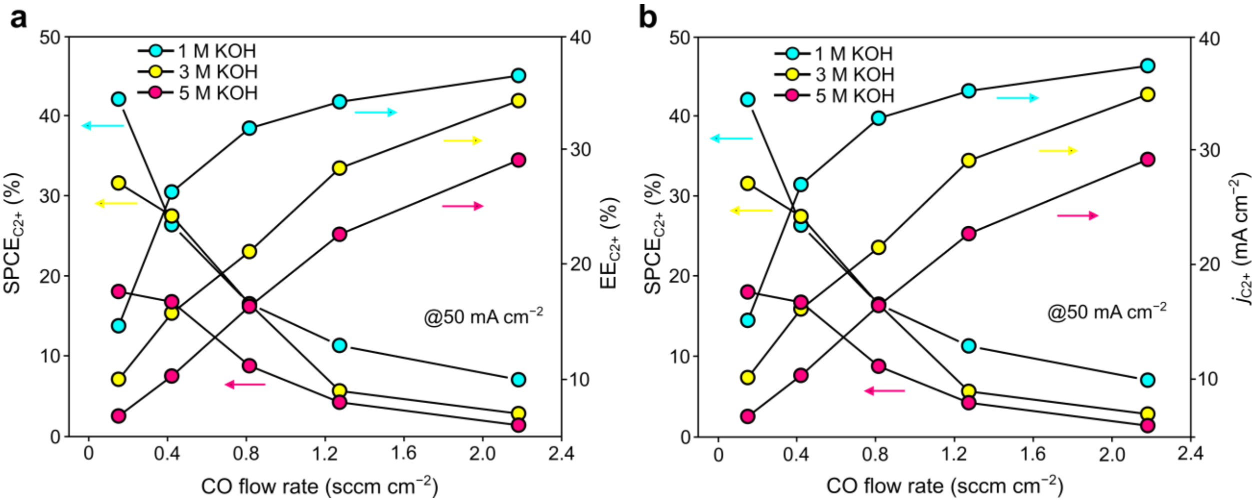

Supplementary Fig. 4 | CORR performance of Cu/PTFE catalyst in an anion exchange membrane (AEM) based membrane electrode assembly (MEA) using anolytes of various KOH concentrations (1 M KOH (pH 13.9), 3 M KOH (pH 14.4), and 5 M KOH (pH 14.7)) under low CO availability at a constant current density of 50 mA cm^{-2}. a, CO-to-C_{2+} single-pass carbon efficiency (SPCE) and energy efficiency (EE) under various CO flow rates. **b,** CO-to-C_{2+} single-pass carbon efficiency (SPCE) and C_{2+} partial current density under various CO flow rates. Operating conditions: anolyte flow rate 20 mL min^{-1}; CO flow rate: varied from ~0.13 sccm cm^{-2} to ~2.3 sccm cm^{-2}; anolyte concentration: varied from 1 M KOH to 5 M KOH; and cell temperature and pressure: atmospheric conditions. At a constant current density of 50 mA cm^{-2}, the electrolytes of various pHs enabled comparable cell potentials in the range of −2.04 V and −2.10 V.

Supplementary Note 3 | COMSOL simulations. This section provides the details of a one-dimensional (1D) reaction-diffusion model that simulates the local concentrations of K^+, OH^- and CO at the catalyst layer with or without COF.

Geometry 1. For the bare Cu electrode, the detailed geometry consists of a Cu catalyst, a bulk electrolyte layer, and a 1 nm reaction interface layer [3] in-between (Supplementary Fig. 10a). Different electrolytes with evenly distributed 1 M KOH or 1 M KOH + 2 M K_2CO_3 were set to the right-hand boundary of the Cu catalyst. Gaseous CO was supplied, and the dissolved aqueous CO concentration was calculated using Henry's law and set at the right-hand boundary of the Cu catalyst. An electrical potential was put at the left-hand boundary of the Cu catalyst. The ground was put at the right-hand boundary of the Cu catalyst. The 1 nm OHP induced a strong negative space charge to modulate the local concentrations of CO, K^+, OH^-, and CO_3^{2-}.

Geometry 2. For the CCBH electrodes, the detailed geometry consists of a Cu catalyst, a COF layer, and a 1 nm reaction interface layer[3] in-between (Supplementary Fig. 10a). A constant concentration of evenly distributed 1 M KOH electrolyte was set to the right-hand boundary of the Cu or COF layer. Gaseous CO was supplied and the dissolved aqueous CO concentration was calculated using Henry's law and set at the right-hand boundary of the Cu or COF layer. An electrical potential was put at the left-hand boundary of the Cu catalyst. A ground condition was applied at the right-hand boundary of the Cu catalyst. The species concentrations were set the same at the right-hand boundary of the Cu or COF layer. The thickness of COF layer was estimated to be less than 100 nm from the experimental results (Supplementary Figs. 15-17), in which 20 nm, 50 nm, and 80 nm were chosen to represent low COF loading, medium COF loading, and high COF loading, respectively. Specifically, the COF layer has the capability of blocking the potassium, decreasing the local K^+ concentration in the COF layer and the reaction interface; it is also hydrophobic, confining the local concentration of OH^- in the COF layer and the reaction interface. As a result, changing the thickness of COF layer provides a means to tune the relative K^+/OH^- concentration ratio at the reaction interface and therefore analyze symmetric vs. asymmetric ion migration/adsorption (Fig. 2). The 1 nm OHP induced a strong negative space charge, resulting in an increase in the K^+ concentration near the catalyst surface.

Detailed COMSOL Physics Setup. CO solubility was calculated using Henry's Law (Supplementary Equation 13a) and Sechenov Constant (Supplementary Equation 13b). The CO was assumed to be the ideal gas, and the solubility was assumed to be depending on pressure, temperature, and salinity effect. Thus, the available CO concentration (Supplementary Equation 13c) can be determined by the sets of equations shown below.

$$K_H = \exp\left(1300[K]\left(\frac{1}{T} - \frac{1}{298[K]}\right)\right) \tag{13a}$$

$$K_s = 10^{-c_K(0.0922+H_{G,0})-c_{OH}(0.0839+H_{G,0})} \tag{13b}$$

$$c_{sat} = P_{CO}K_H K_s \tag{13c}$$

where C_K and C_{OH} represent the local concentration of potassium and hydroxide, respectively[4]. $H_{G,0}$ is the Sechenov constant for CO, which is 0.006. P_{CO} represents the partial pressure of CO, which is 0.00099 M/bar.

Ohm's Law (Supplementary Equation 14) is applied to the cathode catalyst layer. An assumption of the catalyst domain consists of 0.6 electrolyte volume fraction with 4.56 S/m electrical conductivity and 0.4 copper catalyst based electrode volume fraction with 8e4 S/m (ref. [5]).

$$i = -\sigma \frac{\partial \phi}{\partial x} \tag{14}$$

where σ is the electrical conductivity of different media.

The electrochemical half-cell CO reduction reactions toward ethylene, acetic acetate, ethanol, and n-propanol productions are listed below (Supplementary Equations 15a-d):

$$2CO + 6H_2O + 8e^- \rightarrow C_2H_4 + 8OH^- \tag{15a}$$

$$2CO + 4H_2O + 4e^- \rightarrow CH_3COOH + 4OH^- \tag{15b}$$

$$2CO + 7H_2O + 8e^- \rightarrow C_2H_5OH + 8OH^- \tag{15c}$$

$$3CO + 10H_2O + 12e^- \rightarrow C_3H_7OH + 12OH^- \tag{15d}$$

The Faraday's equations for the CO reduction (r_{CO}) and OH^- production (r_{OH^-}) at a catalyst with a predetermined reaction rate are shown in Supplementary Equations 16a and b, in which the Faradic efficiency of each product is obtained from the experimental result. The electrochemical reactions were calculated in a manner similar to that in ref. [6].

$$r_{CO} = -\frac{i}{F} * \left(\frac{FE_{C2H4}}{8} + \frac{FE_{CH3COOH}}{4} + \frac{FE_{C2H5OH}}{8} + \frac{FE_{C3H8O}}{12}\right) * \frac{\varepsilon}{L} \tag{16a}$$

$$r_{OH^-} = \frac{i}{F} * \frac{\varepsilon}{L} \tag{16b}$$

$i, \varepsilon, F, and\ L$ represent the current density (100 mA cm^{-2}), porosity of the catalyst layer (60%), Faraday's constant, and thickness of the catalyst, respectively.

Diffusion and electromigration were considered in the species transportation. The Nernst-Planck set of equations for the Cu catalyst layer and COF domains were applied (Supplementary Equations 17a and b). The Millington and Quirk set of equations were applied to calculate the effective diffusivity of species (Supplementary Equations 17c and d).

$$\frac{\partial c_i}{\partial t} + \frac{\partial j_i}{\partial x} + r_i = \Sigma R_i \tag{17a}$$

$$J_i = -\frac{D_i \partial c_i}{\partial x} - \frac{z_i D_i}{RT} F c_i \frac{\partial V}{\partial x} \tag{17b}$$

$$\tau_{F,i} = \epsilon_p^{-1/3} \tag{17c}$$

$$D_i = \frac{\epsilon_p}{\tau_{F,i}} D_{F,i} \tag{17d}$$

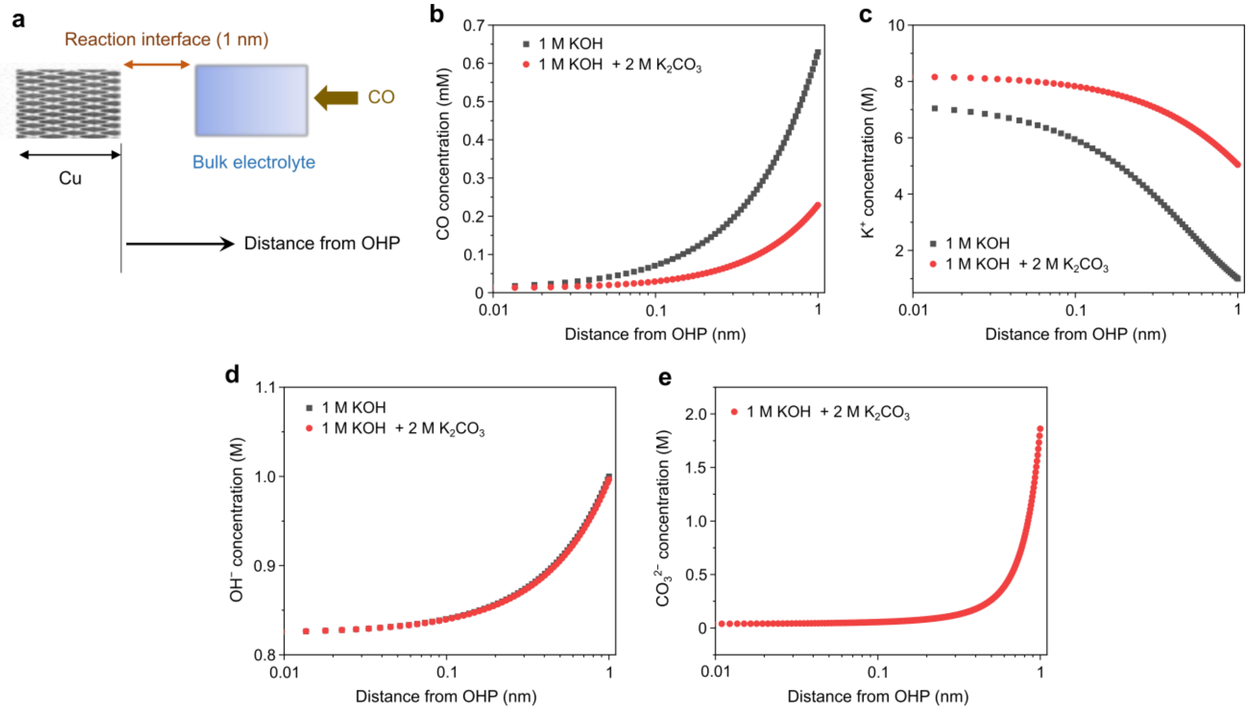

Supplementary Fig. 5 | COMSOL simulation results on Cu with different electrolytes. a, Schematic of a one-dimensional (1D) COMSOL model, in which a reaction interface of 1 nm is defined to enable diffusion of K^+, OH^-, and CO due to electromigration and CO reduction; the bulk electrolyte layer is defined at a distance >1 nm from the outer Helmholtz plane (OHP), in which 1 M KOH and 1 M KOH + 2 M K_2CO_3 electrolytes are applied to simulate the local concentrations of CO, K^+, OH^-, and CO_3^{2-}. **b,** Simulated concentration of CO on the Cu catalyst at different electrolytes as a function of distance from the OHP. **c,** Simulated concentration of K^+ on the Cu catalyst at different electrolytes as a function of distance from the OHP. **d,** Simulated concentration of OH^- on the Cu catalyst at different electrolytes as a function of distance from the OHP. **e,** Simulated concentration of CO_3^{2-} on the Cu catalyst at different electrolytes as a function of distance from the OHP. The results show that the addition of K_2CO_3 leads to a further accumulation of K^+ at the Cu catalyst without changing the local pH, resulting in a drastic decrease of the local CO availability.

Supplementary Note 4 | Impurity analysis. According to the certificate of analysis of KOH (99.99%), the pellets contain 0.4 ppm of Fe and 0.8 ppm of Ni. We therefore carried out analysis to estimate the impurity coverage on the surface of bare Cu and CCBH catalysts. We first prepared 1 M KOH solutions (50 mL) and carried out 25 hours of continuous CORR operation – a typical experimental duration for the CORR performance tests carried out in this work (Supplementary Figs. 6 and 46). We then used an inductively coupled plasma optical emission spectrometer (Thermo Scientific iCAP Pro ICP OES) to determine the Ni and Fe concentrations in 1 M KOH solutions (neutralized with equivalent volumes of 1 M nitric acid solutions before testing) before CORR and after 25 hours of CORR. We also extracted the Cu, Ni, and Fe compositions in the bare Cu and CCBH catalysts (dissolved in 70% nitric acid and diluted for 100 times before testing) after 25 hours of continuous CORR. We prepared different standard solutions containing 0.001 ppm, 0.01 ppm, 0.1 ppm, and 1 ppm Ni, Fe and Cu for the calibration. As shown in Supplementary Table 14, the changes in concentration of Ni and Fe, before and after CORR, were negligible, suggesting that Ni and Fe species remain in the electrolyte and do not migrate to the cathode through an anion exchange membrane during CORR. No Ni and Fe impurities were detected on the Cu and CCBH catalysts after 25 hours of CORR.

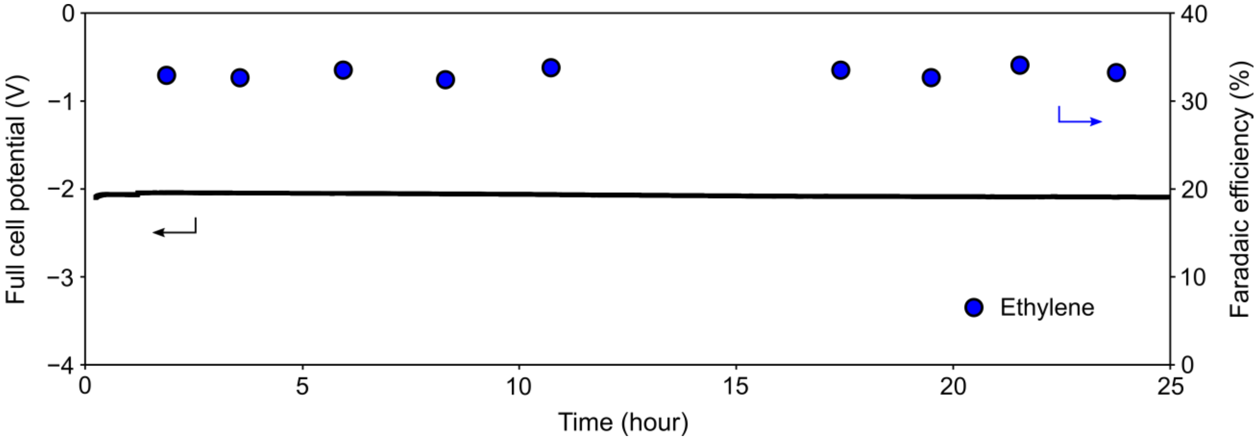

Supplementary Fig. 6 | CORR performance of Cu/PTFE catalyst for impurity analysis. CORR performance of Cu/PTFE catalyst in an anion exchange membrane (AEM) based membrane electrode assembly using 1 M KOH (pH 13.9) as anolyte at 100 mA cm^{-2}. An average ethylene FE of 33% maintained for 25 hours of continuous operation. The 1 M KOH electrolyte was analyzed via ICP-OES for any Ni and Fe impurities before and after 25 hours of continuous CORR (see also Supplementary Note 4 and Supplementary Table 14). Operating conditions: anolyte flow rate 20 mL min^{-1}; CO flow rate: ~1 sccm cm^{-2}; and cell temperature and pressure: atmospheric conditions.

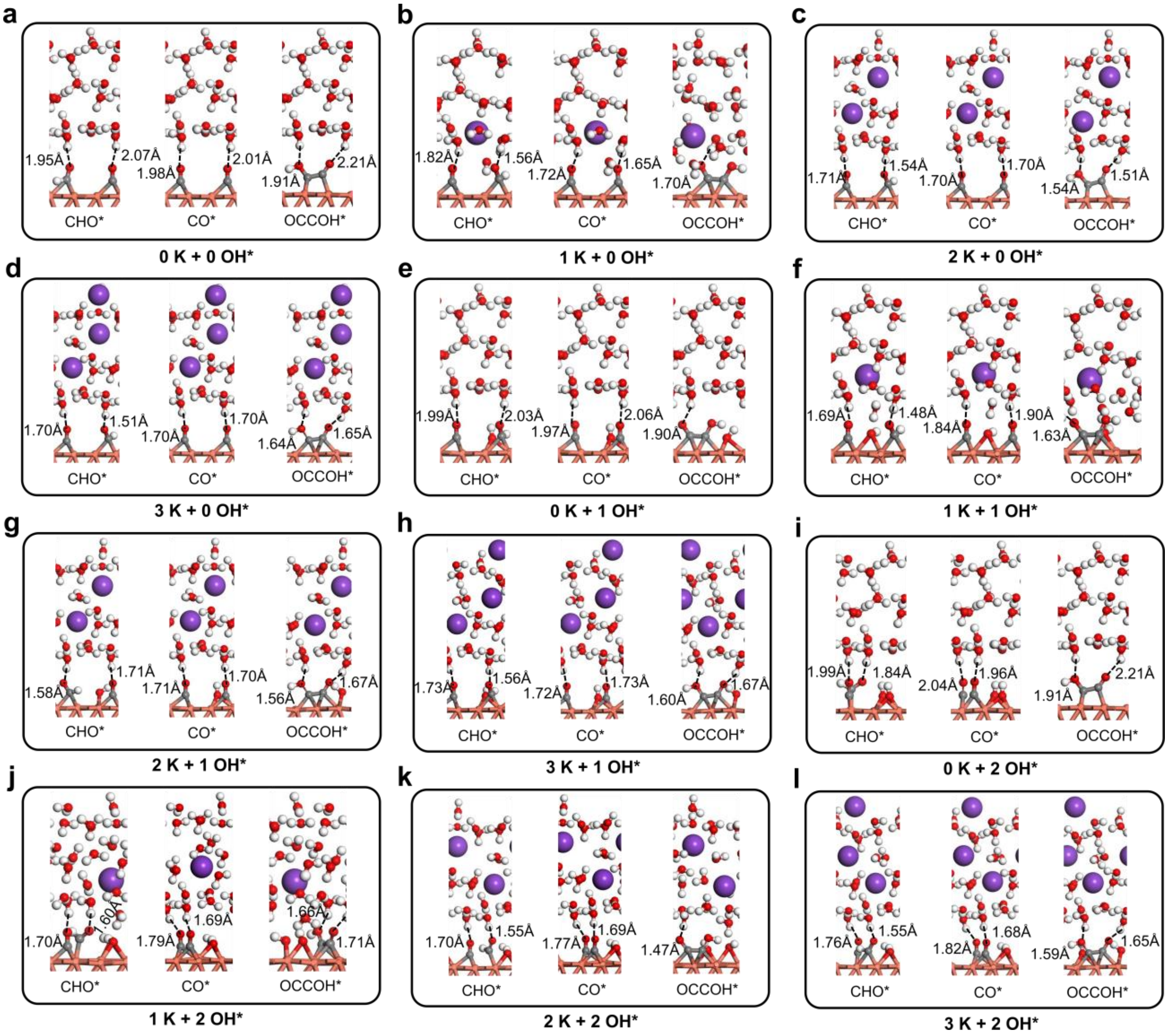

Supplementary Fig. 7 | The most stable configurations of CO protonation and C–C coupling. The different adsorption structures consider zero, one, two OH^- adsorption on the Cu(111) surface and zero, one, two, three potassium atoms in the water layers, respectively. a, 0 K + 0 OH*. **b,** 1 K + 0 OH*. **c,** 2 K + 0 OH*. **d,** 3 K + 0 OH*. **e,** 0 K + 1 OH*. **f,** 1 K + 1 OH*. **g,** 2 K + 1 OH*. **h,** 3 K + 1 OH*. **i,** 0 K + 2 OH*. **j,** 1 K + 2 OH*. **k,** 2 K + 2 OH*. **l,** 3 K + 2 OH*. Grey represents C atom, red represents O atom, white represents H atom, and purple represents K atom.

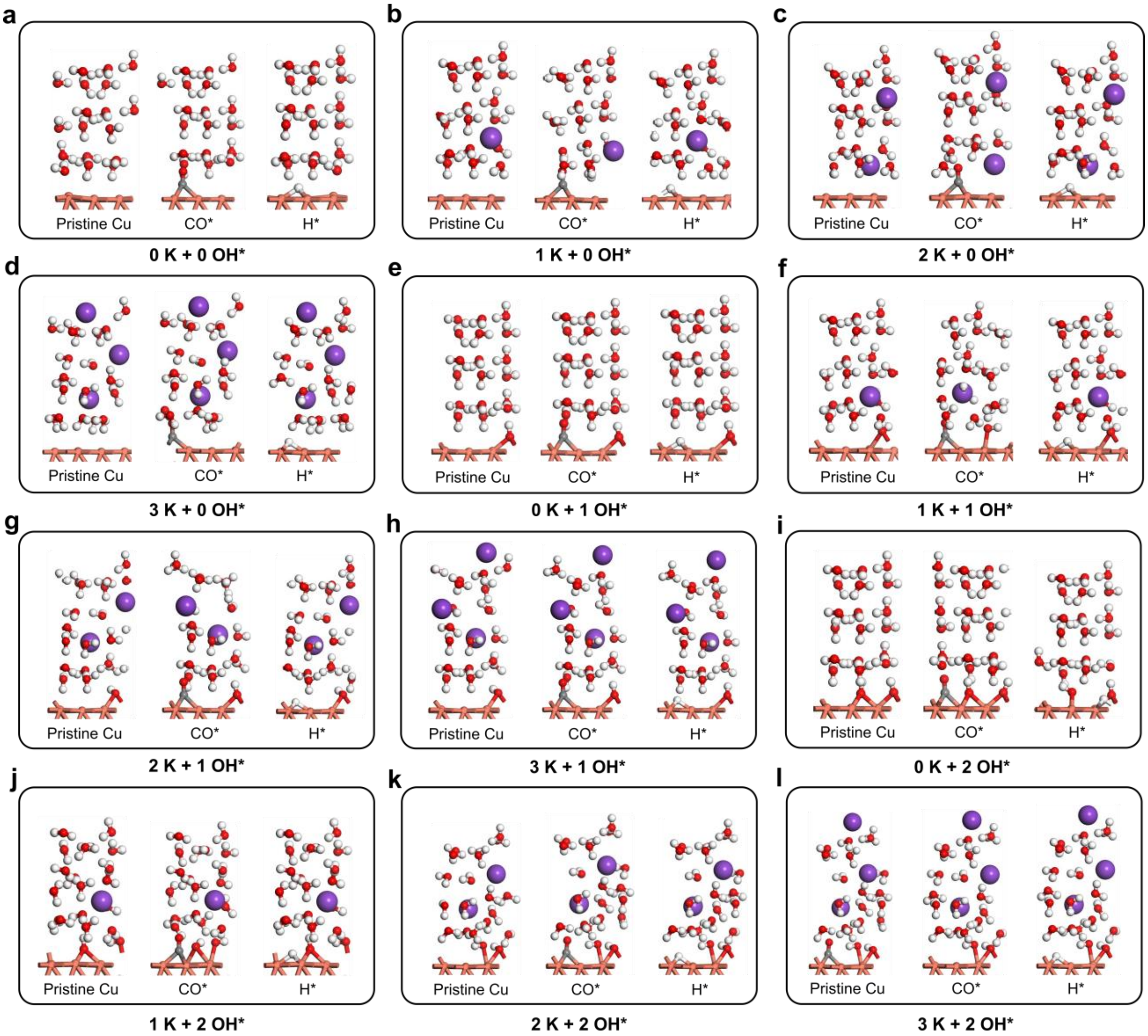

Supplementary Fig. 8 | The optimized periodic atomic structures under various K$^+$ concentrations and OH* coverages. a, 0 K + 0 OH*. **b,** 1 K + 0 OH*. **c,** 2 K + 0 OH*. **d,** 3 K + 0 OH*. **e,** 0 K + 1 OH*. **f,** 1 K + 1 OH*. **g,** 2 K + 1 OH*. **h,** 3 K + 1 OH*. **i,** 0 K + 2 OH*. **j,** 1 K + 2 OH*. **k,** 2 K + 2 OH*. **l,** 3 K + 2 OH*. Grey represents C atom, red represents O atom, white represents H atom, and purple represents K atom.

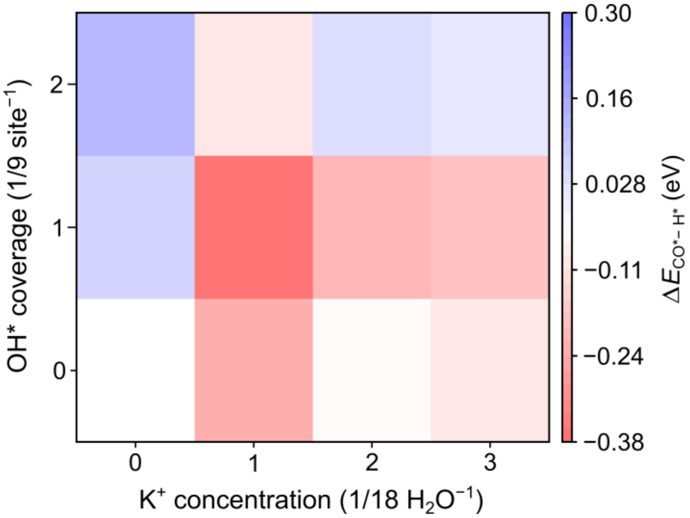

Supplementary Fig. 9 | The adsorption energy difference of CO* and H* on a Cu surface ($\Delta E_{\mathrm{CO}*-\mathrm{H}*} = \Delta E_{ads}^{CO*} - \Delta E_{ads}^{H*}$) at various K$^+$ concentrations and OH* coverages.

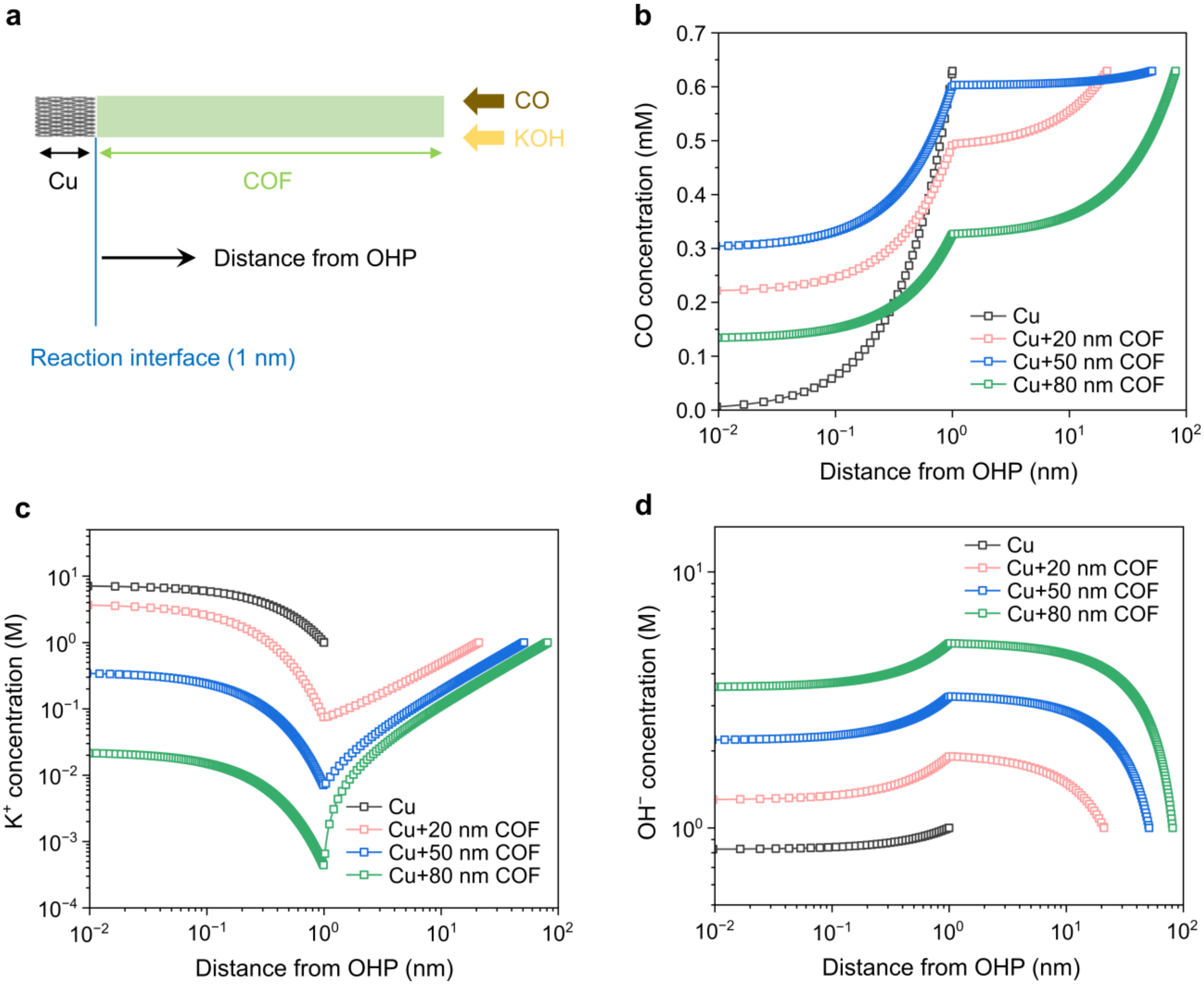

Supplementary Fig. 10 | COMSOL simulation results. a, Schematic of a one-dimensional (1D) COMSOL model, in which a reaction interface of 1 nm is defined to enable diffusion of K^+, OH^-, and CO due to electromigration and CO reduction; the bulk catalyst layer is defined at a distance >1 nm from the outer Helmholtz (OHP), in which a COF layer with various thicknesses (i.e., 20 nm, 50 nm, and 80 nm) is included to control the local concentrations of K+, OH^-, and CO. **b,** Simulated concentration of CO on the Cu catalyst with various COF loadings (represented by the thickness) and without COF as a function of distance from the OHP. **c,** Simulated concentration of K^+ on the Cu with various COF loadings (represented by the thickness) and without COF as a function of distance from the OHP. **d,** Simulated concentration of OH^- on the Cu with various COF loadings (represented by the thickness) and without COF as a function of distance from the OHP. A discussion on the effect of COF on the reaction environment is provided in Supplementary Note 5.

Supplementary Note 5 | Discussion on COMSOL simulations. Using COMSOL simulations, we explored how the local concentrations of K^+, OH^- and CO at the catalyst layer would be modified with an additional COF layer. To do so, we introduced a hydrophobic porous intermediate layer (HPIL) at various thickness (i.e. 20 nm, 50 nm, and 80 nm) between the catalyst surface and bulk with a reaction interface thickness of 1 nm for CO electroreduction. This HPIL layer has a lower K^+ diffusivity than the bulk catalyst layer.

As the thickness of HPIL increases, the local K^+ concentration at the reaction interface could be reduced by three orders of magnitude (Supplementary Fig. 10c), whereas the local OH^- concentration at the reaction interface is promoted (Supplementary Fig. 10d). As a result, the local CO concentration, determined by Supplementary Equations 13a and 13b, is enhanced and approaches an optima in the reaction interface layer at a moderate HPIL thickness of 50 nm, resulting in improved performance of CO electroreduction (Supplementary Fig. 10b). In contrast, for a standard bare Cu catalyst configuration, the local CO concentration decreases to zero at the catalyst surface, due to an accumulation of K^+ and a depletion of OH^-.

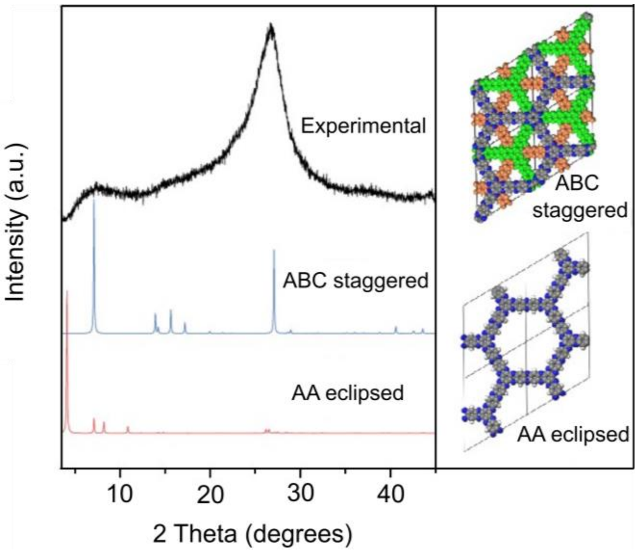

Supplementary Fig. 11 | The powder X-ray diffraction (PXRD) patterns of Hex−Aza−COF compared with different probable stacking models.

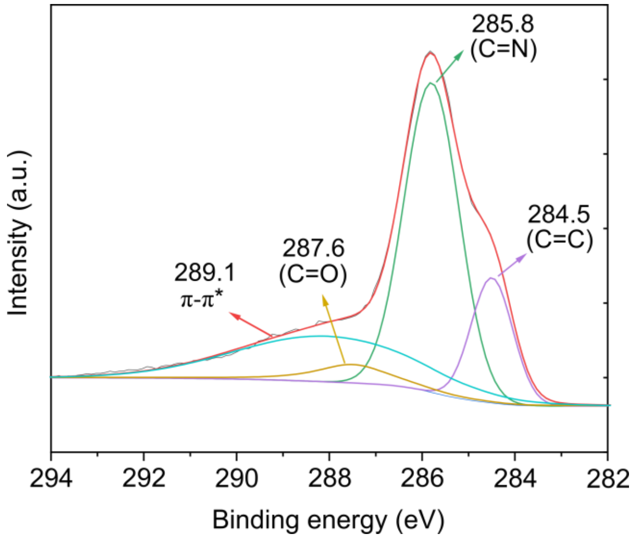

Supplementary Fig. 12 | High-resolution C 1s spectra of bare Hex–Aza–COF. Peaks at 289.1 eV, 289.1 eV, 285.8 eV, 284.5 eV are attributed to π−π*, C=O, C=N, and C=C bonds, respectively.

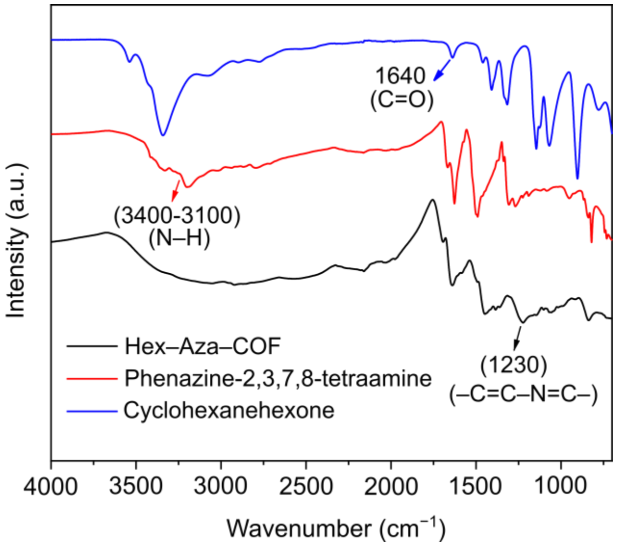

Supplementary Fig. 13 | Fourier-transform infrared spectroscopy (FT-IR) of bare Hex–Aza–COF compared with starting materials.

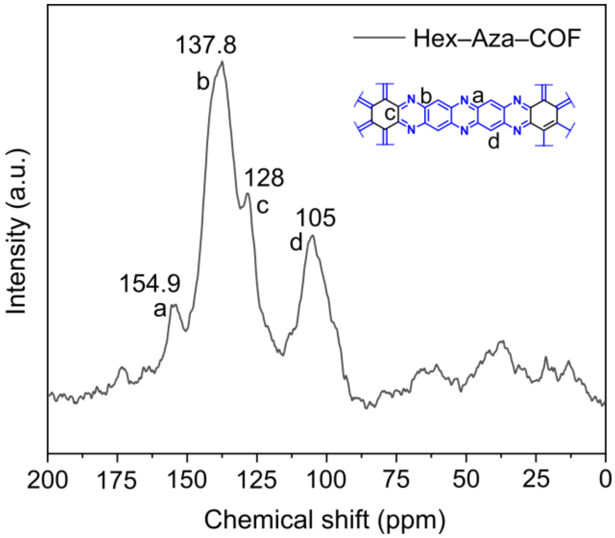

Supplementary Fig. 14 | Spinning carbon-13 nuclear magnetic resonance spectroscopy (^{13}C-NMR CP/MAS) for Hex−Aza−COF.

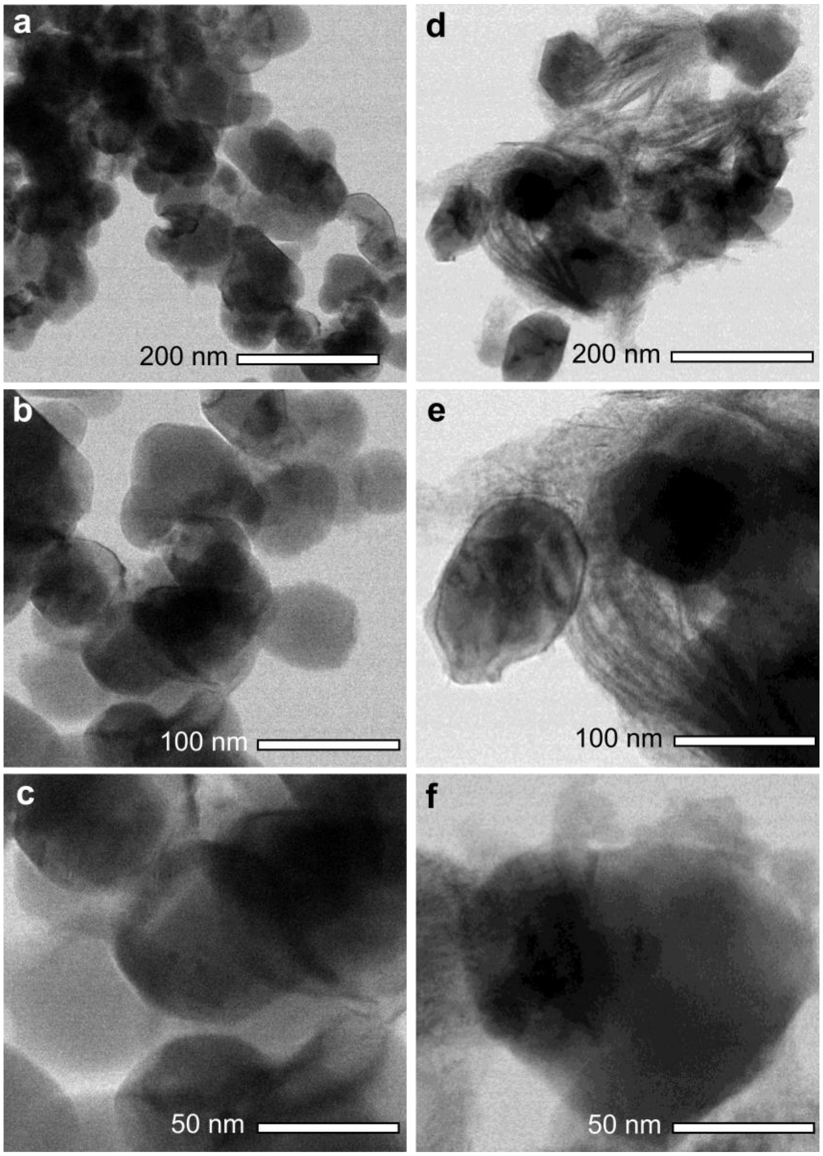

Supplementary Fig. 15 | Transmission electron microscopy (TEM) images. a-c, Cu NPs at 200 nm, 100 nm, and 50 nm, respectively. **d-f,** CCBH catalyst with 15 wt% COF loading at 200 nm, 100 nm, and 50 nm, respectively. The CCBH catalyst consists of Cu NPs surrounded by COF exfoliated into 2D nanosheets.

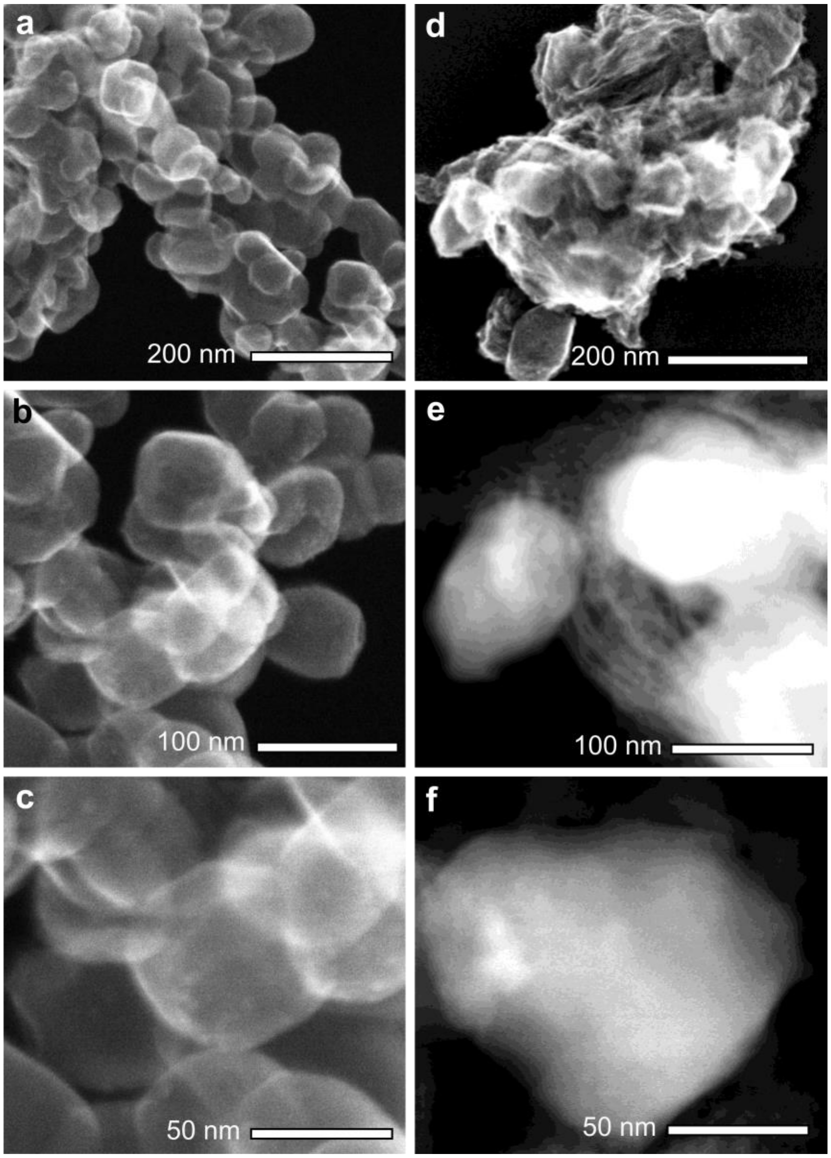

Supplementary Fig. 16 | Transmission electron microscopy (TEM) images. a-c, Cu NPs at 200 nm, 100 nm, and 50 nm, respectively. **d-f,** CCBH catalyst with a 25 wt% COF loading at 200 nm, 100 nm, and 50 nm, respectively.

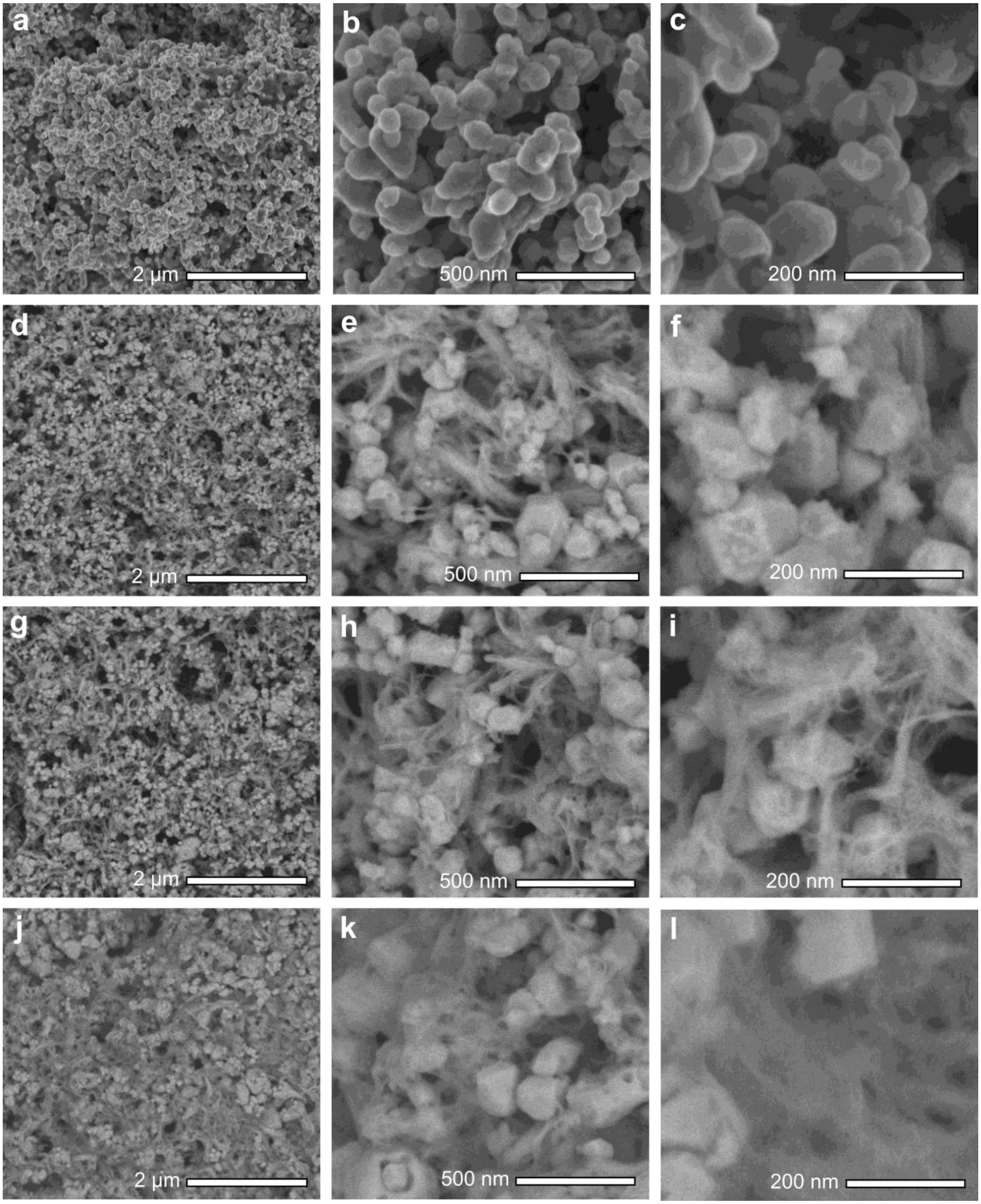

Supplementary Fig. 17 | Scanning electron microscopy (SEM) images. a-c, Cu NPs supported on a carbon paper at 2 µm, 500 nm, and 200 nm, respectively. **d-f,** CCBH catalyst with a 5 wt%

COF loading supported on a carbon paper at 2 µm, 500 nm, and 200 nm, respectively. **g-i,** CCBH catalyst with 15 wt% COF loading supported on a carbon paper at 2 µm, 500 nm, and 200 nm, respectively. **j-l,** CCBH catalyst with a 25 wt% COF loading supported on a carbon paper at 2 µm, 500 nm, and 200 nm, respectively.

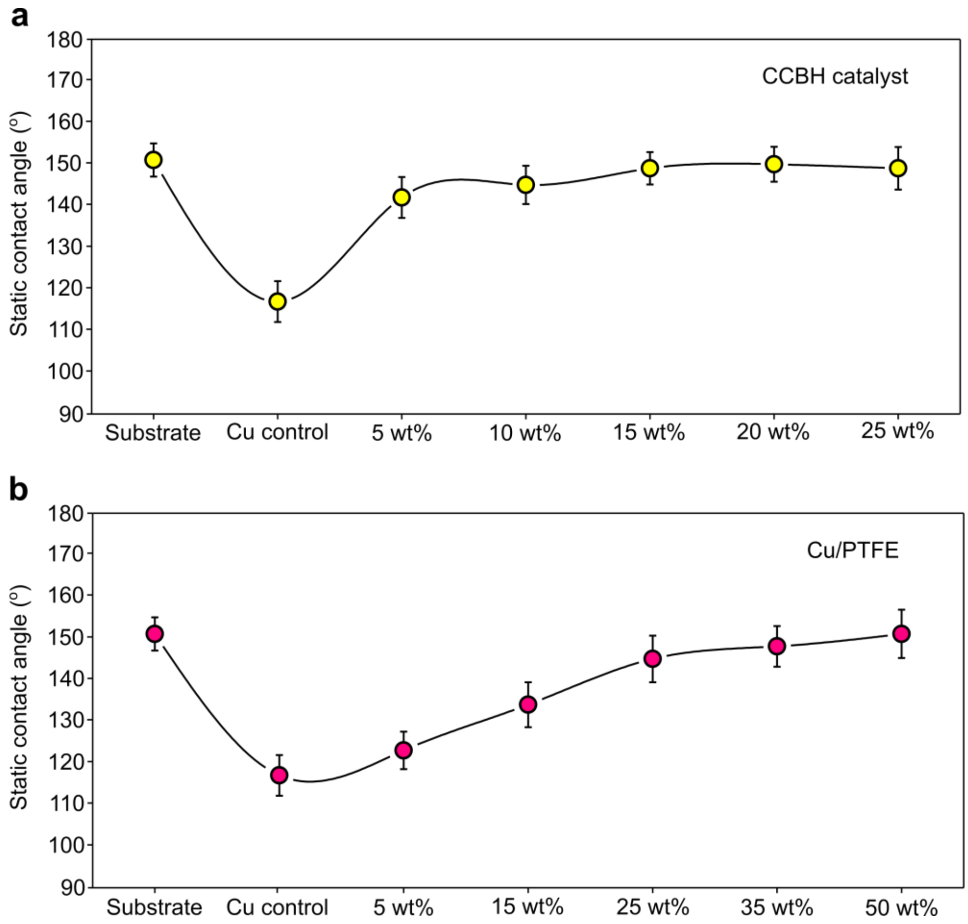

Supplementary Fig. 18 | Static contact angles on various surfaces. a, CCBH catalyst with various COF mass loadings. Error bars represent the standard deviation of three independent measurements. Data are presented as mean values ± standard deviation. **b,** Bare Cu NPs with various polytetrafluoroethylene (PTFE) hydrophobic agent mass loadings. Error bars represent the standard deviation of three independent measurements. Data are presented as mean values ± standard deviation. Substrate stands for the carbon paper used as a base substrate. Control Cu stands for the Cu NPs spray-deposited onto the carbon paper.

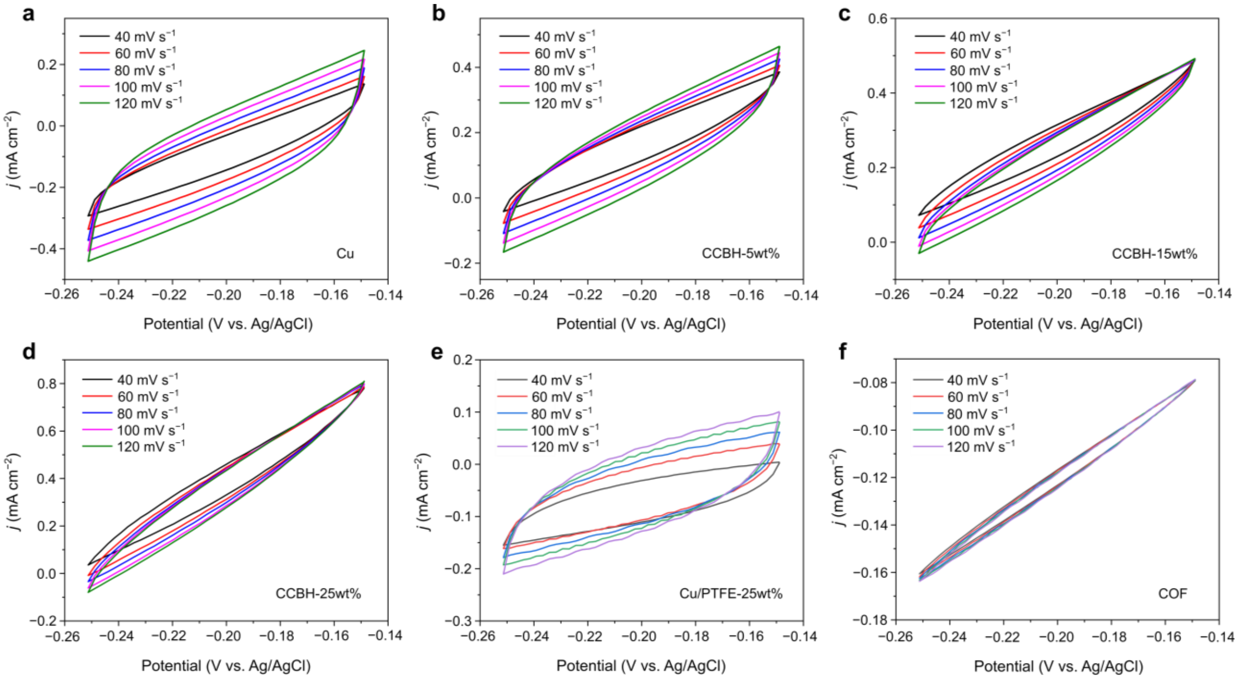

Supplementary Fig. 19 | Electrochemical surface area (ECSA) measurements. a, Voltametric profiles in the double-layer region over a range of scan rates for control Cu (Cu NPs). **b,** Voltametric profiles in the double-layer region over a range of scan rates for CCBH catalyst with 5 wt% COF loading. **c,** Voltametric profiles in the double-layer region over a range of scan rates for CCBH catalyst with 15 wt% COF loading. **d,** Voltametric profiles in the double-layer region over a range of scan rates for CCBH catalyst with 25 wt% COF loading. **e,** Voltametric profiles in the double-layer region over a range of scan rates for Cu NPs with 25 wt% PTFE hydrophobic agent loading. **f,** Voltametric profiles in the double-layer region over a range of scan rates for bare COF with a mass loading same with the CCBH-15 wt% catalyst. The measurements were repeated three or more times to obtain the spectra for various scan rates.

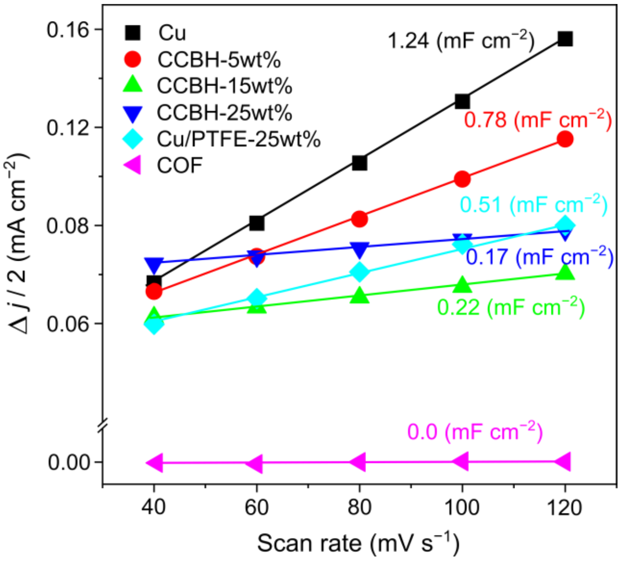

Supplementary Fig. 20 | Double-layer capacitance of various electrodes. Current plotted against the scan rate for the determination of double-layer capacitance. Cu control indicates the electrode composed of Cu NPs. The 5 wt%, 15 wt%, and 25 wt% labels indicate COF mass loadings on Cu NP electrodes. Cu/PTFE-25 wt% indicates the electrode composed of Cu NPs with 25% polytetrafluoroethylene (PTFE) hydrophobic agent mass loading. COF corresponds to the bare COF case, with a mass loading same with the CCBH-15 wt% catalyst. Here we show that the bare COF electrode has a zero capacitance, and thus does not influence the ECSA determination of the CCBH electrode. The total mass loading of Cu NPs was kept constant at 1 mg/cm^2. The measurements were repeated three or more times to obtain the spectra for various scan rates.

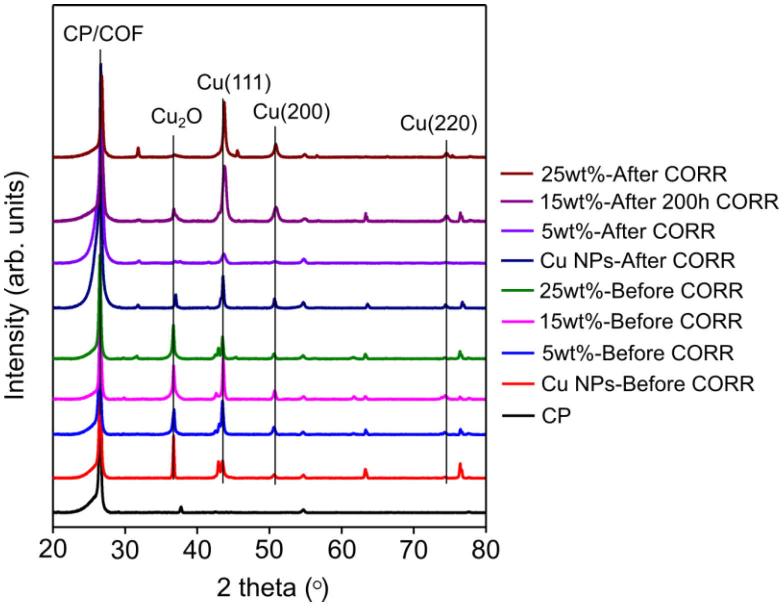

Supplementary Fig. 21 | X-ray diffraction (XRD) patterns of the CCBH catalysts with various COF loadings and bare Cu NPs before and after CORR in an anion exchange membrane (AEM) based membrane electrode assembly (MEA) using 1 M KOH as anolyte at 240 mA cm^{-2}.

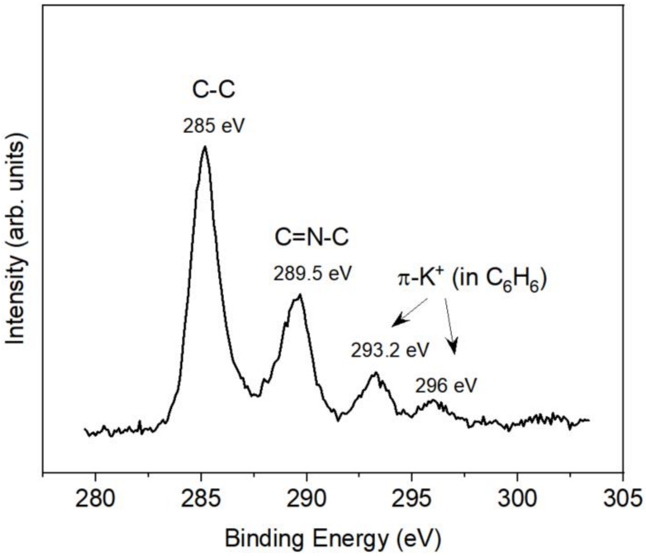

Supplementary Fig. 22 | The C 1s XPS of the CCBH catalyst with 15 wt% COF loading after CORR. Peaks at 285 eV and 289.5 eV are attributed to C–C and C=N–C bonds, respectively. Peaks at 293.2 eV and 296 eV are due the reaction of K^+ and sp^2 carbon from the benzene ring of COF[7].

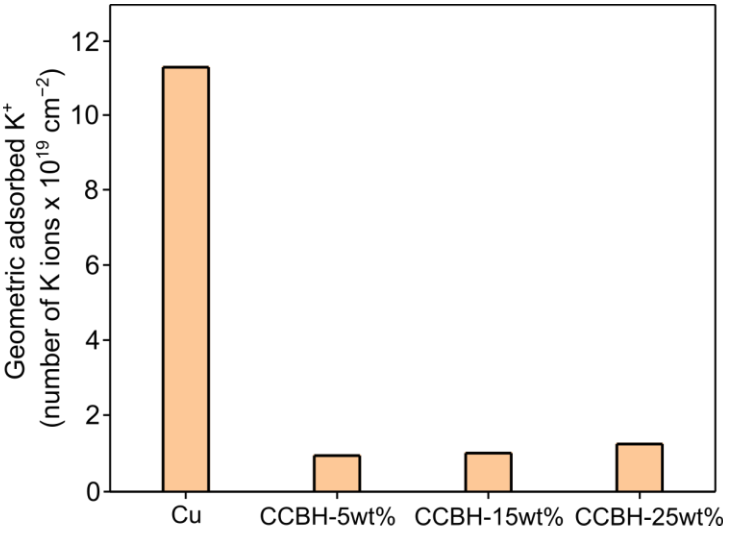

Supplementary Fig. 23 | Adsorbed K$^+$ concentrations on CCBH catalysts with 5 wt%, 15 wt%, and 25 wt% COF loadings and bare Cu catalyst. The values presented are based on geometric area of the electrodes.

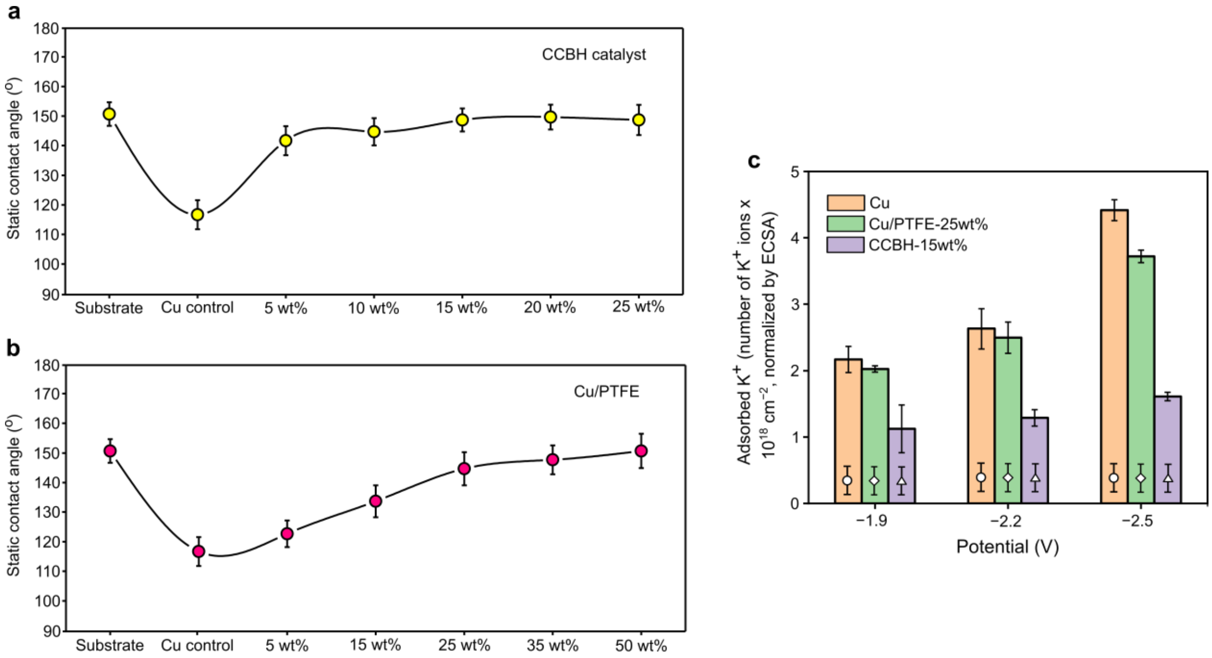

Supplementary Fig. 24 | ECSA-normalized absorbed K$^+$ concentration on catalysts with similar hydrophobicity. a, Static contact angles on CCBH catalyst with various COF mass loadings. Error bars represent the standard deviation of three independent measurements. Data are presented as mean values ± standard deviation. **b,** Static contact angles on Cu NPs with various polytetrafluoroethylene (PTFE) hydrophobic agent mass loadings. Error bars represent the standard deviation of three independent measurements. Data are presented as mean values ± standard deviation. **c,** ECSA-normalized absorbed K$^+$ concentration on catalysts with similar hydrophobicity at cell potentials of −1.9 V, −2.2 V, and −2.5 V. Error bars represent the standard deviation of three independent measurements. Data are presented as mean values ± standard deviation. CCBH catalyst with 15 wt% COF loading and Cu NPs with 25 wt% PTFE hydrophobic agent loading yield a similar static contact angle of ~145^o. Control Cu stands for the Cu NPs spray-deposited onto the carbon paper. The total mass loading of Cu NPs in all electrodes was kept constant at 1 mg/cm^2.

Supplementary Note 6 | K^+ diffusion measurements. This section provides the details of K^+ retention measurements. A time-lag method was applied to determine the quantity of K^+ diffused from anolyte (1 M KOH) to catholyte (pure water) through the membrane with or without COF in a two-electrode flow cell system during CORR (Supplementary Fig. 25). The concentration of K^+ in the pure water (due to the K^+ crossing over from the anode to the cathode) increases linearly with the time and reaches a steady-state condition in 4 hours. The experiments were also carried out under the same conditions by introducing a COF layer. The COF addition decreased the cross-over rate of K^+ by three orders of magnitude.

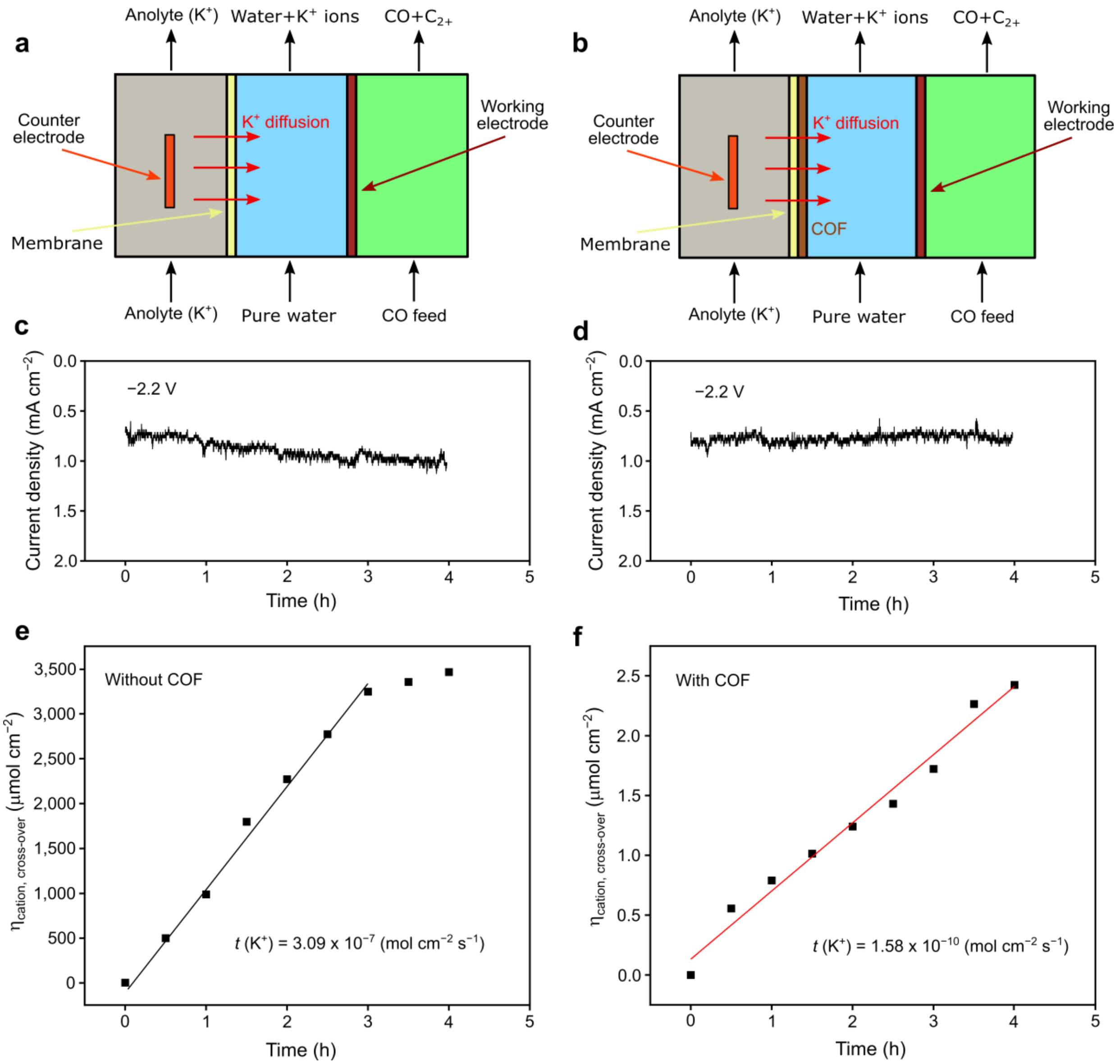

Supplementary Fig. 25 | K$^+$ diffusion measurements. a, Schematic of a two-electrode flow cell system without COF for K$^+$ cross-over measurements. **b,** Schematic of a two-electrode flow cell system with COF for K$^+$ cross-over measurements. **c,** Chrono-potentiometry profile of two-electrode flow cell system without COF at a constant potential of −2.2 V. **d,** Chrono-potentiometry profile of two-electrode flow cell system with COF at a constant potential of −2.2 V. **e,** Inductively coupled plasma optical emission spectroscopy (ICP-OES) quantification of K$^+$ cross-over through membrane without COF during CORR in a two-electrode flow cell system. **f,** Inductively coupled plasma optical emission spectroscopy (ICP-OES) quantification of K$^+$ cross-over through membrane and COF during CORR in a two-electrode flow cell system. The total mass loading of COF was kept constant at 0.15 mg/cm^2, which is the same with the amount used in the highest performing CCBH catalyst (CCBH-15 wt%). The details of the K^+ diffusion measurements are provided in Supplementary Note 6 and Methods.

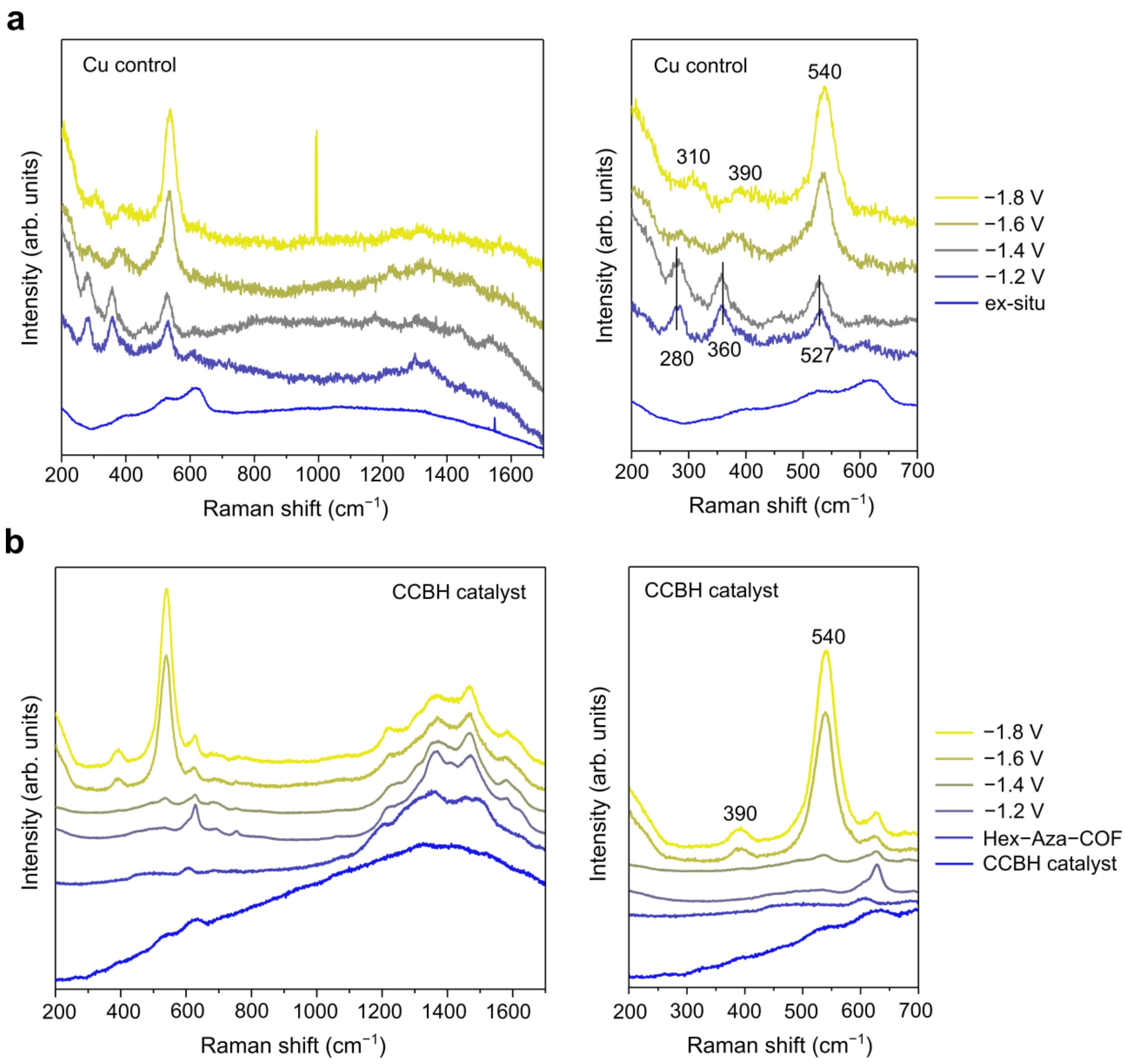

Supplementary Fig. 26 | Raman spectra. a, Ex- and in-situ Raman spectra of bare Cu NPs. **b,** Ex- and in-situ Raman spectra of the CCBH catalyst with 15 wt% COF loading and bare COF (Hex–Aza–COF). The voltages are presented versus Ag/AgCl.

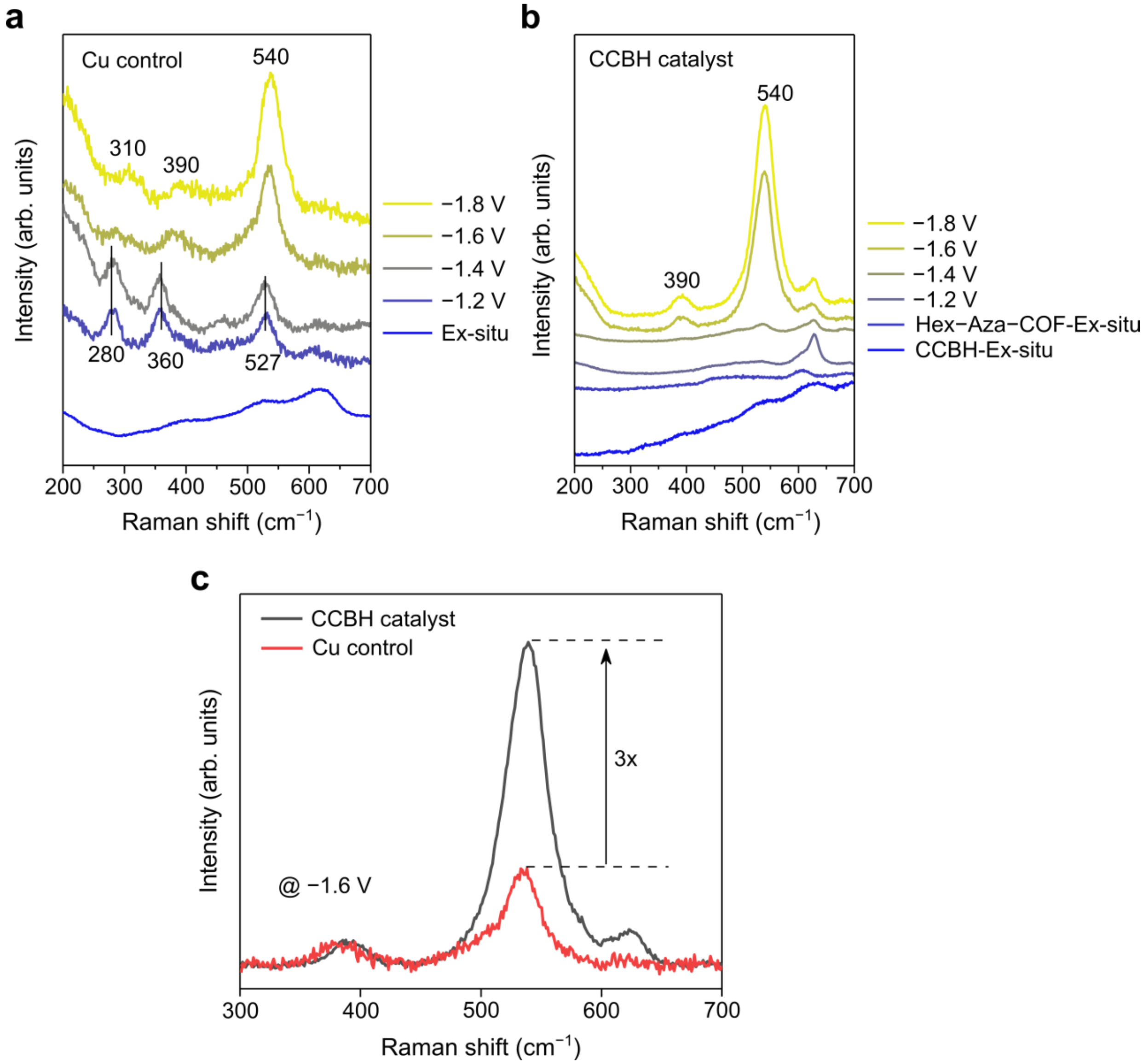

Supplementary Fig. 27 | Raman spectra. a, Ex- and in-situ Raman spectra of bare Cu NPs. **b,** Ex- and in-situ Raman spectra of CCBH catalyst with 15 wt% COF loading. **c,** Comparison of in-situ Raman spectra of bare Cu and CCBH catalyst at −1.6 V versus Ag/AgCl.

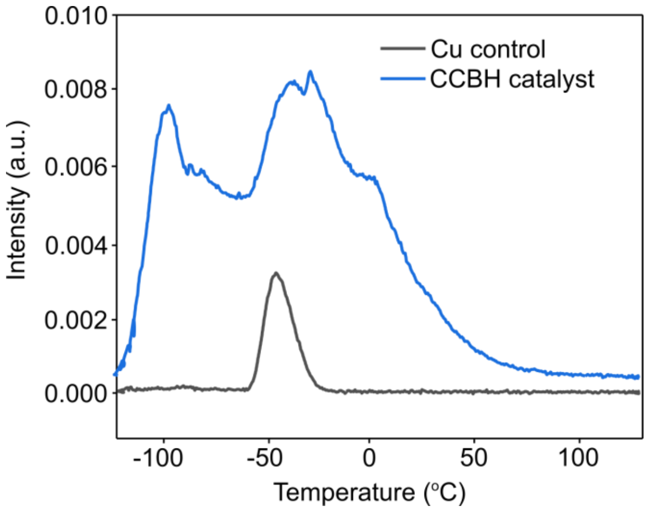

Supplementary Fig. 28 | Thermal desorption spectroscopy (TPD) profiles of CO on CCBH catalyst with 15 wt% COF loading and bare Cu NPs.

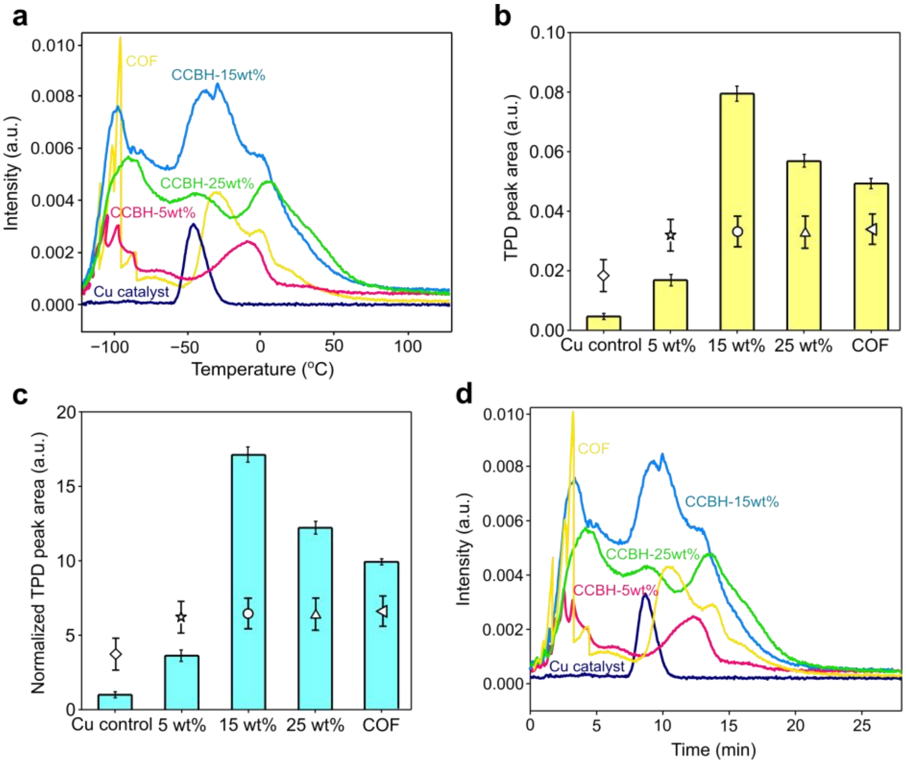

Supplementary Fig. 29 | Thermal desorption spectroscopy (TPD) measurements. a, TPD profiles of the CCBH catalyst with various COF mass loadings and bare Cu NPs. **b,** TPD peak areas of the CCBH catalysts with various COF mass loadings and bare Cu NPs. Error bars represent the standard deviation of two independent measurements. Data are presented as mean values ± standard deviation. **c,** Normalized TPD peak areas of the CCBH catalysts with various COF mass loadings and bare Cu NPs. Error bars represent the standard deviation of two independent measurements. Data are presented as mean values ± standard deviation. **d,** TPD profiles versus time of the CCCB catalysts with various COF mass loadings and bare Cu NPs (Peak area calculated from the chemisorption software is automatically derived from the TPD time profile graph).

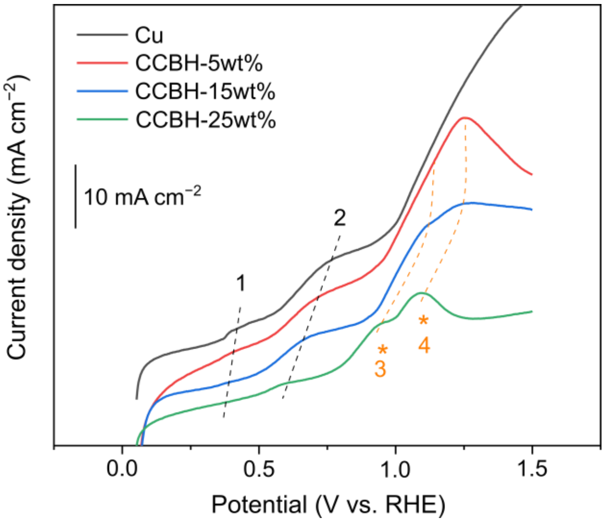

Supplementary Fig. 30 | CO stripping voltammetry profiles of bare Cu NPs and CCBH catalysts with various COF mass loadings. Cu control stands for the catalyst composed of Cu NPs. 5 wt%, 15 wt%, and 25 wt% stand for the catalysts of Cu NPs with various COF mass loadings. The total mass loading of Cu NPs in all electrodes was kept constant at 1 mg/cm^2. Peaks 1 and 2 could be assigned to CO desorption from Cu surfaces[8], which shift to more negative potentials with increasing COF loadings, indicating a relatively higher CO binding strength on Cu modulated by COF. Two additional peaks 3 and 4 on the CCBH catalysts are likely due to CO desorption at the Cu/COF interfaces.

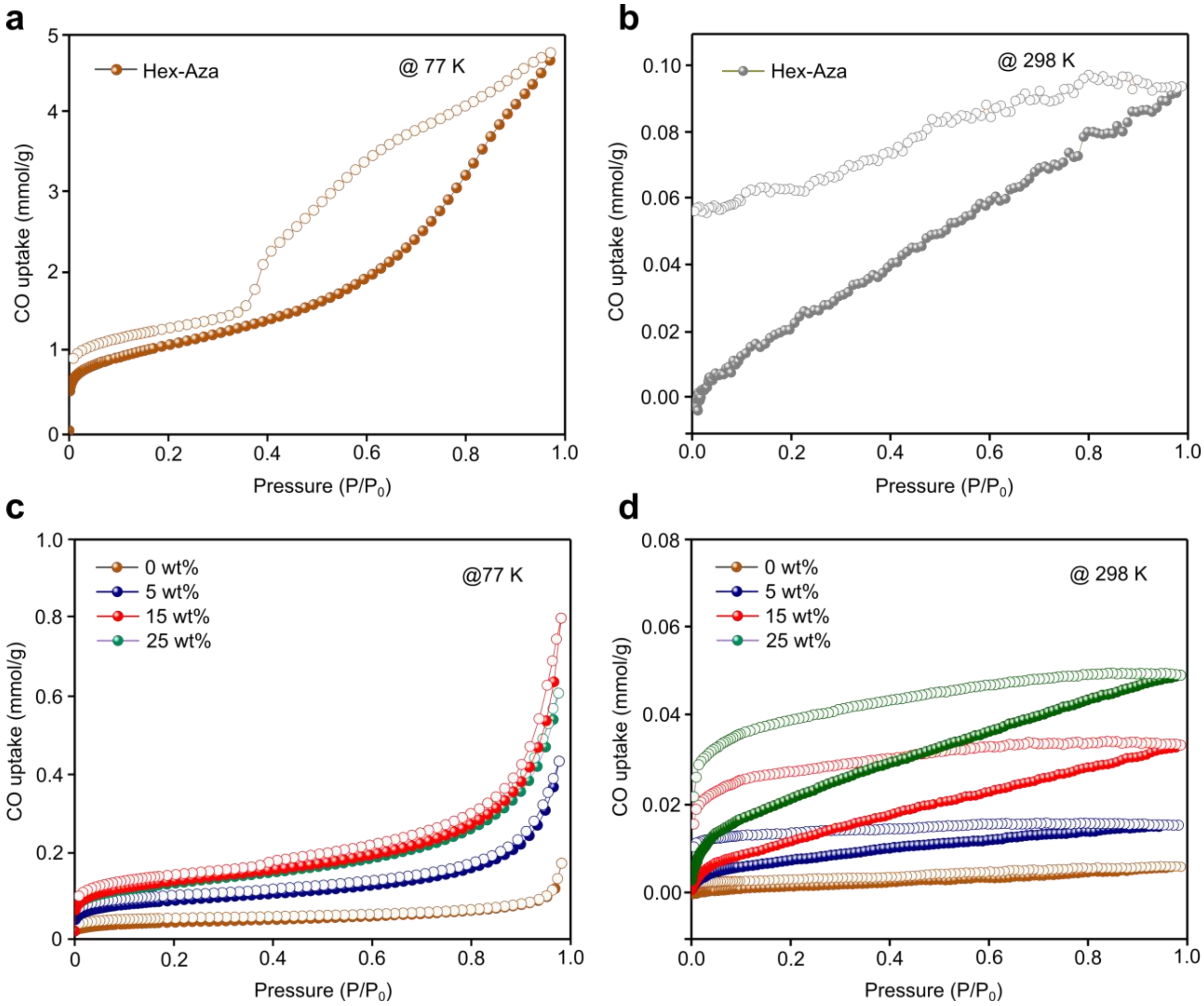

Supplementary Fig. 31 | Static CO adsorption profiles of CCBH catalysts with various COF mass loadings. a, Static CO adsorption profile of bare COF (Hex–Aza–COF) at a temperature of 77 K. **b,** Static CO adsorption profile of bare COF (Hex–Aza–COF) at a temperature of 298 K. **c,** Static CO adsorption profile of CCBH catalysts with various COF mass loadings (5 wt%, 15 wt%, and 25 wt%) at a temperature of 77 K. **d,** Static CO adsorption profile of CCBH catalysts with various COF mass loadings (5 wt%, 15 wt%, and 25 wt%) at a temperature of 298 K.

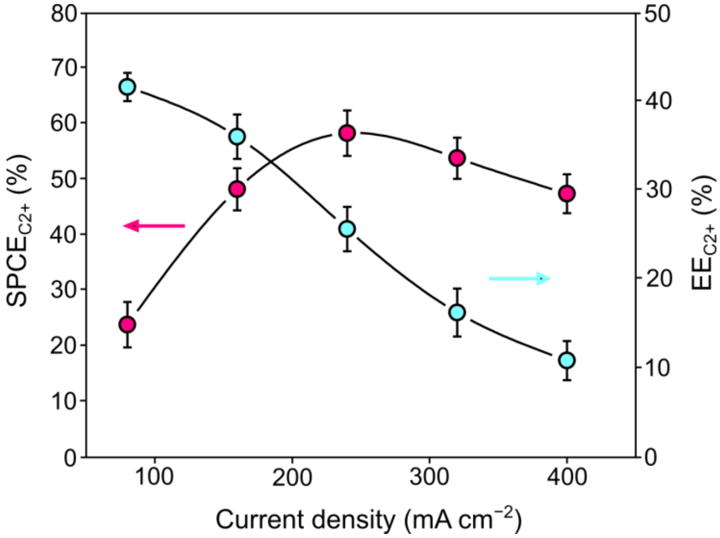

Supplementary Fig. 32 | CORR single-pass carbon efficiency (SPCE) versus energy efficiency (EE) performance of bare Cu NPs in anion exchange membrane (AEM) based membrane electrode assembly (MEA) using 1 M KOH as anolyte. Operating conditions: anolyte flow rate 20 mL min^{-1}; CO flow rate: ~1 sccm cm^{-2}; and cell temperature and pressure: atmospheric conditions. Error bars represent the standard deviation of three independent measurements. Data are presented as mean values ± standard deviation.

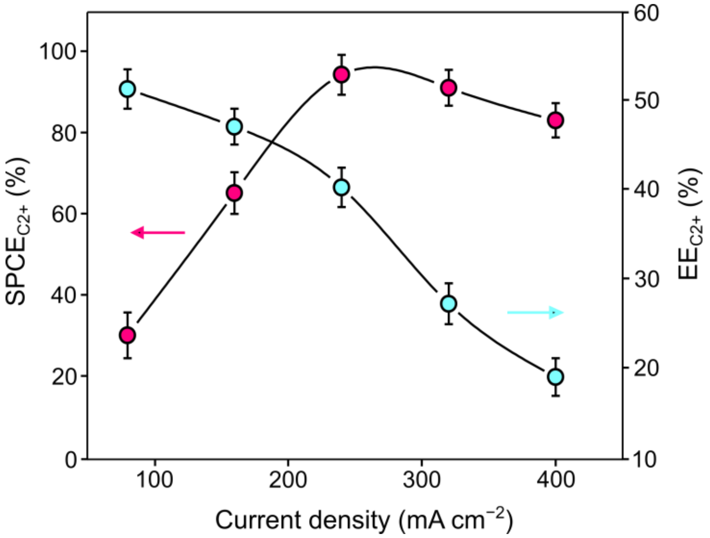

Supplementary Fig. 33 | CORR single-pass carbon efficiency (SPCE) versus energy efficiency (EE) performance of the CCBH catalyst with 15 wt% COF loading in anion exchange membrane (AEM) based membrane electrode assembly (MEA) using 1 M KOH as anolyte. Operating conditions: anolyte flow rate 20 mL min^{-1}; CO flow rate: ~1 sccm cm^{-2}; and cell temperature and pressure: atmospheric conditions. Error bars represent the standard deviation of three independent measurements. Data are presented as mean values ± standard deviation.

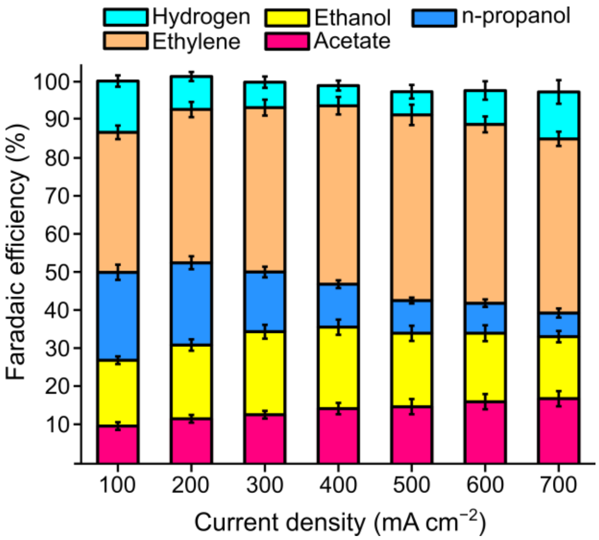

Supplementary Fig. 34 | CORR Faradaic efficiency versus current density performance of the CCBH catalyst with 15 wt% COF loading in an anion exchange membrane (AEM) based membrane electrode assembly (MEA) using 1 M KOH as anolyte. Operating conditions: anolyte flow rate 20 mL min^{-1}; CO flow rate: ~10 sccm cm^{-2}; and cell temperature and pressure: atmospheric conditions. Error bars represent the standard deviation of three independent measurements. Data are presented as mean values ± standard deviation. A discussion on the product distributions as a function of current density is provided in Supplementary Note 7.

Supplementary Note 7 | Product distribution of CCBH catalyst. At a constant CO flow rate of 10 sccm cm^{-2}, the CCBH catalyst with 15 wt% COF loading yields a typical CORR products of ethylene, ethanol, n-propanol, and acetate over a wide range of current densities (100-700 mA cm^{-2}). The total FE toward C_{2+} products achieves a plateau of 94% at 400 mA cm^{-2}, where the FE toward H_2 remains around 5%. Over this wide current density range, ethylene remains the major CORR product, and its FE reaches a plateau of 49% at 500 mA cm^{-2}. The CCBH catalyst produces n-propanol with the highest FE of 23% at a current density of 100 mA cm^{-2}, and increasing the current density further leads to a gradual decrease in the FE of n-propanol. The FE toward ethanol, however, increases from 17% to 22% with the current density increasing from 100 mA cm^{-2} to 300 mA cm^{-2} and starts decreasing gradually down to 16% with the current density increasing from 300 mA cm^{-2} to 700 mA cm^{-2}. The FE toward acetate, on the other hand, gradually increases from 10% to 17.1% with the current density increasing from 100 mA cm^{-2} to 700 mA cm^{-2}, where the FE toward H_2 reaches 12% and FE toward C_{2+} products reduces to 85% (see also Supplementary Figure 34 and Supplementary Table 22 for the details of full performance metrics).

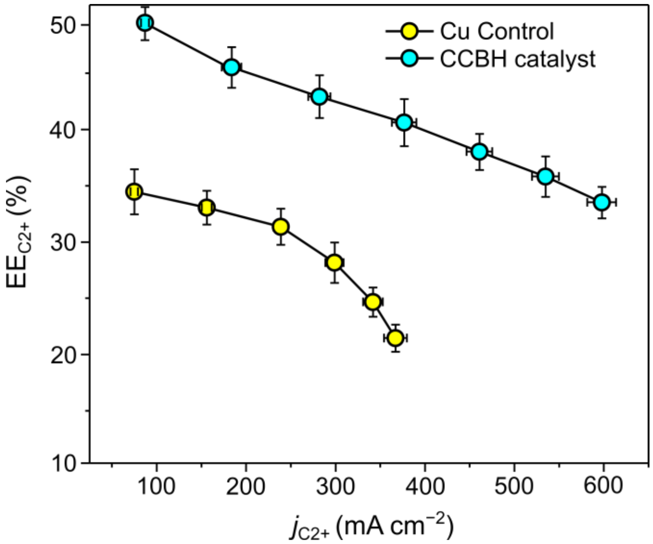

Supplementary Fig. 35 | Comparison of CORR performance of the CCBH catalyst with 15 wt% COF loading with that of bare Cu NPs in anion exchange membrane (AEM) based membrane electrode assembly (MEA) under their highest energy efficiency operation modes. Operating conditions: anolyte flow rate 20 mL min^{-1}; CO flow rate: ~10 sccm cm^{-2}; and cell temperature and pressure: atmospheric conditions. Error bars represent the standard deviation of three independent measurements. Data are presented as mean values ± standard deviation.

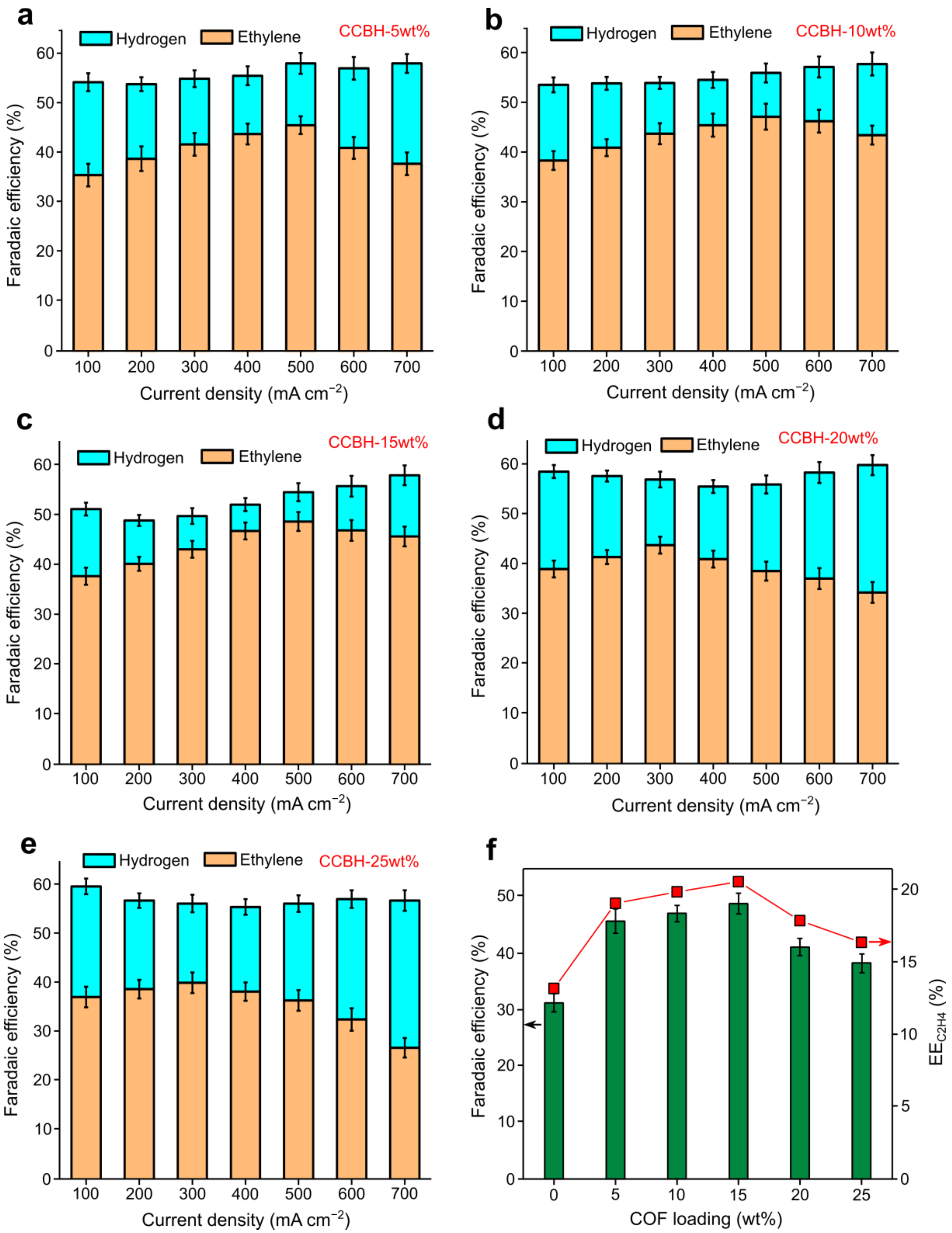

Supplementary Fig. 36 | CORR performance of CCBH catalysts with various COF mass loadings. a, Faradaic efficiency versus current density performance of the CCBH catalyst with 5 wt% COF loading. Error bars represent the standard deviation of three independent measurements.

Data are presented as mean values ± standard deviation. **b,** Faradaic efficiency versus current density performance of the CCBH catalyst with 10 wt% COF loading. Error bars represent the standard deviation of three independent measurements. Data are presented as mean values ± standard deviation. **c,** Faradaic efficiency versus current density performance of the CCBH catalyst with 15 wt% COF loading. Error bars represent the standard deviation of three independent measurements. Data are presented as mean values ± standard deviation. **d,** Faradaic efficiency versus current density performance of the CCBH catalyst with 20 wt% COF loading. Error bars represent the standard deviation of three independent measurements. Data are presented as mean values ± standard deviation. **e,** Faradaic efficiency versus current density performance of the CCBH catalyst with 25 wt% COF loading. Error bars represent the standard deviation of three independent measurements. Data are presented as mean values ± standard deviation. **f,** COF mass loading versus current density and EE_{C2H4} performance of the CCBH catalysts with various COF mass loadings. Error bars represent the standard deviation of three independent measurements. Data are presented as mean values ± standard deviation. Operating conditions: anolyte flow rate 20 mL min^{-1}; CO flow rate: ~10 sccm cm^{-2}; and cell temperature and pressure: atmospheric conditions.

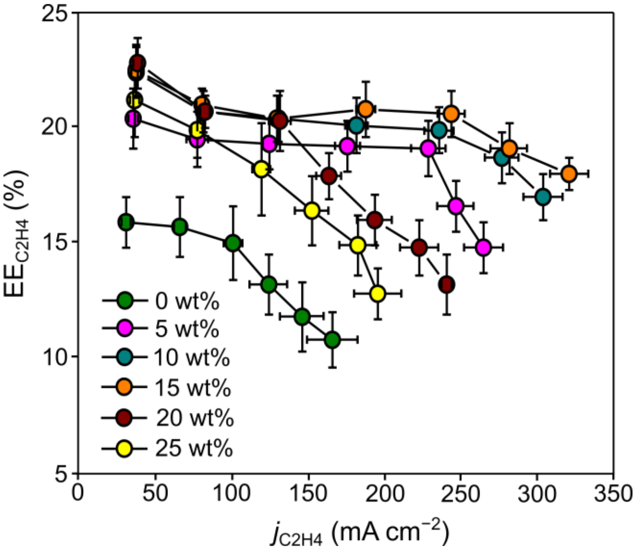

Supplementary Fig. 37 | Effect of COF mass loading (wt%) (weight/ by weight ratio between COF and Cu NPs) on the ethylene energy efficiency (EE) versus ethylene partial current density performance of CCBH catalyst in an anion exchange membrane (AEM) based membrane electrode assembly (MEA) using 1 M KOH as anolyte. Operating conditions: anolyte flow rate 20 mL min^{-1}; CO flow rate: ~10 sccm cm^{-2}; and cell temperature and pressure: atmospheric conditions. Error bars represent the standard deviation of three independent measurements. Data are presented as mean values ± standard deviation.

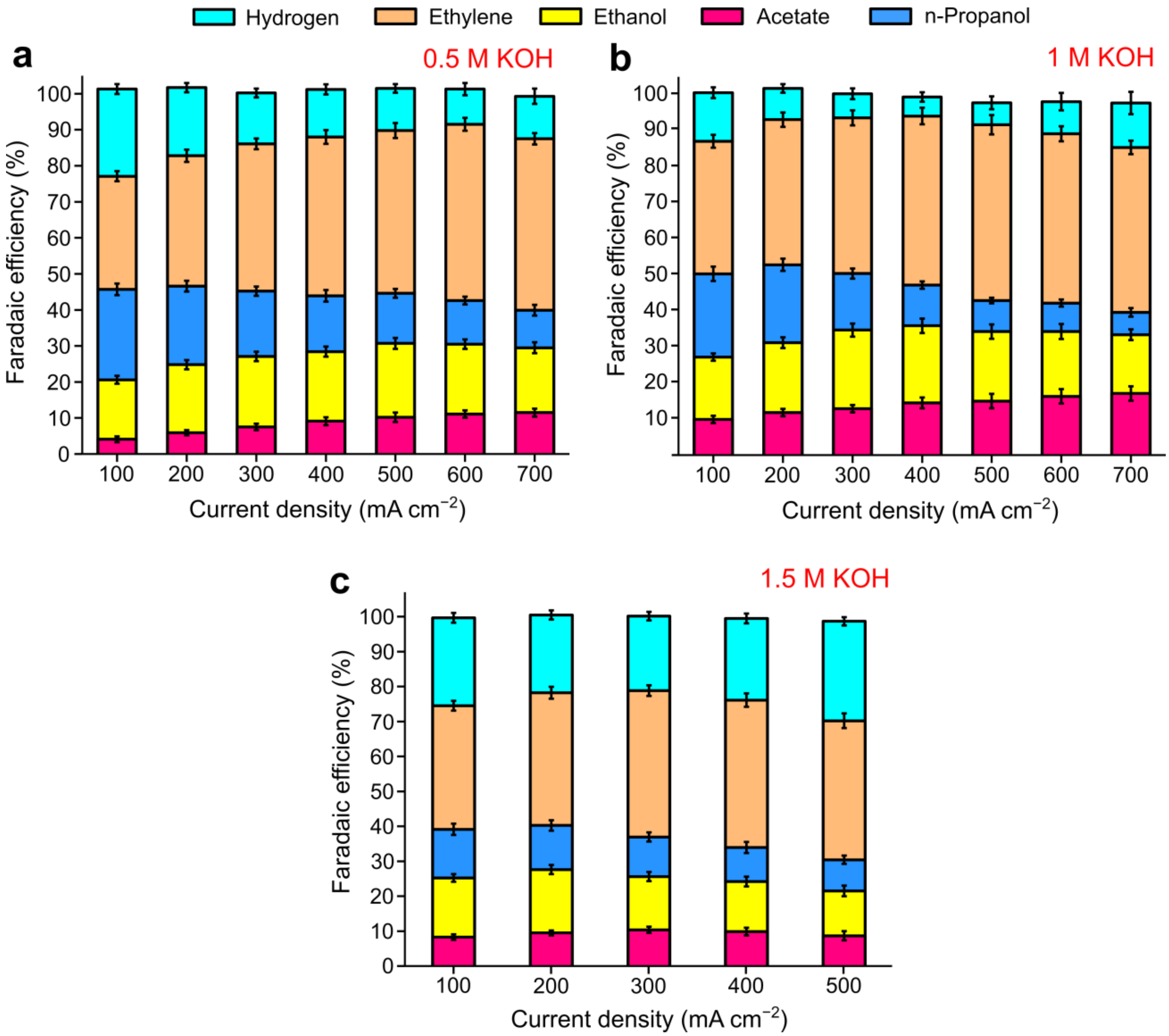

Supplementary Fig. 38 | CORR Faradaic efficiency versus current density performance of CCBH catalyst with 15 wt% COF loading in an anion exchange membrane (AEM) based membrane electrode assembly (MEA) using various KOH concentrations. a, 0.5 M KOH (pH 13.6). Error bars represent the standard deviation of three independent measurements. Data are presented as mean values ± standard deviation. **b,** 1 M KOH (pH 13.9). Error bars represent the standard deviation of three independent measurements. Data are presented as mean values ± standard deviation. **c,** 1.5 M KOH (pH 14.1). Error bars represent the standard deviation of three independent measurements. Data are presented as mean values ± standard deviation. Operating conditions: anolyte flow rate 20 mL min^{-1}; CO flow rate: ~10 sccm cm^{-2}; and cell temperature and pressure: atmospheric conditions.

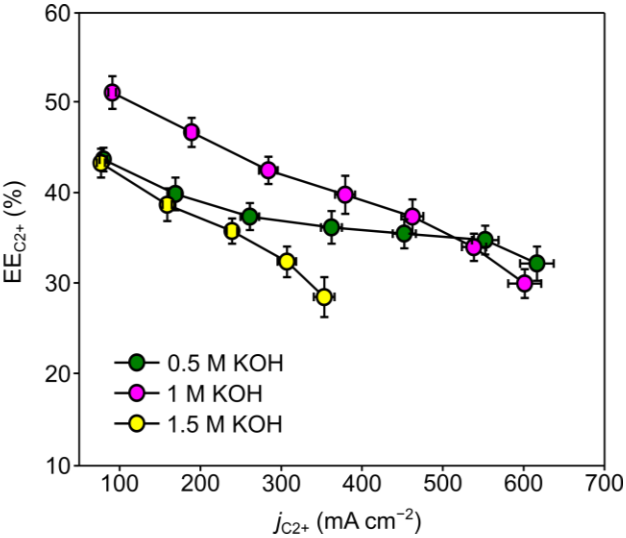

Supplementary Fig. 39 | CORR partial current density versus energy efficiency (EE) performance of the CCBH catalyst with 15 wt% COF loading in anion exchange membrane (AEM) based membrane electrode assembly (MEA) using KOH with various concentrations as anolyte (0.5 M KOH (pH 13.6), 1 M KOH (pH 13.9), and 1.5 M KOH (pH 14.1)). Operating conditions: anolyte flow rate 20 mL min^{-1}; CO flow rate: ~10 sccm cm^{-2}; and cell temperature and pressure: atmospheric conditions. Error bars represent the standard deviation of three independent measurements. Data are presented as mean values ± standard deviation.

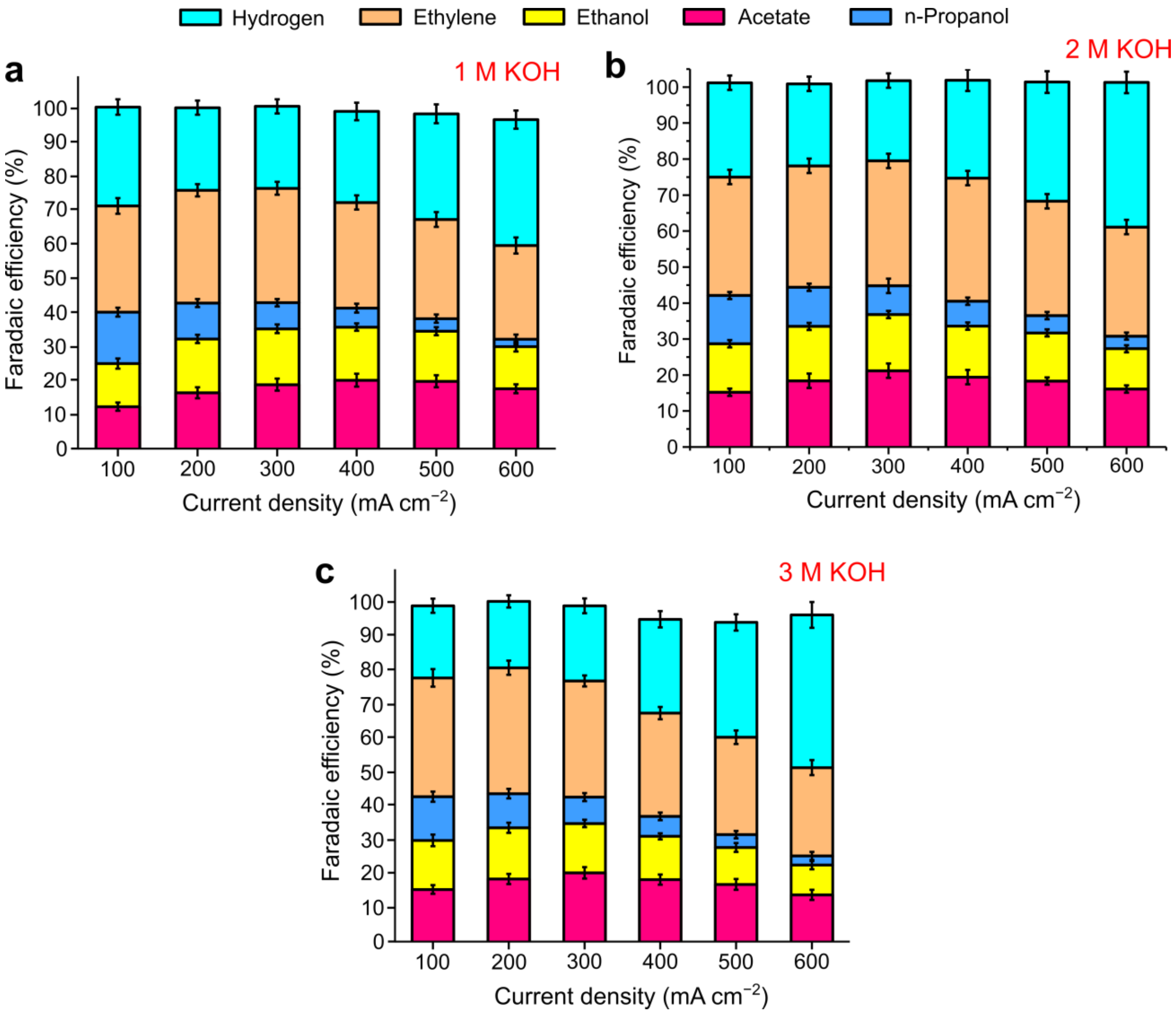

Supplementary Fig. 40 | CORR Faradaic efficiency versus current density performance of bare Cu NPs in an anion exchange membrane (AEM) based membrane electrode assembly (MEA) using various KOH concentrations. a, 1 M KOH (pH 13.9). Error bars represent the standard deviation of three independent measurements. Data are presented as mean values ± standard deviation. **b,** 2 M KOH (pH 14.2). Error bars represent the standard deviation of three independent measurements. Data are presented as mean values ± standard deviation. **c,** 3 M KOH (pH 14.4). Error bars represent the standard deviation of three independent measurements. Data are presented as mean values ± standard deviation. Operating conditions: anolyte flow rate 20 mL min^{-1}; CO flow rate: ~10 sccm cm^{-2}; and cell temperature and pressure: atmospheric conditions.

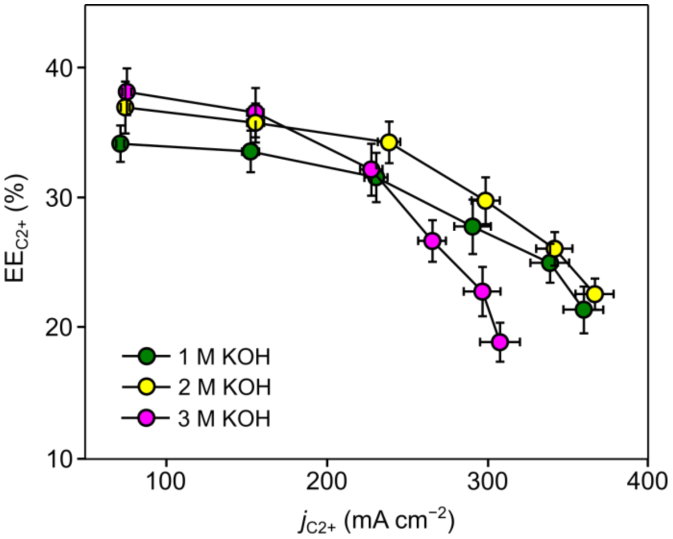

Supplementary Fig. 41 | CORR energy efficiency (EE) versus CORR partial current density (j_{C2+}) performance of Cu NPs in an anion exchange membrane (AEM) based membrane electrode assembly (MEA) using KOH with various concentrations as anolyte (1 M KOH (pH 13.9), 2 M KOH (pH 14.2), and 3 M KOH (pH 14.4)). Operating conditions: anolyte flow rate 20 mL min^{-1}; CO flow rate: ~10 sccm cm^{-2}; and cell temperature and pressure: atmospheric conditions. Error bars represent the standard deviation of three independent measurements. Data are presented as mean values ± standard deviation.

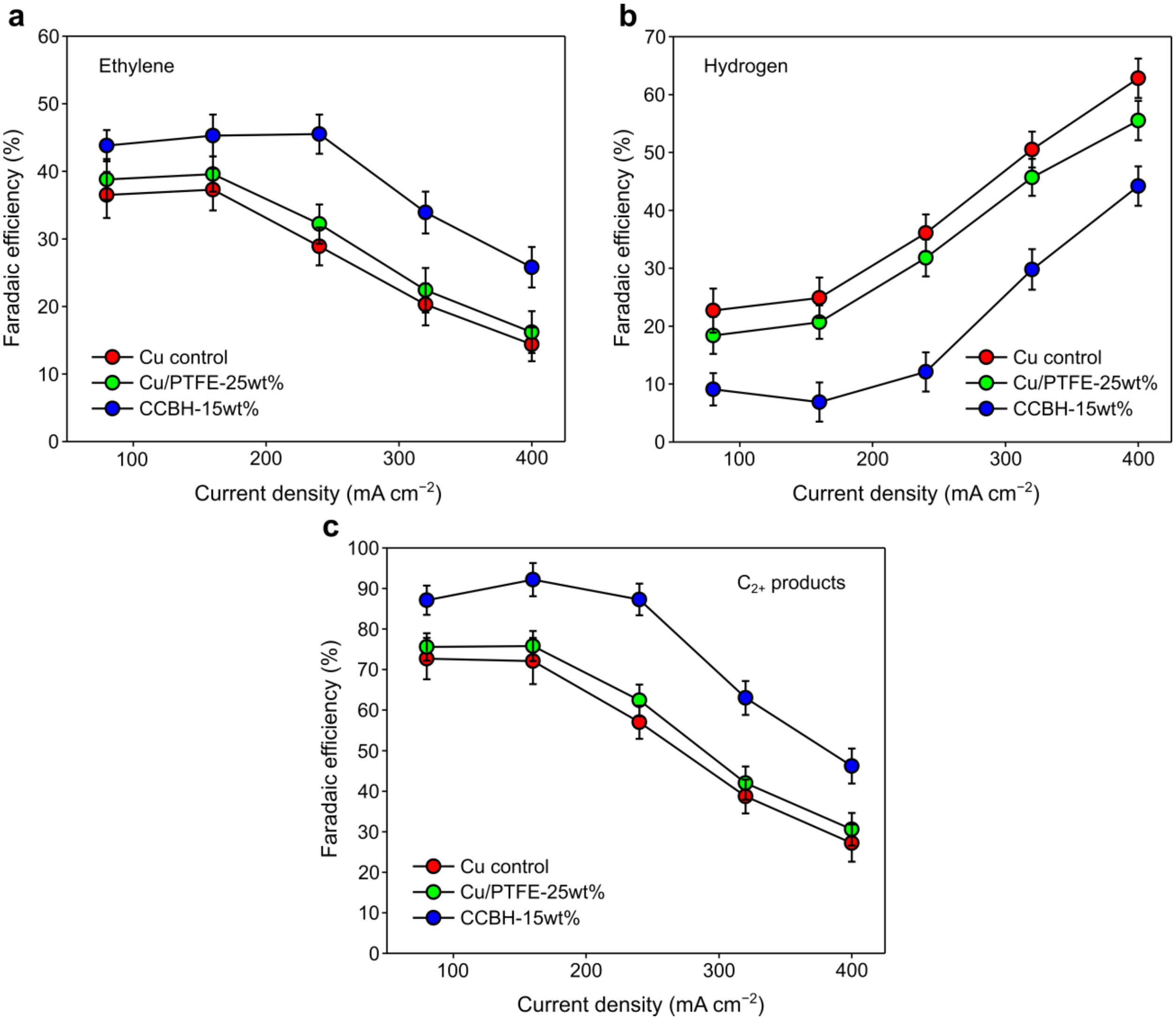

Supplementary Fig. 42 | CORR performance of CCBH catalyst with 15 wt% COF loading, Cu NPs loaded with 25 wt% hydrophobic polytetrafluoroethylene (PTFE) loading, and bare Cu NPs in an anion exchange membrane (AEM) based membrane electrode assembly (MEA) using 1 M KOH (pH 13.9) as anolyte under low CO availability. a, Ethylene Faradaic efficiency versus current density. Error bars represent the standard deviation of three independent measurements. Data are presented as mean values ± standard deviation. **b,** Hydrogen Faradaic efficiency versus current density. Error bars represent the standard deviation of three independent measurements. Data are presented as mean values ± standard deviation. **c,** C$_{2+}$ Faradaic efficiency versus current density. Error bars represent the standard deviation of three independent measurements. Data are presented as mean values ± standard deviation. Operating conditions: anolyte flow rate 20 mL min^{-1}; CO flow rate: ~1 sccm cm^{-2}; anolyte type: 1 KOH; and cell temperature and pressure: atmospheric conditions.

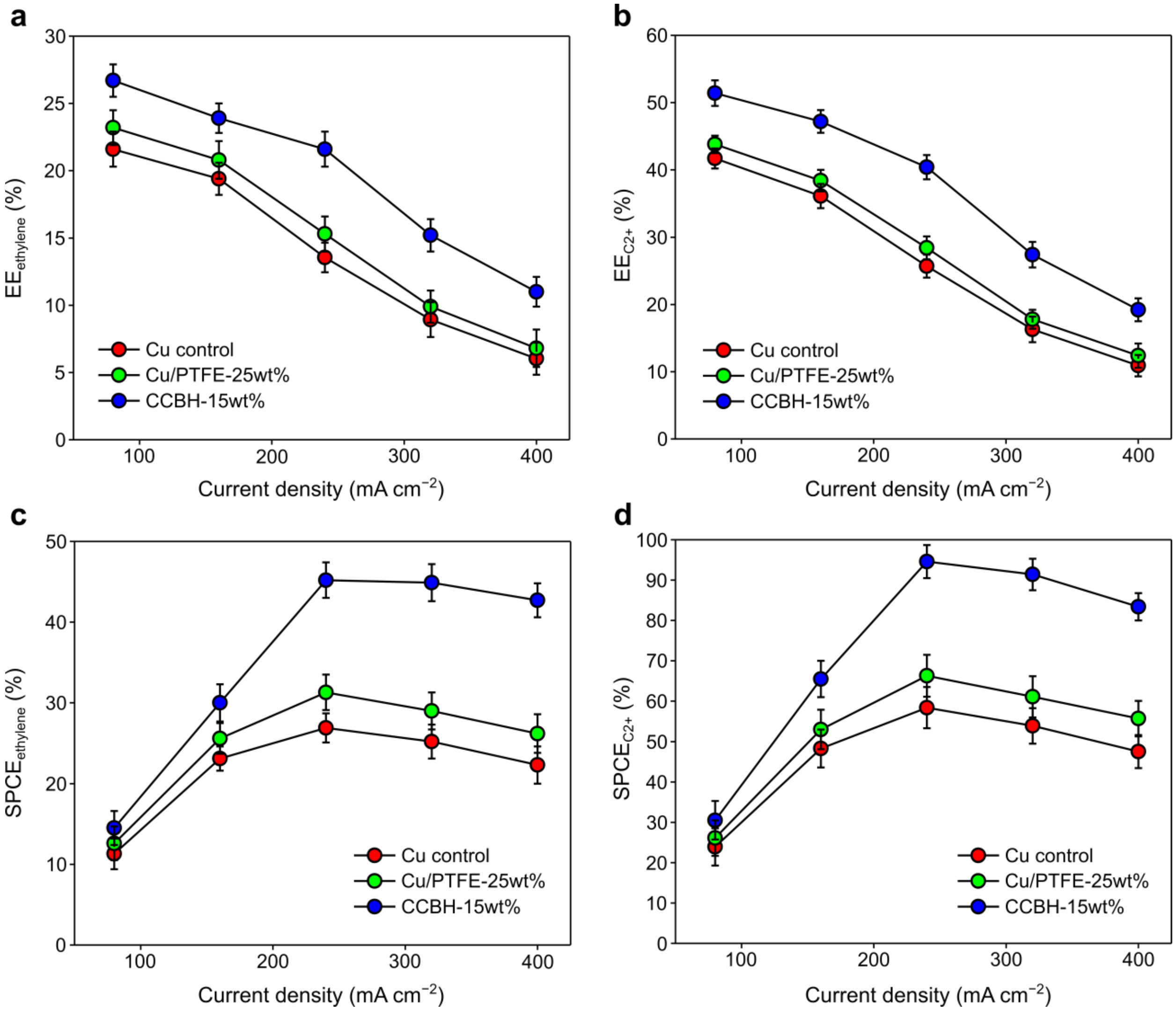

Supplementary Fig. 43 | CORR performance of CCBH catalyst with 15 wt% COF loading, Cu NPs loaded with 25 wt% hydrophobic polytetrafluoroethylene (PTFE) loading, and bare Cu NPs in an anion exchange membrane (AEM) based membrane electrode assembly (MEA) using 1 M KOH (pH 13.9) as anolyte under low CO availability. a, CO-to-ethylene energy efficiency (EE) versus current density. Error bars represent the standard deviation of three independent measurements. Data are presented as mean values ± standard deviation. **b,** CO-to-C_{2+} energy efficiency (EE) versus current density. Error bars represent the standard deviation of three independent measurements. Data are presented as mean values ± standard deviation. **c,** CO-to-ethylene single-pass carbon efficiency (SPCE) versus current density. Error bars represent the standard deviation of three independent measurements. Data are presented as mean values ± standard deviation. **d,** CO-to-C_{2+} single-pass carbon efficiency (SPCE) versus current density. Error bars represent the standard deviation of three independent measurements. Data are presented as mean values ± standard deviation. Operating conditions: anolyte flow rate 20 mL min^{-1}; anolyte type: 1 M KOH; CO flow rate: ~1 sccm cm^{-2}; and cell temperature and pressure: atmospheric conditions.

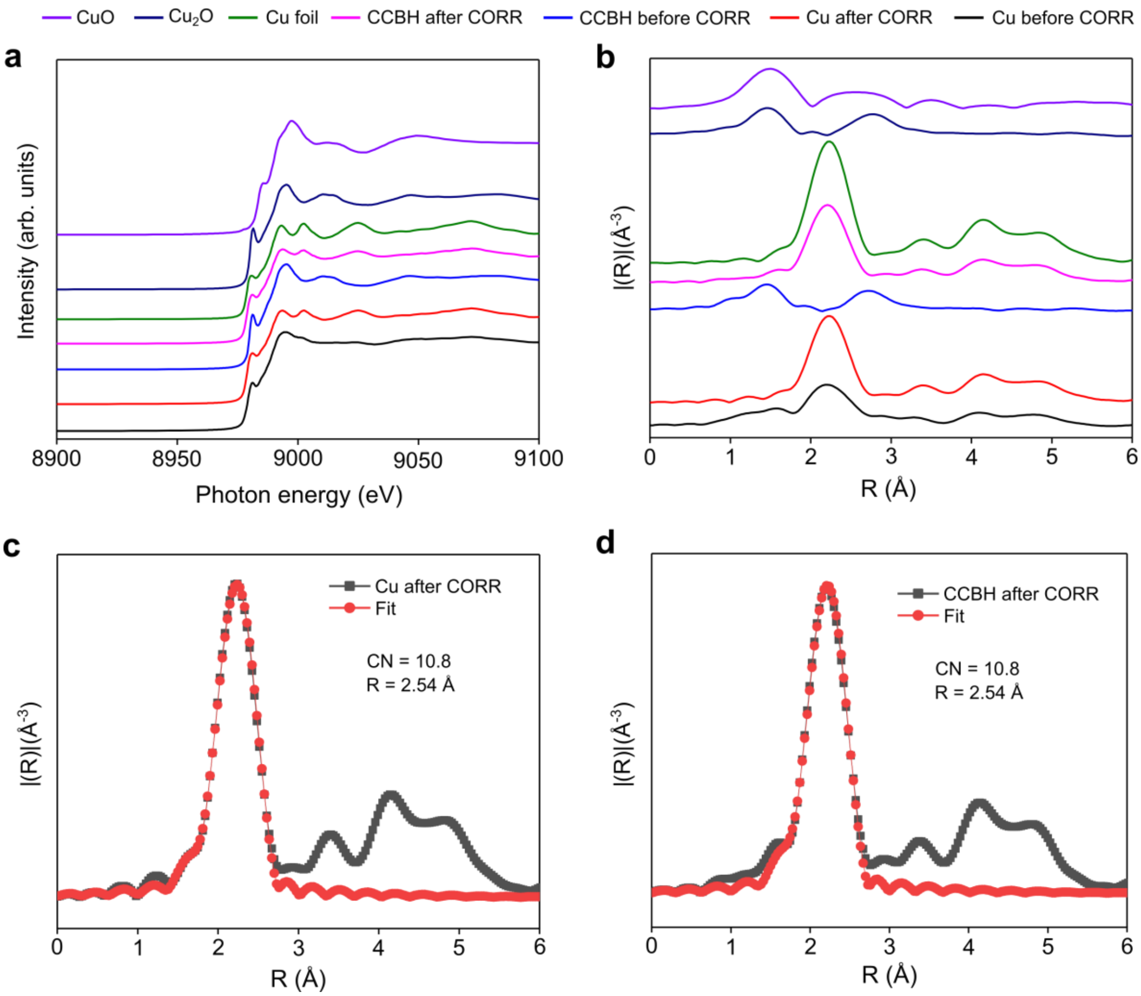

Supplementary Fig. 44 | X-ray adsorption spectroscopy (XAS) measurements. a, The Cu K-edge XAS of bare Cu and CCBH catalysts before and after CORR and Cu standards (metallic Cu foil, Cu_2O, and CuO). **b,** Fourier-transformed Cu K-edge XAS of bare Cu and CCBH catalysts before and after CORR and Cu standards (metallic Cu foil, Cu_2O, and CuO). **c,** Fitting of the Fourier-transformed Cu K-edge XAS of bare Cu after CORR. **d,** Fitting of the Fourier-transformed Cu K-edge XAS of CCBH catalyst after CORR.

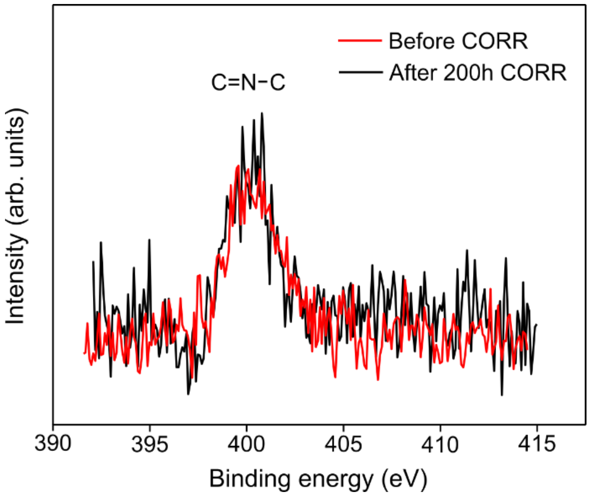

Supplementary Fig. 45 | X-ray photoelectron spectroscopy (XPS) of the CCBH catalyst with 15 wt% COF loading before and after 200 h of continuous CORR in anion exchange membrane (AEM) based membrane electrode assembly (MEA) using 1 M KOH as anolyte at 240 mA cm^{-2}.

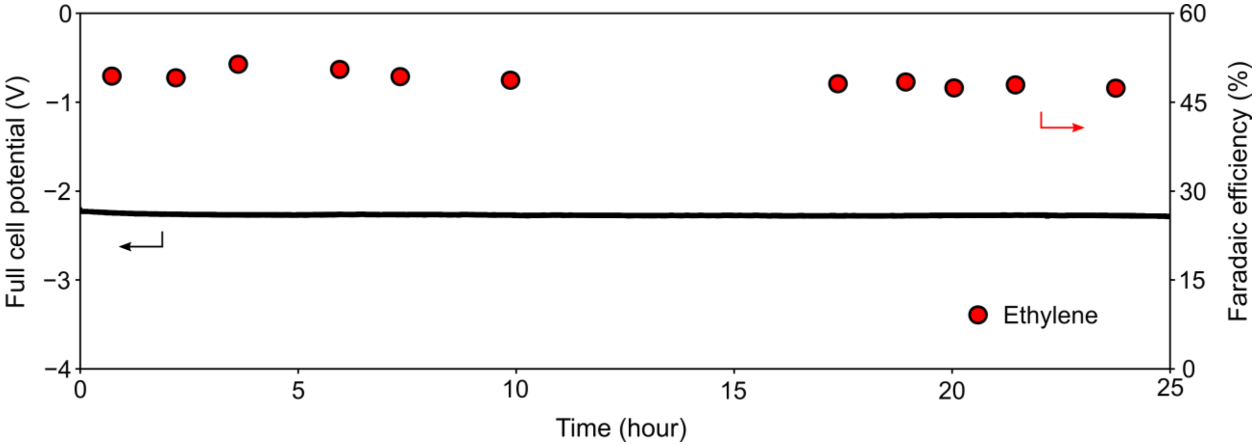

Supplementary Fig. 46 | CORR performance of the CCBH catalyst for impurity analysis. CORR performance of the CCBH catalyst in an anion exchange membrane (AEM) based membrane electrode assembly using 1 M KOH (pH 13.9) as anolyte at 240 mA cm^{-2}. An average ethylene FE of 47% maintained for 25 hours of continuous operation. The 1 M KOH electrolyte was analyzed via ICP-OES for any Ni and Fe impurities before and after 25 hours of continuous CORR (see also Supplementary Note 4 and Supplementary Table 14). Operating conditions: anolyte flow rate 20 mL min^{-1}; CO flow rate: ~1 sccm cm^{-2}; and cell temperature and pressure: atmospheric conditions.

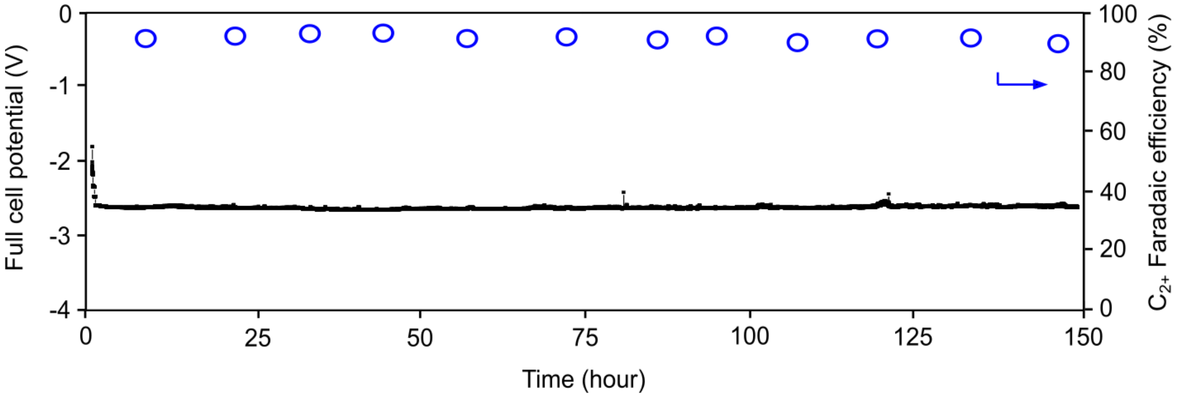

Supplementary Fig. 47 | Extended CORR performance of the CCBH catalyst with 15 wt% COF loading in anion exchange membrane (AEM) based membrane electrode assembly (MEA) using 1 M KOH as anolyte at 600 mA cm^{-2}. An average EE_{C2+} of 34% is maintained for initial 150 hours of continuous operation. Operating conditions: anolyte flow rate 20 mL min^{-1}; CO flow rate: ~10 sccm cm^{-2}; and cell temperature and pressure: atmospheric conditions.

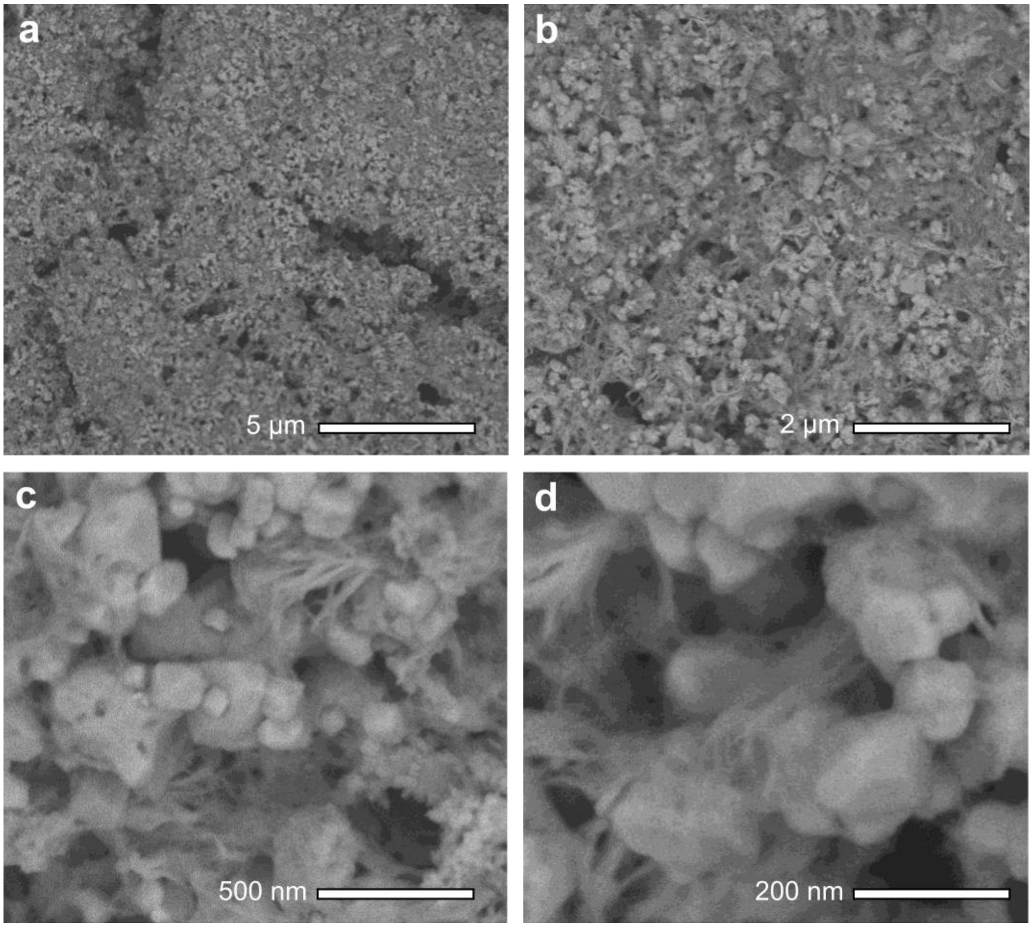

Supplementary Fig. 48 | Scanning electron microscopy (SEM) images of the CCBH catalyst with 15 wt% COF loading upon completion of 200 h of continuous CORR in an anion exchange membrane (AEM) based membrane electrode assembly (MEA) using 1 M KOH as anolyte at 240 mA cm^{-2}.

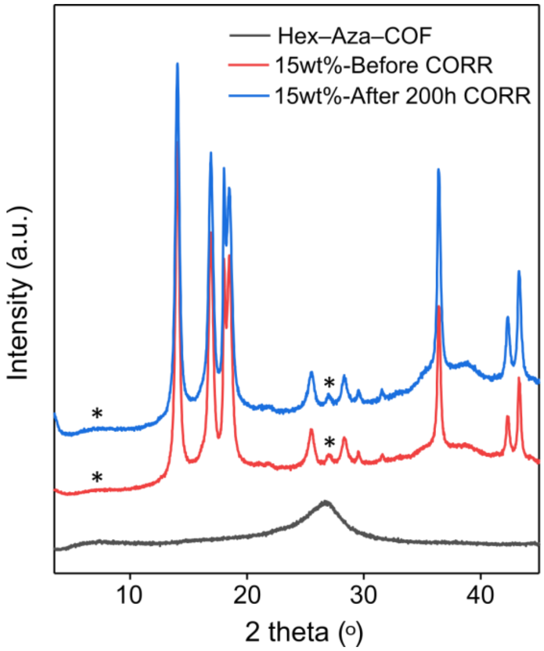

Supplementary Fig. 49 | Powder X-Ray diffraction (PXRD) patterns of the bare COF (Hex-Aza-COF), the CCBH catalyst with 15 wt% COF loading before and after 200 h of continuous CORR in anion exchange membrane (AEM) based membrane electrode assembly (MEA) using 1 M KOH as anolyte at 240 mA cm^{-2}. Peaks corresponding to COFs are marked as *.

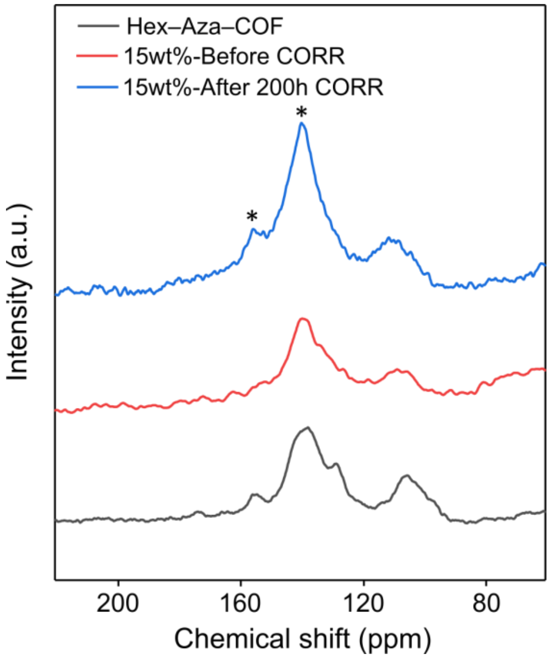

Supplementary Fig. 50 | Carbon-13 nuclear magnetic resonance (^{13}C-NMR) spectroscopy measurements for the bare COF (Hex-Aza-COF), the CCBH catalyst with 15 wt% COF loading before and after 200 h of continuous CORR in anion exchange membrane (AEM) based membrane electrode assembly (MEA) using 1 M KOH as anolyte at 240 mA cm^{-2}. Peaks corresponding to −C=N− carbons marked as *.

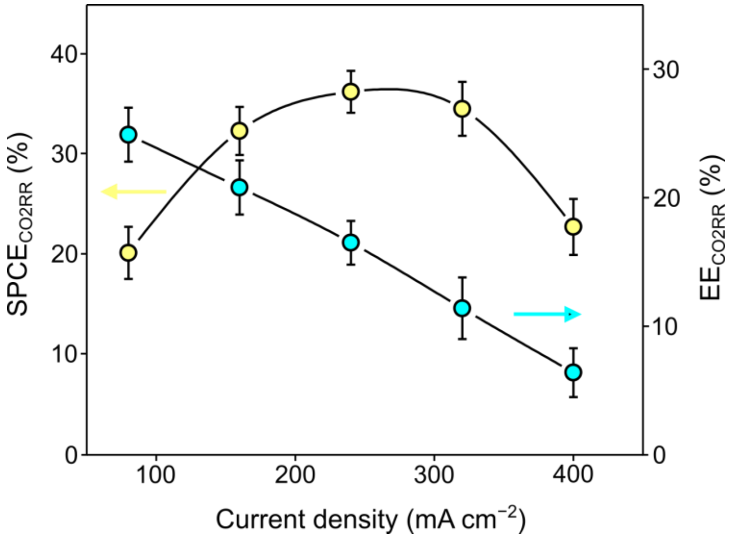

Supplementary Fig. 51 | CO$_2$RR single-pass carbon efficiency (SPCE) versus energy efficiency (EE) performance of bare Cu NPs in an anion exchange membrane (MEA) based membrane electrode assembly (MEA) using 0.1 M KHCO$_3$ as anolyte. Operating conditions: anolyte flow rate 20 mL min^{-1}; CO$_2$ inlet flow rate: ~1 sccm cm^{-2}; and cell temperature and pressure: atmospheric conditions. Error bars represent the standard deviation of three independent measurements. Data are presented as mean values ± standard deviation.

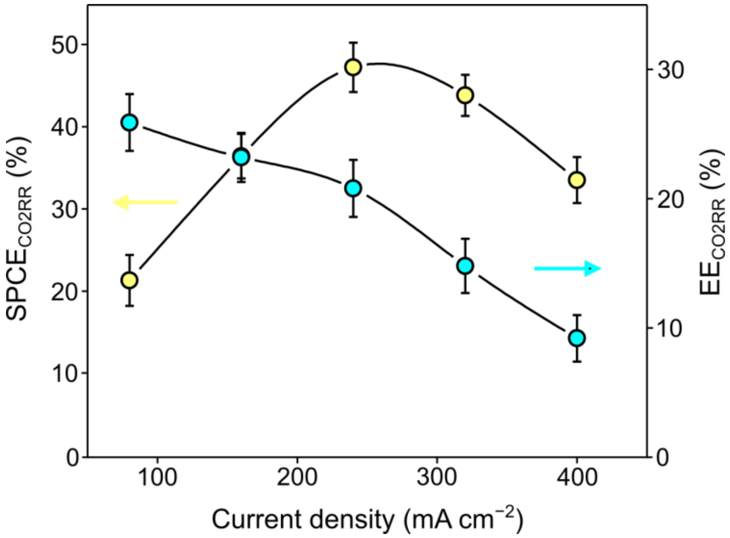

Supplementary Fig. 52 | CO_2RR single-pass carbon efficiency (SPCE) versus energy efficiency (EE) performance of the CCBH catalyst with 15 wt% COF loading in an anion exchange membrane (AEM) based membrane electrode assembly (MEA) using 0.1 M $KHCO_3$ as anolyte. Operating conditions: anolyte flow rate 20 mL min^{-1}; CO_2 inlet flow rate: ~1 sccm cm^{-2}; and cell temperature and pressure: atmospheric conditions. Error bars represent the standard deviation of three independent measurements. Data are presented as mean values ± standard deviation.

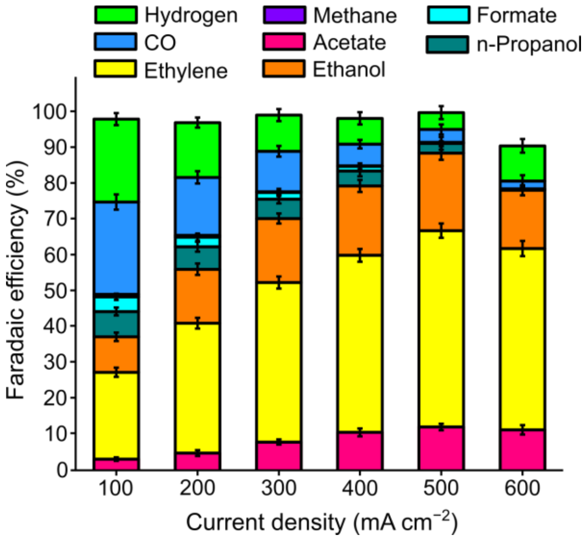

Supplementary Fig. 53 | CO$_2$RR Faradaic efficiency versus current density performance of CCBH catalyst with 15 wt% COF loading in an anion exchange membrane (AEM) based membrane electrode assembly (MEA) using 0.1 M KHCO$_3$ as anolyte. Operating conditions: anolyte flow rate 20 mL min^{-1}; CO$_2$ flow rate: ~10 sccm cm^{-2}; and cell temperature and pressure: atmospheric conditions. Error bars represent the standard deviation of three independent measurements. Data are presented as mean values ± standard deviation.

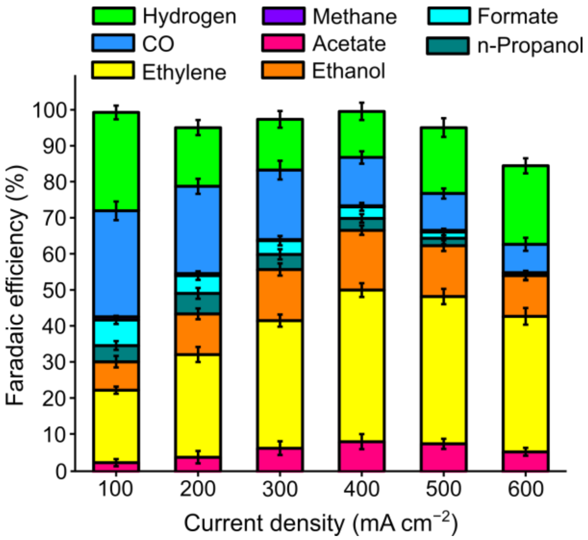

Supplementary Fig. 54 | CO_2RR Faradaic efficiency versus current density performance of bare Cu NPs in an anion exchange membrane (AEM) based membrane electrode assembly (MEA) using 0.1 M $KHCO_3$ as anolyte. Operating conditions: anolyte flow rate 20 mL min^{-1}; CO_2 flow rate: ~10 sccm cm^{-2}; and cell temperature and pressure: atmospheric conditions. Error bars represent the standard deviation of three independent measurements. Data are presented as mean values ± standard deviation.

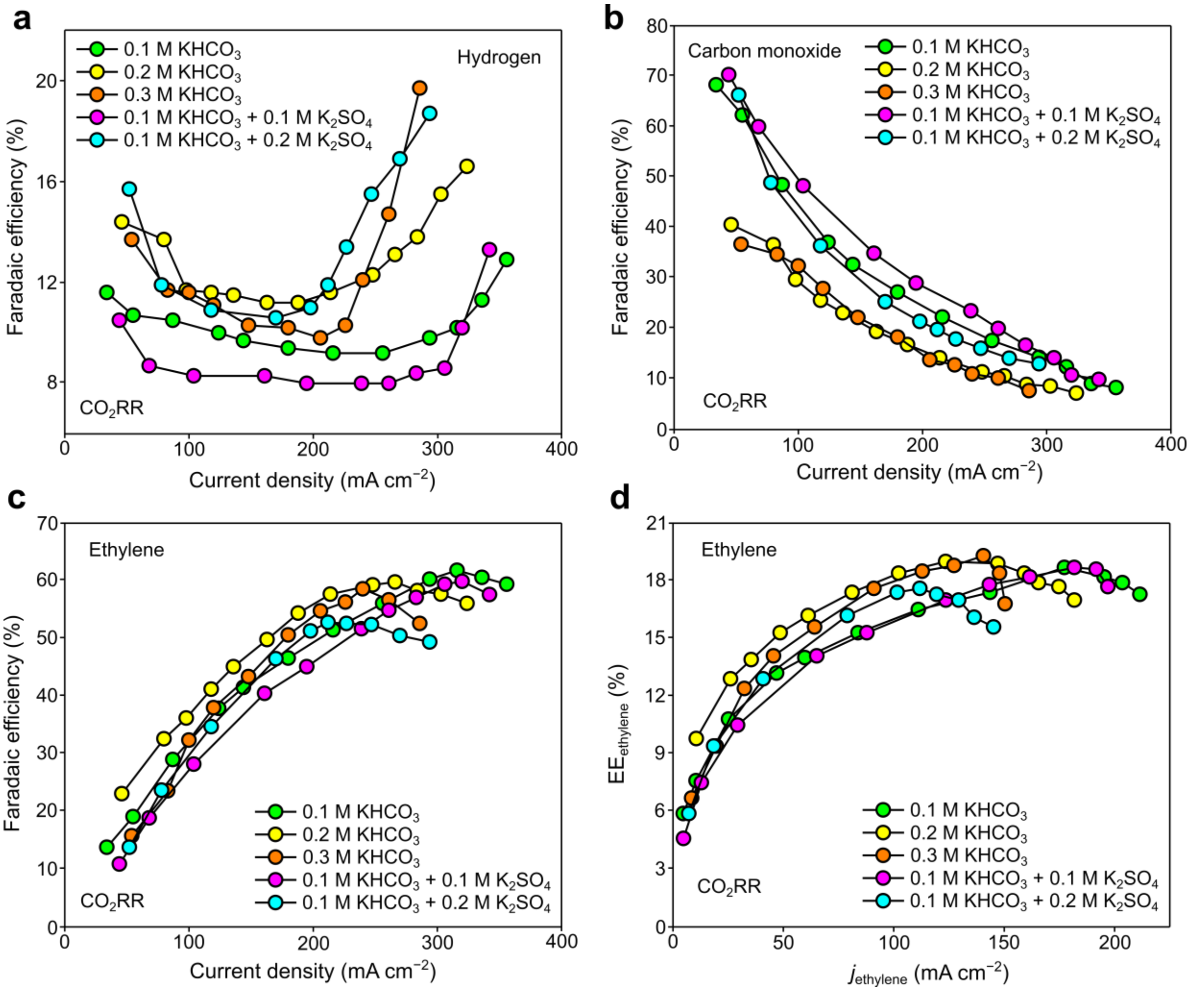

Supplementary Fig. 55 | CO_2RR performance of Cu NPs supported on a Cu/PTFE substrate in an anion exchange membrane (AEM) based membrane electrode assembly (MEA) using anolytes of various K^+ concentrations at similar pHs (0.1 M $KHCO_3$ (pH 8.4), 0.2 M $KHCO_3$ (pH 8.4), 0.3 M $KHCO_3$ (pH 8.4), 0.1 M $KHCO_3$ + 0.1 M K_2SO_4 (pH 8.4), 0.1 M $KHCO_3$ + 0.2 M K_2SO_4 (pH 8.4)). a, Hydrogen Faradaic efficiency versus current density. **b,** Carbon monoxide Faradaic efficiency versus current density. **c,** Ethylene Faradaic efficiency versus current density. **d,** Ethylene energy efficiency versus CORR partial current density. Operating conditions: anolyte flow rate 20 mL min^{-1}; CO_2 flow rate: ~10 sccm cm^{-2}; and cell temperature and pressure: atmospheric conditions.

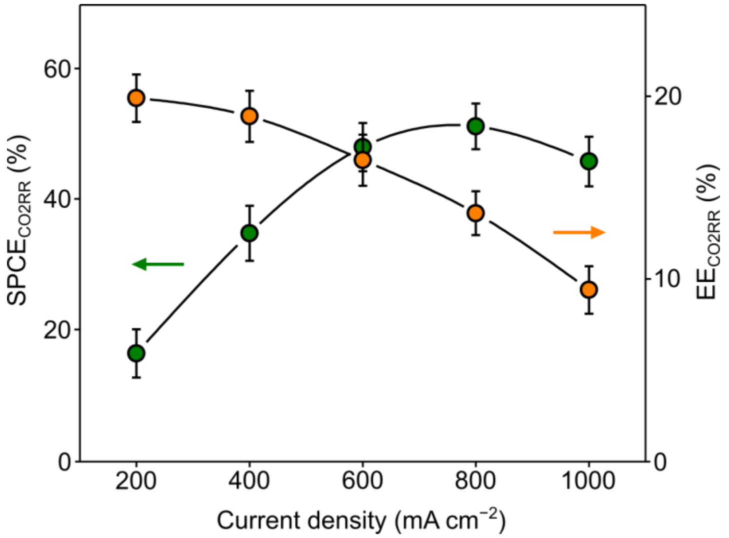

Supplementary Fig. 56 | CO_2RR single-pass carbon efficiency (SPCE) and energy efficiency (EE) versus current density performance of bare Cu NPs supported onto Cu/PTFE in a liquid-electrode flow cell using 1 M H_3PO_4 + 1 M KCl (pH ~0.8) electrolytes under low CO_2 input flow rate. Operating conditions: anolyte flow rate 20 mL min^{-1}; CO_2 inlet flow rate: ~3.6 sccm cm^{-2}; and cell temperature and pressure: atmospheric conditions. Error bars represent the standard deviation of three independent measurements. Data are presented as mean values ± standard deviation.

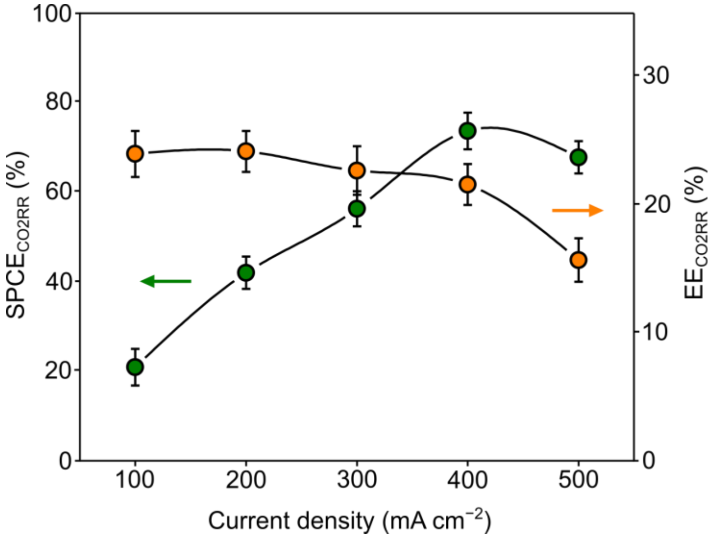

Supplementary Fig. 57 | CO_2RR single-pass carbon efficiency (SPCE) and energy efficiency (EE) versus current density performance of the CCBH catalyst with 15 wt% COF loading in a liquid-electrode flow cell using 1 M H_3PO_4 + 1 M KCl (pH ~0.8) electrolytes under low CO_2 input flow rate. Operating conditions: anolyte flow rate 20 mL min^{-1}; CO_2 inlet flow rate: ~1 sccm cm^{-2}; and cell temperature and pressure: atmospheric conditions. Error bars represent the standard deviation of three independent measurements. Data are presented as mean values ± standard deviation.

Supplementary Table 1 | Summary of input performance metrics and energy breakdown to achieve a target energy intensity of 80 GJ ton^{-1} in electrosynthesis of ethylene in the idealized case of 100% FE in the CO-to-ethylene conversion (represented by Case 1 dashed line in Supplementary Fig. 1).

$\text{SPCE}_{\text{ethylene}}$ (%)	$\text{EE}_{\text{ethylene}}$ (%)	$\text{FE}_{\text{ethylene}}$ (%)	Cell potential (V)	CO_2-to-CO conversion in SOEC (GJ ton^{-1})	Electrolyzer electricity (GJ ton^{-1})	Cathode separation (GJ ton^{-1})	Total energy (GJ ton^{-1})
4.9	100	100	1.05	20	28.94	31.3	80.62
5.1	95.0	100	1.1	20	30.32	30.04	80.5
5.4	90.5	100	1.16	20	31.97	28.33	79.3
5.8	85.4	100	1.23	20	33.9	26.3	80.2
6	83.3	100	1.26	20	34.73	25.4	80.1
6.4	79.5	100	1.32	20	36.4	23.8	80.2
6.9	76.1	100	1.38	20	38.04	22.0	80.1
7.6	71.9	100	1.46	20	40.2	19.9	80.1
8.3	69.1	100	1.52	20	41.9	18.2	80.1
8.8	67.3	100	1.56	20	43.0	17.1	80.1
9.3	66.03	100	1.59	20	43.8	16.1	80.03
9.7	64.8	100	1.62	20	44.7	15.4	80.2
11.1	62.1	100	1.69	20	46.6	13.4	80.0
12.3	60.3	100	1.74	20	47.97	12.0	80.0
14.1	58.4	100	1.8	20	49.61	10.36	80.0
15.6	57.1	100	1.84	20	50.72	9.3	80.0
16.6	56.5	100	1.86	20	51.3	8.7	80.0
17.1	56.1	100	1.87	20	51.6	8.4	80.0
18.2	55.6	100	1.89	20	52.1	7.9	80.0
19.9	54.7	100	1.92	20	52.9	7.1	80.0
21.6	54.1	100	1.94	20	53.5	6.5	80.0
23.2	53.6	100	1.96	20	54.0	6.0	80.0
24.2	53.3	100	1.97	20	54.3	5.7	80.0
25.2	53.0	100	1.98	20	54.6	5.4	80.0
27.8	52.8	100	2.00	20	55.1	4.9	80.0
30.7	51.9	100	2.02	20	55.7	4.3	80.0
32.7	51.7	100	2.03	20	56.0	4.0	80.0
34.7	51.5	100	2.04	20	56.2	3.7	80.0
36.8	51.2	100	2.05	20	56.5	3.5	80.0
39.2	50.9	100	2.06	20	56.8	3.2	80.0
42.5	50.7	100	2.07	20	57.1	2.9	80.0
45.5	50.5	100	2.08	20	57.3	2.7	80.0
49.7	50.2	100	2.09	20	57.6	2.4	80.0
54.5	50.0	100	2.10	20	57.9	2.1	80.0
59.8	49.8	100	2.11	20	58.2	1.8	80.0
66.8	49.5	100	2.12	20	58.4	1.6	80.0
71.3	49.4	100	2.125	20	58.6	1.4	80.0
76.1	49.3	100	2.13	20	58.7	1.3	80.0
81.6	49.2	100	2.135	20	58.85	1.14	80.0
87.5	49.1	100	2.14	20	59.0	1.0	80.0
94.8	48.95	100	2.145	20	59.13	0.87	80.0
99.9	48.8	100	2.15	20	59.7	0.3	80.0

Notes: Energy assessment was performed by using a techno-economic (TEA) model as well as assumptions similar to those reported in refs. [1,2]. The energy intensity of 80 GJ ton^{-1} corresponds to a total process efficiency of ~55% and a lower heating value of ethylene (45 GJ ton^{-1}). A constant energy intensity of 20 GJ ton^{-1} for electrosynthesis of CO from CO_2 in a SOEC was considered. Energy intensities given for SOEC (CO_2-to-CO conversion) are given for 2 tons of CO produced, which is the amount required to produce 1 ton of ethylene. A constant operating current density of 200 mA cm^{-2} and a constant ethylene FE of 100% were considered. Highly optimistic $EE_{ethylene}$ values in Supplementary Fig. 1 were modeled by inputting cell potentials closer to theoretical values. The dashed line (Case 1) represents the $EE_{ethylene}$ and $SPCE_{ethylene}$ combinations presented in this table.

Supplementary Table 2 | Summary of input performance metrics and energy breakdown to achieve a target energy intensity of 80 GJ ton^{-1} in electrosynthesis of ethylene in the idealized case of 100% FE in the CO-to-ethylene conversion (represented by Case 2 dashed line in Supplementary Fig. 1).

$\mathrm{SPCE}_{\mathrm{ethylene}}$ (%)	$\mathrm{EE}_{\mathrm{ethylene}}$ (%)	$\mathrm{FE}_{\mathrm{ethylene}}$ (%)	Cell potential (V)	CO_2-to-CO conversion in SOEC (GJ ton^{-1})	Electrolyzer electricity (GJ ton^{-1})	Cathode separation (GJ ton^{-1})	Total energy (GJ ton^{-1})
7	100	100	1.05	30	28.94	21.67	80.62
7.5	95.0	100	1.1	30	30.32	27.8	80.5
8.7	90.5	100	1.16	30	31.97	17.29	79.3
9.2	85.4	100	1.23	30	33.9	16.3	80.2
10	83.3	100	1.26	30	34.93	14.94	79.7
11	79.5	100	1.32	30	36.4	13.5	79.9
12.5	76.1	100	1.38	30	38.04	11.8	79.8
15.0	71.9	100	1.46	30	40.2	9.7	79.9
17.5	69.1	100	1.52	30	41.9	8.2	80.1
20	67.3	100	1.56	30	43.0	7.1	80.1
22.5	66.03	100	1.59	30	43.8	6.2	80.03
25	64.8	100	1.62	30	44.65	5.5	80.2
30	63.3	100	1.66	30	45.7	4.5	80.2
35	62.1	100	1.69	30	46.6	3.7	80.2
40	61.4	100	1.71	30	47.1	3.1	80.2
45	60.6	100	1.73	30	47.7	2.7	80.4
50	60.3	100	1.74	30	47.97	2.4	80.3
55	60.0	100	1.75	30	48.2	2.1	80.3
60	59.7	100	1.76	30	48.5	1.8	80.3
65	59.3	100	1.77	30	48.8	1.6	80.4
70	59.2	100	1.775	30	48.9	1.45	80.4
75	58.99	100	1.78	30	49.1	1.3	80.4
80	58.82	100	1.785	30	49.2	1.18	80.4
85	58.7	100	1.79	30	49.3	1.06	80.4
90	58.5	100	1.795	30	49.48	0.96	80.4
95	58.4	100	1.8	30	49.61	0.58	80.2
100	58.2	100	1.805	30	50.1	0.0	80.1

Notes: Energy assessment was performed by using a techno-economic (TEA) model as well as assumptions similar to those reported in refs [1,2]. The energy intensity of 80 GJ ton^{-1} corresponds to a total process efficiency of ~55% and a lower heating value of ethylene (45 GJ ton^{-1}). A constant energy intensity of 30 GJ ton^{-1} for electrosynthesis of CO from CO_2 in a SOEC was considered. Energy intensities given for SOEC (CO_2-to-CO conversion) are given for 2 tons of CO produced, which is the amount required to produce 1 ton of ethylene. A constant operating current density of 200 mA cm^{-2} and a constant ethylene FE of 100% were considered. Highly optimistic $\mathrm{EE}_{\mathrm{ethylene}}$ values ($\mathrm{EE}_{\mathrm{ethylene}}$ of >90%) in Supplementary Fig. 1 were modeled by inputting cell potentials closer to theoretical values. The dashed line (Case 2) represents the $\mathrm{EE}_{\mathrm{ethylene}}$ and $\mathrm{SPCE}_{\mathrm{ethylene}}$ combinations presented in this table.

Supplementary Table 3 | Summary of input performance metrics and energy breakdown to achieve a target energy intensity of 80 GJ ton^{-1} in electrosynthesis of ethylene in the idealized case of 100% FE in the CO-to-ethylene conversion (represented by Case 3 dashed line in Supplementary Fig. 1).

SPCE$_{ethylene}$ (%)	**EE$_{ethylene}$ (%)**	**FE$_{ethylene}$ (%)**	**Cell potential (V)**	**CO_2-to-CO conversion in SOEC (GJ ton^{-1})**	**Electrolyzer electricity (GJ ton^{-1})**	**Cathode separation (GJ ton^{-1})**	**Total energy (GJ ton^{-1})**
13.15	100	100	1.05	40	28.94	11.17	80.11
15.20	95.0	100	1.1	40	30.32	9.72	80.04
17.75	90.5	100	1.16	40	31.97	8.07	80.04
20.0	85.4	100	1.23	40	33.9	7.07	79.97
26.0	83.3	100	1.26	40	34.73	5.26	79.99
29.0	79.5	100	1.32	40	36.4	3.76	80.16
44.0	78.5	100	1.35	40	37.21	2.78	79.99
52.0	77.3	100	1.37	40	37.77	2.23	80.0
70.0	75.7	100	1.40	40	38.59	1.46	80.05
81.0	75.17	100	1.41	40	38.87	1.15	80.02
95.0	74.6	100	1.42	40	39.15	0.87	80.02
98.0	74.4	100	1.425	40	39.28	0.81	80.09

Notes: Energy assessment was performed by using a techno-economic (TEA) model as well as assumptions similar to those reported in refs. [1,2]. The energy intensity of 80 GJ ton^{-1} corresponds to a total process efficiency of ~55% and a lower heating value of ethylene (45 GJ ton^{-1}). A constant energy intensity of 30 GJ ton^{-1} for electrosynthesis of CO from CO_2 in a SOEC was considered. Energy intensities given for SOEC (CO_2-to-CO conversion) are given for 2 tons of CO produced, which is the amount required to produce 1 ton of ethylene. A constant operating current density of 200 mA cm^{-2} and a constant ethylene FE of 100% were considered. Highly optimistic EE$_{ethylene}$ values in Supplementary Fig. 1 were modeled by inputting cell potentials closer to theoretical values. The dashed line (Case 3) represents the EE$_{ethylene}$ and SPCE$_{ethylene}$ combinations presented in this table.

CORR performance of the Cu/PTFE substrate in an anion exchange membrane based membrane electrode assembly (MEA) using anolytes of various pHs. Operating conditions: anolyte flow rate: 20 mL min^{-1}; CO flow rate: ~1 sccm cm^{-2}; and cell temperature and pressure: atmospheric conditions. Error bars represent the standard deviation of three independent measurements.

Supplementary Table 4 | 0.1 M $KHCO_3$ (pH 8.4).

Full cell potential (V)	**Current density (mA cm^{-2})**	**Faradaic efficiency (%)**					**J_{C2+} (mA cm^{-2})**	**$SPCE_{CO\text{-}to\text{-}C2+}$ (%)**	**EE_{C2+} (%)**
		Acetate	**C_2H_4**	**EtOH**	**n-PrOH**	**H_2**			
2.3	12	2.8	18.9	6.1	6.4	62.7	4.1	1.6	15.3
2.5	40	3.9	25.2	8.3	7.5	48.4	18.0	7.3	18.5
2.7	70	4.7	29.1	8.9	6.8	42.1	34.7	14.2	18.8
2.9	115	5.6	29.8	8.3	6.2	40.5	57.4	23.9	17.6
3.1	180	4.7	25.1	6.5	4.4	49.4	73.3	30.6	13.4

Supplementary Table 5 | 0.1 M KOH (pH 13).

Full cell potential (V)	**Current density (mA cm^{-2})**	**Faradaic efficiency (%)**					**J_{C2+} (mA cm^{-2})**	**$SPCE_{CO\text{-}to\text{-}C2+}$ (%)**	**EE_{C2+} (%)**
		Acetate	**C_2H_4**	**EtOH**	**n-PrOH**	**H_2**			
1.9	13	4.1	22.3	7.1	7.7	56.9	5.4	2.2	22.2
2.1	28	4.5	28.7	8.2	7.9	47.3	13.8	5.6	24.1
2.3	45	4.8	31.8	9.1	7.4	40.2	23.9	9.7	23.7
2.5	85	6.1	32.4	8.6	7.2	37.8	46.2	19.2	22.2
2.8	140	5.8	27.3	6.7	5.9	47.9	64.0	27.0	16.7

Supplementary Table 6 | 1 M KOH (pH 13.9).

Full cell potential (V)	**Current density (mA cm^{-2})**	**Faradaic efficiency (%)**					**J_{C2+} (mA cm^{-2})**	**$SPCE_{CO\text{-}to\text{-}C2+}$ (%)**	**EE_{C2+} (%)**
		Acetate	**C_2H_4**	**EtOH**	**n-PrOH**	**H_2**			
1.9	18	6.2	30.1	9.4	7.9	44.3	9.6	4.0	28.8
2.0	26	7.2	34.1	10.8	8.2	36.8	15.7	6.6	30.8
2.1	45	7.5	36.3	9.6	7.9	33.9	27.6	11.6	29.8
2.2	60	7.7	36.7	8.4	7.1	34.3	35.9	15.2	27.7
2.3	80	7.4	33.5	6.9	6.4	39.7	43.4	18.5	24.0
2.4	115	6.9	29.8	5.7	5.2	46.1	54.7	23.5	20.1

Supplementary Table 7 | 3 M KOH (pH 14.4).

Full cell potential (V)	Current density (mA cm^{-2})	Faradaic efficiency (%)					J_{C2+} (mA cm^{-2})	$SPCE_{CO-to-C2+}$ (%)	EE_{C2+} (%)
		Acetate	C_2H_4	EtOH	n-PrOH	H_2			
1.9	20	7.3	35.4	8.2	6.4	41.6	11.5	4.8	30.7
2.0	33	7.6	36.8	9.1	7.1	36.4	20.0	8.4	30.9
2.1	50	8.3	33.2	7.3	5.5	41.9	27.2	11.7	26.2
2.2	68	7.4	30.1	6.2	4.4	47.7	32.7	14.2	22.1
2.3	85	6.3	26.2	5.6	3.5	55.3	35.4	15.3	18.4

Supplementary Table 8 | 5 M KOH (pH 14.7).

Full cell potential (V)	Current density (mA cm^{-2})	Faradaic efficiency (%)					J_{C2+} (mA cm^{-2})	$SPCE_{CO-to-C2+}$ (%)	EE_{C2+} (%)
		Acetate	C_2H_4	EtOH	n-PrOH	H_2			
1.9	23	6.2	36.7	7.6	6.1	40.8	13.0	5.4	30.5
2.0	35	5.9	34.3	6.5	4.9	44.7	18.1	7.6	26.4
2.1	55	5.1	27.9	5.2	4.1	53.6	23.3	9.8	20.6
2.2	75	3.5	14.4	3.1	2.3	69.1	17.5	7.5	10.7

CORR performance of the Cu/PTFE catalyst in an anion exchange membrane based membrane electrode assembly (MEA) under low CO input flow rates at a constant current density of 50 mA cm^{-2} using various anolyte concentrations. Operating conditions: anolyte flow rate: 20 mL min^{-1}; cell temperature and pressure: atmospheric conditions.

Supplementary Table 9 | 1 M KOH (pH 13.9).

CO input flow rate (sccm cm^{-2})	**Current density (mA cm^{-2})**	**Faradaic efficiency (%)**					**J_{C2+} (mA cm^{-2})**	**$CE_{CO\text{-}to\text{-}C2+}$ (%)**	**EE_{C2+} (%)**
		Acetate	**C_2H_4**	**EtOH**	**n-PrOH**	**H_2**			
2.10	50	7.8	40.2	15.8	11.2	24.3	37.5	7.1	36.6
1.20	50	7.2	39.4	13.7	10.3	28.1	35.3	11.4	34.3
0.65	50	6.9	37.9	11.8	9.1	32.9	32.9	16.6	32.0
0.38	50	5.7	32.8	8.7	6.9	41.8	27.1	26.5	26.4
0.16	50	3.9	18.1	5.2	3.1	65.6	15.2	42.2	14.7

Note: An average full cell potential of ~2.1 V was maintained at a constant current density of 50 mA cm^{-2}.

Supplementary Table 10 | 3 M KOH (pH 14.4).

CO input flow rate (sccm cm^{-2})	**Current density (mA cm^{-2})**	**Faradaic efficiency (%)**					**J_{C2+} (mA cm^{-2})**	**$CE_{CO\text{-}to\text{-}C2+}$ (%)**	**EE_{C2+} (%)**
		Acetate	**C_2H_4**	**EtOH**	**n-PrOH**	**H_2**			
2.10	50	9.1	41.2	11.2	8.5	28.8	35.0	7.0	34.4
1.20	50	8.7	35.1	8.6	5.9	39.9	29.2	9.0	28.5
0.65	50	6.1	25.9	7.1	4.1	53.6	21.6	16.6	21.2
0.38	50	4.7	18.8	5.9	2.9	65.1	16.2	24.3	15.8
0.16	50	2.6	11.7	4.1	1.9	81.2	10.2	27.2	10.0

Note: An average full cell potential of ~2.07 V was maintained at a constant current density of 50 mA cm^{-2}.

Supplementary Table 11 | 5 M KOH (pH 14.7).

CO input flow rate (sccm cm^{-2})	**Current density (mA cm^{-2})**	**Faradaic efficiency (%)**					**J_{C2+} (mA cm^{-2})**	**$CE_{CO\text{-}to\text{-}C2+}$ (%)**	**EE_{C2+} (%)**
		Acetate	**C_2H_4**	**EtOH**	**n-PrOH**	**H_2**			
2.10	50	8.2	35.3	8.3	6.8	38.2	29.3	6.0	29.2
1.20	50	6.3	28.2	6.4	4.6	51.2	22.8	8.0	22.7
0.65	50	4.6	20.6	4.8	2.9	64.1	16.5	11.2	16.4
0.38	50	2.8	12.4	3.3	2.2	76.8	10.4	16.8	10.3
0.16	50	1.9	7.8	2.4	1.5	86.3	6.8	17.7	6.8

Note: An average full cell potential of ~2.04 V was maintained at a constant current density of 50 mA cm^{-2}.

Supplementary Table 12 | 1 M KOH + 2 M K_2CO_3 (pH 13.9).

CO input flow rate (sccm cm^{-2})	Current density (mA cm^{-2})	Faradaic efficiency (%)					J_{C2+} (mA cm^{-2})	$CE_{CO\text{-}to\text{-}C2+}$ (%)	EE_{C2+} (%)
		Acetate	C_2H_4	EtOH	n-PrOH	H_2			
2.10	50	5.5	35.6	11.6	8.6	35.9	30.7	5.8	30.2
1.20	50	6.2	35.3	11.2	8.2	37.6	30.4	10.1	29.9
0.65	50	5.1	33.4	9.9	7.6	41.1	28.0	13.2	27.6
0.38	50	4.3	29.3	7.8	5.7	41.8	27.1	21.1	23.3
0.16	50	3.1	14.1	3.5	1.9	71.6	11.3	29.1	11.1

Note: An average full cell potential of ~2.07 V was maintained at a constant current density of 50 mA cm^{-2}.

Supplementary Table 13 | 5 M KOH + 2 M K_2CO_3 (pH 14.7).

CO input flow rate (sccm cm^{-2})	Current density (mA cm^{-2})	Faradaic efficiency (%)					J_{C2+} (mA cm^{-2})	$CE_{CO\text{-}to\text{-}C2+}$ (%)	EE_{C2+} (%)
		Acetate	C_2H_4	EtOH	n-PrOH	H_2			
2.10	50	6.4	26.3	5.8	5.1	50.3	21.8	4.4	21.5
1.20	50	5.1	22.2	4.9	4.2	57.9	18.2	6.4	18.0
0.65	50	3.9	17.3	4.2	2.3	69.6	13.9	9.1	13.7
0.38	50	2.7	10.1	2.3	1.9	82.4	8.5	10.8	8.3
0.16	50	1.4	5.2	1.7	1.3	89.4	4.8	12.0	4.7

Note: An average full cell potential of ~2.06 V was maintained at a constant current density of 50 mA cm^{-2}.

Supplementary Table 14 | Summary of ICP-OES results.

Sample	Element	Calculated concentration (mg L^{-1})
1 M pure KOH (99.99%)	Fe	0.012
	Ni	0.026
1 M KOH after 25-h CORR on Cu	Fe	0.008
	Ni	0.028
1 M KOH after 25-h CORR on CCBH catalyst	Fe	0.010
	Ni	0.028
The Cu catalyst after 25-h CORR	Cu	138.6
	Fe	0
	Ni	0
The CCBH catalyst after 25-h CORR	Cu	169.7
	Fe	0
	Ni	0

Supplementary Table 15 | The difference of reaction free energies from CO to OCCOH and CHO. A lower value indicates a more favorable conversion from CO to OCCOH, promoting C_{2+} products.

ΔG (eV)	**0 K (in the 18 H_2O)**	**1 K (in the 18 H_2O)**	**2 K (in the 18 H_2O)**	**3 K (in the 18 H_2O)**
0 OH* (on the 9 Cu sites)	0.54	−0.05	0.47	0.46
1 OH* (on the 9 Cu sites)	0.43	−0.12	−0.01	0.04
2 OH* (on the 9 Cu sites)	0.15	0.09	−0.08	0.02

Supplementary Table 16 | The free energy corrections *G* for various adsorbed species.

Species	ZPE (eV)	$\int \mathrm{CpdT}$	−T.S (eV)	G – E (eV)
0 OH* (on the 9 Cu sites)	0.54	−0.05	0.47	0.46
1 OH* (on the 9 Cu sites)	0.43	−0.12	−0.01	0.04
2 OH* (on the 9 Cu sites)	0.15	0.09	−0.08	0.02

Supplementary Table 17 | The difference of adsorption energies of CO* and H*. A lower value indicates a more favorable CO* over H*, promoting CO reduction over hydrogen evolution reaction.

ΔG (eV)	**0 K (in the 18 H_2O)**	**1 K (in the 18 H_2O)**	**2 K (in the 18 H_2O)**	**3 K (in the 18 H_2O)**
0 OH* (on the 9 Cu sites)	0.30	−0.24	−0.05	−0.09
1 OH* (on the 9 Cu sites)	0.06	−0.38	−0.22	−0.18
2 OH* (on the 9 Cu sites)	0.13	−0.08	0.05	0.02

Supplementary Table 18 | Capacitance values and surface roughness factors obtained on CCBH catalysts with various COF mass loadings, bare Cu NPs, Cu NPs with 25% PTFE loading, and Cu foil. Error bars represent the standard deviation of three independent measurements.

Electrode	**Capacitance**	**Surface roughness factor**
Cu foil	29 µF	1
Cu nanoparticles	1.24±0.14 mF	43±5
Cu nanoparticles/5 wt% Hex–Aza–COF	0.78±0.20 mF	27±7
Cu nanoparticles/15 wt% Hex–Aza–COF	0.22±0.09 mF	8±3
Cu nanoparticles/25 wt% Hex–Aza–COF	0.17±0.03 mF	6±1
Cu nanoparticles/25 wt% PTFE	0.51±0.09 mF	18±3

The surface roughness factor for Cu foil is defined as 1 in ref. [9].

CORR performance in an anion exchange membrane based membrane electrode assembly (MEA) using 1 M KOH as analyte under low CO input flow rate.

Supplementary Table 19 | Bare Cu NPs.

Full cell potential (V)	**Current density (mA cm^{-2})**	**Faradaic efficiency (%)**					**J_{C2+} (mA cm^{-2})**	**SPCE$_{CO\text{-}to\text{-}C2+}$ (%)**	**EE$_{C2+}$ (%)**
		Acetate	**EtOH**	**n-PrOH**	**C_2H_4**	**H_2**			
1.79	80	6.7	13.2	16.3	36.5	22.7	58±3.2	23.9±4.6	41.7±1.5
2.04	160	7.8	12.8	14.2	37.3	24.9	115±6.5	48.3±4.7	36.1±1.8
2.26	240	7.1	11.1	9.9	28.9	36.1	137±7.1	58.4±5.1	25.7±1.7
2.41	320	5.4	8.2	4.8	20.3	50.5	124±6.7	53.9±4.4	16.3±1.9
2.53	400	3.7	6.9	2.2	14.4	62.8	109±6.2	47.5±4.1	10.9± 1.6

Operating conditions: anolyte flow rate: 20 mL min^{-1}; average CO inlet flow rate: ~1 sccm cm^{-2}; and cell temperature and pressure: atmospheric conditions. Error bars represent the standard deviation of three independent measurements.

Supplementary Table 20 | CCBH catalyst with 15 wt% COF loading.

Full cell potential (V)	**Current density (mA cm^{-2})**	**Faradaic efficiency (%)**					**J_{C2+} (mA cm^{-2})**	**SPCE$_{CO\text{-}to\text{-}C2+}$ (%)**	**EE$_{C2+}$ (%)**
		Acetate	**EtOH**	**n-PrOH**	**C_2H_4**	**H_2**			
1.74	80	7.8	15.9	19.6	43.8	9.1	70±3.6	30.5±4.8	51.4±1.8
2.01	160	9.0	19.1	19.2	45.3	6.9	148±5.2	65.5±4.5	47.2±1.6
2.23	240	9.7	19.4	12.7	45.5	12.1	210±7.1	94.6±4.1	40.4±1.7
2.37	320	7.1	14.2	7.8	33.9	29.8	202±7.9	91.4±3.9	27.4±1.8
2.49	400	4.9	10.3	5.2	25.8	44.2	185±8.4	83.4±3.4	19.2±1.6

Operating conditions: anolyte flow rate: 20 mL min^{-1}; average CO inlet flow rate: ~1 sccm cm^{-2}; and cell temperature and pressure: atmospheric conditions. Error bars represent the standard deviation of three independent measurements.

Supplementary Table 21 | Comparison of performance metrics of the highest performing CCBH catalyst (CCBH catalyst with 15 wt% COF loading) with those of literature benchmark CO_2RR/CORR systems.

Catalyst	**Feedstock**	**FE$_{C2+}$ (%)**	**j_{C2+} (mA cm^{-2})**	**Stability (h)**	**SPCE$_{C2+}$ (%)**	**Full cell EE$_{C2+}$**	**References**
Graphite/Carbon/Cu/PTFE	CO_2	71	78	1	**0.3**	**34**	10
F–Cu	CO_2	77	102	–	**0.5**	**37**	11
Cu/PTFE	CO_2	33	33	–	**43.2**	**10.1**	12
Cu/PFSA	CO_2	48	576	–	**29**	**13.1**	13
Cu:Py:SSC	CO	76	91	40	**32.2**	**32.2**	1
OD–Cu/GDE	CO	83	415	1	**19.2**	**25.5**	14
Cu/GDE	CO	72	104	24	**66**	**24**	15
Cu	CO	87	367	–	**65.5**	**47**	**This work**
CCBH	CO	87	210	200	**94.6**	**41**	**This work**

Supplementary Table 22 | CORR performance of CCBH catalyst with 15 wt% COF loading in an anion exchange membrane based membrane electrode assembly (MEA) using 1 M KOH as anolyte.

Full cell potential (V)	Current density (mA cm^{-2})	Faradaic efficiency (%)					J_{C2+} (mA cm^{-2})	EE$_{C2H4}$ (%)	EE$_{C2+}$ (%)
		Acetate	EtOH	n-PrOH	C_2H_4	H_2			
1.78	100	9.9	17.3	23.1	37.8	13.5	88±4.6	22.5±1.0	50.4±1.7
2.03	200	11.8	19.4	21.6	40.3	8.7	186±7.9	21.0±1.2	46.6±1.6
2.24	300	12.9	21.8	15.7	43.2	6.7	281±10.4	20.4±1.3	42.4±1.5
2.39	400	14.5	21.4	11.3	46.9	5.2	376±12.9	20.8±1.4	39.8±1.8
2.51	500	15.0	19.3	8.6	48.8	5.9	459±14.2	20.6±1.3	34.1±1.7
2.61	600	16.3	18.0	7.9	47.0	8.9	535±16.4	19.1±1.2	34.3±1.5
2.69	700	17.1	16.3	6.2	45.8	12.3	598±21.3	18.1±1.0	31.7±1.6

Operating conditions: anolyte flow rate: 20 mL min^{-1}; CO flow rate: ~10 sccm cm^{-2}; and cell temperature and pressure: atmospheric conditions. Error bars represent the standard deviation of three independent measurements.

CORR performance of CCBH catalyst with various COF mass loadings in an anion exchange membrane based membrane electrode assembly (MEA) using 1 M KOH as anolyte. Operating conditions: anolyte flow rate: 20 mL min^{-1}; CO flow rate: ~10 sccm cm^{-2}; and cell temperature and pressure: atmospheric conditions. Error bars represent the standard deviation of three independent measurements.

Supplementary Table 23 | CCBH catalyst 5 wt% COF loading.

Full cell potential (V)	**Current density (mA cm^{-2})**	**Faradaic efficiency (%)**			***j*$_{C2H4}$ (mA cm^{-2})**	**EE$_{C2H4}$ (%)**
		H_2	**CH_4**	**C_2H_4**		
1.85	100	18.8	0.1	35.6	36±2.9	20.4±1.3
2.11	200	15.1	0.1	38.9	78±3.9	19.5±1.2
2.29	300	13.3	0.1	41.8	125±4.6	19.3±1.0
2.42	400	11.8	0.2	43.9	176±6.1	19.2±1.1
2.53	500	12.5	0.3	45.7	229±7.3	19.1±1.2
2.63	600	16.1	0.4	41.1	247±8.2	16.6±1.3
2.72	700	20.3	0.6	37.9	265±9.4	14.8±1.2

Supplementary Table 24 | CCBH catalyst 10 wt% COF loading.

Full cell potential (V)	**Current density (mA cm^{-2})**	**Faradaic efficiency (%)**			***j*$_{C2H4}$ (mA cm^{-2})**	**EE$_{C2H4}$ (%)**
		H_2	**CH_4**	**C_2H_4**		
1.81	100	15.2	0.0	38.3	38±2.7	22.4±1.3
2.09	200	12.9	0.0	40.9	82±3.5	20.7±1.2
2.27	300	10.2	0.0	43.7	131±4.1	20.4±1.1
2.40	400	9.1	0.0	45.4	182±5.6	20.1±1.2
2.51	500	8.8	0.1	47.1	236±6.7	19.9±1.4
2.62	600	10.9	0.2	46.2	277±7.5	18.7±1.3
2.71	700	14.3	0.2	43.4	304±8.4	17.0±1.2

Supplementary Table 25 | CCBH catalyst 15 wt% COF loading.

Full cell potential (V)	**Current density (mA cm^{-2})**	**Faradaic efficiency (%)**			***j*$_{C2H4}$ (mA cm^{-2})**	**EE$_{C2H4}$ (%)**
		H_2	**CH_4**	**C_2H_4**		
1.78	100	13.5	0.0	37.8	38±1.9	22.5±1.0

2.03	200	8.7	0.0	40.3	81±3.5	21.0±1.2
2.24	300	6.7	0.0	43.2	130±3.9	20.4±1.3
2.39	400	5.2	0.1	46.9	188±4.9	20.8±1.4
2.51	500	5.9	0.2	48.8	244±7.1	20.6±1.3
2.61	600	8.9	0.2	47.0	282±8.4	19.1±1.2
2.69	700	12.3	0.3	45.8	321±9.1	18.0±1.0

Supplementary Table 26 | CCBH catalyst 20 wt% COF loading.

Full cell potential (V)	**Current density (mA cm^{-2})**	**Faradaic efficiency (%)**			**j_{C2H4} (mA cm^{-2})**	**EE_{C2H4} (%)**
		H_2	**CH_4**	**C_2H_4**		
1.82	100	19.6	0.0	39.1	39±2.1	22.8±1.2
2.13	200	16.3	0.1	41.5	83±3.7	20.7±1.1
2.29	300	13.2	0.2	43.9	132±4.8	20.3±1.3
2.43	400	14.6	0.3	41.1	164±5.9	17.9±1.2
2.56	500	17.4	0.5	38.7	194±7.3	16.0±1.3
2.67	600	21.3	0.6	37.2	223±8.9	14.8±1.3
2.77	700	25.6	0.8	34.4	241±9.8	13.2±1.3

Supplementary Table 27 | CCBH catalyst 25 wt% COF loading.

Full cell potential (V)	**Current density (mA cm^{-2})**	**Faradaic efficiency (%)**			**j_{C2H4} (mA cm^{-2})**	**EE_{C2H4} (%)**
		H_2	**CH_4**	**C_2H_4**		
1.86	100	22.6	0.1	37.2	37±2.6	21.2±1.2
2.07	200	18.1	0.1	38.8	78±3.7	19.9±1.3
2.34	300	16.2	0.2	40.1	120±4.7	18.2±1.6
2.47	400	17.3	0.2	38.3	153±6.8	16.4±1.5
2.60	500	19.8	0.3	36.5	183±8.7	14.9±1.3
2.71	600	24.6	0.5	32.6	196±9.1	12.8±1.2

CORR performance of CCBH catalyst with 15 wt% COF loading in an anion exchange membrane based membrane electrode assembly (MEA) using anolytes with various KOH concentrations. Operating conditions: anolyte flow rate: 20 mL min^{-1}; CO flow rate: ~10 sccm cm^{-2}; and cell temperature and pressure: atmospheric conditions. Error bars represent the standard deviation of three independent measurements.

Supplementary Table 28 | 0.5 M KOH (pH 13.6).

Full cell potential (V)	**Current density (mA cm^{-2})**	**Faradaic efficiency (%)**					**J_{C2+} (mA cm^{-2})**	**EE$_{C2H4}$ (%)**	**EE$_{C2+}$ (%)**
		Acetate	**EtOH**	**n-PrOH**	**C_2H_4**	**H_2**			
1.82	100	4.1	16.5	25.1	31.4	24.2	77±4.1	18.3±1.1	43.8±1.6
2.13	200	5.9	18.9	21.8	36.2	18.9	166±7.2	18.0±1.2	40.0±1.7
2.36	300	7.5	19.6	18.1	40.9	14.1	258±9.8	18.4±1.3	37.5±1.5
2.48	400	9.1	19.3	15.5	44.1	13.2	359±13.2	18.9±1.3	36.3±1.7
2.58	500	10.2	20.5	13.9	45.2	11.7	449±15.7	18.6±1.2	35.6±1.6
2.67	600	11.1	19.4	12.1	48.9	9.8	549±17.2	19.4±1.3	34.9±1.5
2.75	700	11.5	18.0	10.4	47.6	11.8	613±20.3	18.3±1.1	32.3±1.7

Supplementary Table 29 | 1 M KOH (pH 13.9).

Full cell potential (V)	**Current density (mA cm^{-2})**	**Faradaic efficiency (%)**					**J_{C2+} (mA cm^{-2})**	**EE$_{C2H4}$ (%)**	**EE$_{C2+}$ (%)**
		Acetate	**EtOH**	**n-PrOH**	**C_2H_4**	**H_2**			
1.78	100	9.9	17.3	23.1	37.8	13.5	88±4.6	22.5±1.0	50.4±1.7
2.03	200	11.8	19.4	21.6	40.3	8.7	186±7.9	21.0±1.2	46.6±1.6
2.24	300	12.9	21.8	15.7	43.2	6.7	281±10.4	20.4±1.3	42.4±1.5
2.39	400	14.5	21.4	11.3	46.9	5.2	376±12.9	20.8±1.4	39.8±1.8
2.51	500	15.0	19.3	8.6	48.8	5.9	459±14.2	20.6±1.3	34.1±1.7
2.61	600	16.3	18.0	7.9	47.0	8.9	535±16.4	19.1±1.2	34.3±1.5
2.69	700	17.1	16.3	6.2	45.8	12.3	598±21.3	18.1±1.0	31.7±1.6

Supplementary Table 30 | 1.5 M KOH (pH 14.1).

Full cell potential (V)	**Current density (mA cm^{-2})**	**Faradaic efficiency (%)**					**J_{C2+} (mA cm^{-2})**	**EE$_{C2H4}$ (%)**	**EE$_{C2+}$ (%)**
		Acetate	**EtOH**	**n-PrOH**	**C_2H_4**	**H_2**			
1.75	100	8.2	16.9	13.9	35.3	25.1	74±3.8	21.4±1.0	43.4±1.5
2.05	200	9.4	18.1	12.6	37.9	22.2	156±5.8	19.6±1.1	38.8±1.6
2.23	300	10.3	15.2	11.3	41.8	21.3	236±6.9	19.9±1.2	35.9±1.4
2.38	400	9.8	14.3	9.7	42.1	23.3	304±9.5	18.8±1.1	32.5±1.7

2.50	500	8.6	12.8	8.9	39.7	28.4	350±11.7	16.8±1.0	28.6±1.9

CORR performance of bare Cu NPs in an anion exchange membrane based membrane electrode assembly (MEA) using anolytes with various KOH concentrations. Operating conditions: anolyte flow rate: 20 mL min^{-1}; CO flow rate: ~10 sccm cm^{-2}; and cell temperature and pressure: atmospheric conditions. Error bars represent the standard deviation of three independent measurements.

Supplementary Table 31 | 1 M KOH (pH 13.9).

Full cell potential (V)	**Current density (mA cm^{-2})**	**Faradaic efficiency (%)**					**J_{C2+} (mA cm^{-2})**	**EE_{C2H4} (%)**	**EE_{C2+} (%)**
		Acetate	**EtOH**	**n-PrOH**	**C_2H_4**	**H_2**			
2.09	100	12.4	12.7	15.2	31.4	29.2	72±3.6	15.9±1.1	34.3±1.5
2.25	200	16.5	15.9	10.6	33.3	24.4	153±4.8	15.7±1.2	33.7±1.7
2.39	300	18.9	16.5	7.7	33.8	24.2	231±5.5	15.0±1.4	31.7±1.8
2.51	400	20.2	15.7	5.6	31.2	26.9	291±6.7	13.2±1.3	27.9±2.0
2.63	500	19.9	14.8	3.7	29.3	31.2	339±8.2	11.8±1.4	25.1±1.8
2.72	600	17.7	12.4	2.2	27.7	37.2	360±10.6	10.8±1.2	21.5±1.9

Supplementary Table 32 | 2 M KOH (pH 14.2).

Full cell potential (V)	**Current density (mA cm^{-2})**	**Faradaic efficiency (%)**					**J_{C2+} (mA cm^{-2})**	**EE_{C2H4} (%)**	**EE_{C2+} (%)**
		Acetate	**EtOH**	**n-PrOH**	**C_2H_4**	**H_2**			
2.04	100	15.2	13.5	13.4	33.9	25.2	75±3.1	17.6±1.1	37.1±1.4
2.21	200	18.4	15.1	10.9	35.7	20.8	156±4.7	17.1±1.2	35.9±1.5
2.36	300	21.2	15.6	8.0	37.7	19.3	239±6.5	16.9±1.3	34.4±1.6
2.49	400	19.4	14.2	6.9	35.2	26.2	299±7.8	15.0±1.2	29.9±1.7
2.60	500	18.3	13.4	4.8	32.8	32.1	342±9.7	13.4±1.2	26.2±1.4
2.69	600	16.1	11.2	3.5	31.3	39.2	367±11.6	12.3±1.1	22.7±1.4

Supplementary Table 33 | 3 M KOH (pH 14.4).

Full cell potential (V)	**Current density (mA cm^{-2})**	**Faradaic efficiency (%)**					**J_{C2+} (mA cm^{-2})**	**EE_{C2H4} (%)**	**EE_{C2+} (%)**
		Acetate	**EtOH**	**n-PrOH**	**C_2H_4**	**H_2**			
2.02	100	15.4	14.5	12.9	35.1	21.3	76±3.5	18.4±1.	38.3±1.7
2.18	200	18.5	15.1	10.1	37.2	19.6	156±4.7	16.6±1.	36.7±1.9
2.34	300	20.3	14.6	7.8	34.3	22.2	228±5.8	15.5±1.	32.3±1.8
2.47	400	18.3	12.8	5.9	30.5	27.7	266±6.7	13.1±1.	26.8±1.6
2.58	500	16.9	10.9	3.8	28.8	33.9	297±8.3	11.8±1.	22.9±1.7
2.66	600	13.8	8.8	2.7	26.1	45.1	308±9.4	10.4±1.	19.0±1.4

CORR performance of Cu NPs loaded with hydrophobic polytetrafluoroethylene (PTFE) agents of various mass loadings in an anion exchange membrane based membrane electrode assembly (MEA) using 1 M KOH as anolyte. Operating conditions: anolyte flow rate: 20 mL min^{-1}; CO flow rate: ~10 sccm cm^{-2}; and cell temperature and pressure: atmospheric conditions. Error bars represent the standard deviation of three independent measurements.

Supplementary Table 34 | 5 wt% PTFE.

Full cell potential (V)	**Current density (mA cm^{-2})**	**Faradaic efficiency (%)**			**J_{C2H4} (mA cm^{-2})**	**EE$_{C2H4}$ (%)**
		H_2	**CH_4**	**C_2H_4**		
2.04	100	31.1	0.1	41.2	41±2.2	21.4±1.2
2.21	200	28.9	0.1	43.4	87±4.3	20.8±1.1
2.36	300	30.2	0.3	41.9	126±5.2	18.8±1.0
2.48	400	33.2	0.5	39.2	157±6.4	16.8±1.3
2.59	500	39.3	0.7	33.8	169±7.7	13.8±1.1

Supplementary Table 35 | 15 wt% PTFE.

Full cell potential (V)	**Current density (mA cm^{-2})**	**Faradaic efficiency (%)**			**J_{C2H4} (mA cm^{-2})**	**EE$_{C2H4}$ (%)**
		H_2	**CH_4**	**C_2H_4**		
2.02	100	25.9	0.2	40.6	42±2.4	21.8±1.1
2.18	200	24.3	0.1	41.8	88±3.8	21.3±1.2
2.34	300	23.5	0.1	42.9	136±5.8	20.5±1.0
2.45	400	26.6	0.3	40.5	170±6.9	18.4±1.2
2.55	500	30.8	0.4	36.3	192±8.4	15.9±1.0

Supplementary Table 36 | 25 wt% PTFE.

Full cell potential (V)	**Current density (mA cm^{-2})**	**Faradaic efficiency (%)**					**J_{C2+} (mA cm^{-2})**	**EE$_{C2H4}$ (%)**	**EE$_{C2+}$ (%)**
		Acetate	**EtOH**	**n-PrOH**	**C_2H_4**	**H_2**			
1.99	100	8.3	15.1	16.7	39.1	21.1	79±3.4	20.8±1.1	40.7±1.8
2.17	200	10.5	16.2	12.4	41.4	18.6	161±6.2	21.9±1.2	36.1±1.7
2.35	300	12.3	17.3	10.1	43.6	17.1	250±7.4	19.7±1.0	35.9±1.9
2.46	400	13.5	15.5	8.4	43.2	19.2	322±10.1	18.8±1.1	33.1±1.8
2.55	500	13.8	13.7	7.6	40.5	23.4	378±12.4	16.8±1.0	29.8±1.6

Supplementary Table 37 | 35 wt% PTFE.

Full cell potential (V)	**Current density (mA cm^{-2})**	**Faradaic efficiency (%)**			**j_{C2H4} (mA cm^{-2})**	**EE_{C2H4} (%)**
		H_2	**CH_4**	**C_2H_4**		
2.01	100	33.2	0.2	38.6	42±2.3	21.8±1.2
2.19	200	30.4	0.1	41.3	88±4.6	21.3±1.1
2.35	300	30.7	0.2	41.1	136±5.9	20.5±1.0
2.46	400	34.9	0.5	36.6	170±7.2	18.4±1.1
2.57	500	38.8	0.8	33.3	192±9.4	15.9±1.0

Supplementary Table 38 | 50 wt% PTFE.

Full cell potential (V)	**Current density (mA cm^{-2})**	**Faradaic efficiency (%)**			**j_{C2H4} (mA cm^{-2})**	**EE_{C2H4} (%)**
		H_2	**CH_4**	**C_2H_4**		
2.06	100	39.4	0.2	35.1	35±1.9	18.1±1.0
2.27	200	42.2	0.4	32.3	65±3.5	15.1±1.1
2.39	300	47.7	0.7	28.1	84±4.6	12.5±0.9
2.54	400	55.1	0.9	21.9	88±5.3	9.1±1.2

CORR performance in an anion exchange membrane based membrane electrode assembly (MEA) using 1 M KOH as analyte under low CO input flow rate.

Supplementary Table 39 | 25 wt% PTFE.

Full cell potential (V)	Current density (mA cm^{-2})	Faradaic efficiency (%)					J_{C2+} (mA cm^{-2})	SPCE$_{CO\text{-}to\text{-}C2+}$ (%)	EE$_{C2+}$ (%)
		Acetate	EtOH	n-PrOH	C_2H_4	H_2			
1.77	80	7.3	13.9	15.6	38.8	19.4	60±3.6	26.1±4.4	43.4±1.3
2.02	160	8.2	13.3	14.7	39.6	21.7	121±6.8	53.0±4.9	38.4±1.5
2.24	240	7.4	12.5	10.3	32.2	32.8	150±7.6	66.3±5.2	28.4±1.6
2.39	320	5.9	8.8	4.9	22.4	46.7	134±7.1	61.1±5.1	17.8±1.4
2.51	400	4.2	7.6	2.6	16.2	56.5	122±6.6	55.7±4.4	12.4± 1.8

Operating conditions: anolyte flow rate: 20 mL min^{-1}; average CO inlet flow rate: ~1 sccm cm^{-2}; and cell temperature and pressure: atmospheric conditions. Error bars represent the standard deviation of three independent measurements.

CO_2RR performance in an anion exchange membrane based membrane electrode assembly (MEA) using 0.1 M $KHCO_3$ as anolyte under low CO_2 input flow rate. Operating conditions: anolyte flow rate: 20 mL min^{-1}; average CO_2 inlet flow rate: ~1 sccm cm^{-2}; and cell temperature and pressure: atmospheric conditions. Error bars represent the standard deviation of three independent measurements.

Supplementary Table 40 | Bare Cu NPs.

Full cell potential (V)	**Current density (mA cm^{-2})**	**Faradaic efficiency (%)**							
		Acetate	**C_2H_4**	**EtOH**	**n-PrOH**	**Formate**	**CO**	**CH_4**	**H_2**
2.95	80	3.1	25.4	6.8	4.1	7.2	14.1	0.8	9.1
3.20	160	3.6	26.2	7.1	3.4	5.4	8.6	0.9	6.9
3.39	240	4.7	23.1	7.2	2.9	3.0	4.3	1.4	12.1
3.53	320	4.2	16.2	5.2	1.2	2.1	2.9	1.7	29.8
3.71	400	1.8	11.2	3.1	–	–	1.7	2.3	44.2

J_{CO2RR} (mA cm^{-2})	**$SPCE_{CO2RR}$ (%)**	**EE_{CO2RR} (%)**	**J_{C2+} (mA cm^{-2})**	**$SPCE_{C2+}$ (%)**	**EE_{C2+} (%)**
49±2.5	20.2±2.9	24.9±1.8	31.5±2.1	7.8±1.9	15.5±1.3
97±5.8	32.4±2.7	20.8±1.9	64.5±3.9	16.1±2.4	14.7±1.2
120±6.9	36.3±2.5	16.5±1.7	90.9±4.7	22.8±1.8	13.1±1.3
123±6.4	34.6±3	11.4±1.6	85.8±4.3	22.1±1.9	9.0±1.1
104±5.9	22.8±3.1	6.4±1.5	64.4±4.9	16.3±1.7	5.1±1.2

Supplementary Table 41 | CCBH catalyst with 15 wt% COF loading.

Full cell potential (V)	**Current density (mA cm^{-2})**	**Faradaic efficiency (%)**							
		Acetate	**C_2H_4**	**EtOH**	**n-PrOH**	**Formate**	**CO**	**CH_4**	**H_2**
2.93	80	3.3	30.3	8.3	4.8	4.6	12.1	0.6	26.8
3.22	160	4.2	32.9	9.2	4.4	3.3	7.8	0.7	28.3
3.39	240	5.1	32.4	11.7	3.5	2.1	4.2	0.9	33.8
3.53	320	4.9	24.7	8.1	1.5	1.1	2.1	1.1	44.5
3.71	400	3.1	17.3	5.4	–	–	1.1	1.7	53.1

J_{CO2RR} (mA cm^{-2})	**$SPCE_{CO2RR}$ (%)**	**EE_{CO2RR} (%)**	**J_{C2+} (mA cm^{-2})**	**$SPCE_{C2+}$ (%)**	**EE_{C2+} (%)**
52±2.4	21.5±3.4	25.9±1.8	37.4±1.8	9.2±2.3	18.4±1.3
100±4.6	36.6±3.1	23.2±1.7	81.1±3.5	20.2±2.5	18.3±1.1
144±6.5	47.4±3.3	20.8±1.6	126.5±5.1	31.6±2.2	18.1±1.4

139±7.6	44.0±3.1	14.8±1.7	125.4±6.2	31.3±2.4	13.1±1.3
114±6.9	33.7±3.2	9.2±1.8	103.2±5.4	26.2±2.1	8.2±1.1

CO_2RR performance in an anion exchange membrane based membrane electrode assembly (MEA) using 0.1 M $KHCO_3$ as anolyte. Operating conditions: anolyte flow rate: 20 mL min^{-1}; CO_2 flow rate: ~10 sccm cm^{-2}; and cell temperature and pressure: atmospheric conditions.

Supplementary Table 42 | CCBH catalyst with 15 wt% COF loading.

Full cell potential (V)	Current density (mA cm^{-2})	Faradaic efficiency (%)									
		Acetate	C_2H_4	EtOH	PrOH	Formate	CH_4	CO	H_2	C_1	C_2
2.95	100	3.1	24.3	9.9	7.1	4.1	0.7	25.8	23.2	30.6	44.4
3.23	200	4.8	36.3	15.1	6.3	2.7	0.5	16.2	15.3	19.4	62.5
3.43	300	7.9	44.6	17.9	5.4	1.9	0.2	11.3	10.1	13.4	75.8
3.62	400	10.6	49.5	19.4	4.2	1.3	0.1	6.1	7.2	7.5	83.7
3.79	500	12.1	54.9	21.7	2.7	−	0.3	3.6	4.7	3.9	91.4
3.92	600	11.3	50.7	16.3	−	−	0.4	2.2	9.8	2.6	78.3

Supplementary Table 43 | Bare Cu NPs.

Full cell potential (V)	Current density (mA cm^{-2})	Faradaic efficiency (%)									
		Acetate	C_2H_4	EtOH	PrOH	Formate	CH_4	CO	H_2	C_1	C_2
2.98	100	2.4	20.1	7.9	4.5	7.1	0.9	29.4	27.3	37.4	34.9
3.26	200	3.9	28.5	11.3	5.7	4.9	0.6	24.2	16.3	29.7	49.4
3.45	300	6.4	35.4	14.2	4.2	3.8	0.3	19.3	14.1	23.4	60.2
3.65	400	8.2	42.1	16.6	3.3	3.2	0.3	13.4	12.8	16.9	70.2
3.83	500	7.6	40.9	14.1	2.1	1.7	0.5	10.2	18.3	12.4	64.7
3.97	600	5.4	37.6	11.3	−	−	0.8	7.9	21.8	8.7	54.3

CO_2RR performance of bare Cu NPs supported onto a Cu/PTFE substrate in an anion exchange membrane based membrane electrode assembly (MEA) using anolytes with various concentrations. Operating conditions: anolyte flow rate: 20 mL min^{-1}; CO_2 flow rate: ~10 sccm cm^{-2}; and cell temperature and pressure: atmospheric conditions.

Supplementary Table 44 | 0.1 M $KHCO_3$ (pH 8.4).

Full cell potential (V)	**Current density (mA cm^{-2})**	**Faradaic efficiency (%)**				**j_{C2H4} (mA cm^{-2})**	**EE_{C2H4} (%)**
		H_2	**CO**	**CH_4**	**C_2H_4**		
2.7	34	11.6	68.3	0.4	13.8	4.7	5.9
2.9	55	10.7	62.3	0.4	19.1	10.5	7.6
3.1	87	10.5	48.5	0.3	29.0	25.2	10.8
3.3	124	10	37.1	0.3	37.9	47.0	13.2
3.4	144	9.7	32.7	0.2	41.5	59.8	14.0
3.5	180	9.4	27.2	0.2	46.6	83.9	15.3
3.6	216	9.2	22.3	0.1	51.5	111.2	16.5
3.7	256	9.2	17.6	0.1	56.1	143.6	17.4
3.8	294	9.8	14.3	0.1	60.3	177.3	18.7
3.85	316	10.2	12.4	0.3	61.8	195.3	18.2
3.9	336	11.3	9.1	0.5	60.6	203.6	17.9
3.95	356	12.9	8.3	0.7	59.4	211.5	17.3

Supplementary Table 45 | 0.2 M $KHCO_3$ (pH 8.4).

Full cell potential (V)	**Current density (mA cm^{-2})**	**Faradaic efficiency (%)**				**j_{C2H4} (mA cm^{-2})**	**EE_{C2H4} (%)**
		H_2	**CO**	**CH_4**	**C_2H_4**		
2.7	46	14.4	40.6	0.5	23.1	10.6	9.8
2.9	80	13.7	36.6	0.4	32.6	26.1	12.9
3.0	98	11.7	29.7	0.4	36.2	35.5	13.9
3.1	118	11.6	25.6	0.3	41.2	48.6	15.3
3.2	136	11.5	23.1	0.3	45.1	61.3	16.2
3.3	163	11.2	19.4	0.2	49.8	81.2	17.4
3.4	188	11.2	16.8	0.2	54.4	102.3	18.4
3.5	214	11.6	14.2	0.2	57.7	123.5	19.0
3.6	248	12.3	11.4	0.1	59.3	147.1	18.9
3.65	266	13.1	10.6	0.2	59.8	159.1	18.4
3.7	284	13.8	8.9	0.3	58.3	165.6	17.9

3.75	303	15.5	8.6	0.4	57.7	174.8	17.7
3.8	324	16.6	7.2	0.5	56.1	181.8	17.0

Supplementary Table 46 | 0.3 M $KHCO_3$ (pH 8.4).

Full cell potential (V)	**Current density (mA cm^{-2})**	**Faradaic efficiency (%)**				**j_{C2H4} (mA cm^{-2})**	**EE_{C2H4} (%)**
		H_2	**CO**	**CH_4**	**C_2H_4**		
2.7	54	13.7	36.7	0.4	15.8	8.5	6.7
2.9	83	11.7	34.7	0.3	23.6	19.6	9.4
3.0	100	11.6	32.4	0.3	32.4	32.4	12.4
3.1	120	11.1	27.9	0.2	38.0	45.6	14.1
3.2	148	10.3	22.2	0.2	43.4	64.2	15.6
3.3	180	10.2	18.3	0.1	50.6	91.1	17.6
3.4	206	9.8	13.8	0.1	54.8	112.9	18.5
3.45	226	10.3	12.8	0.1	56.3	127.3	18.8
3.5	240	12.1	11.0	0.2	58.6	140.6	19.3
3.55	261	14.7	10.2	0.4	56.7	147.9	18.4
3.6	286	19.7	7.7	0.6	52.6	150.4	16.8

Supplementary Table 47 | 0.1 M $KHCO_3$ + 0.1 M K_2SO_4 (pH 8.4).

Full cell potential (V)	**Current density (mA cm^{-2})**	**Faradaic efficiency (%)**				**j_{C2H4} (mA cm^{-2})**	**EE_{C2H4} (%)**
		H_2	**CO**	**CH_4**	**C_2H_4**		
2.7	44	10.5	70.3	0.5	10.9	4.8	4.6
2.9	68	8.7	60.0	0.4	18.9	12.9	7.5
3.1	104	8.3	48.3	0.4	28.2	29.3	10.5
3.3	161	8.3	34.9	0.3	40.5	65.2	14.1
3.4	195	8.0	29.0	0.3	45.1	87.9	15.3
3.5	239	8.0	23.5	0.2	51.7	123.6	17.0
3.55	261	8.0	20.0	0.2	54.9	143.3	17.8
3.6	283	8.4	16.7	0.1	57.1	161.6	18.2
3.65	306	8.6	14.2	0.1	59.4	181.8	18.7
3.7	320	10.2	10.8	0.2	59.9	191.7	18.6
3.75	342	13.3	9.9	0.4	57.6	197.0	17.7

Supplementary Table 48 | 0.1 M $KHCO_3$ + 0.2 M K_2SO_4 (pH 8.4).

Full cell potential (V)	**Current density (mA cm^{-2})**	**Faradaic efficiency (%)**				**j_{C2H4} (mA cm^{-2})**	**EE_{C2H4} (%)**
		H_2	**CO**	**CH_4**	**C_2H_4**		
2.7	52	15.7	66.3	0.6	13.8	7.2	5.9
2.9	78	11.9	48.9	0.5	23.7	18.5	9.4
3.1	118	10.9	36.4	0.4	34.7	40.9	12.9
3.3	170	10.6	25.3	0.3	46.5	79.0	16.2
3.4	198	11.0	21.4	0.3	51.3	101.6	17.4
3.45	212	11.9	19.8	0.4	52.8	111.9	17.6
3.5	227	13.4	17.9	0.5	52.6	119.4	17.3
3.55	247	15.5	16.1	0.6	52.4	129.4	17.0
3.6	270	16.9	14.1	0.7	50.5	136.4	16.1
3.65	294	18.7	13.0	0.9	49.4	145.2	15.6

CO_2RR performance in a liquid-electrolyte flow cell using 1 M H_3PO_4 + 1 M KCl (pH ~0.8) electrolytes under low CO_2 input flow rate.

Supplementary Table 49 | Bare Cu NPs. Operating conditions: anolyte flow rate: 20 mL min^{-1}; average CO_2 inlet flow rate: ~3.6 sccm cm^{-2}; and cell temperature and pressure: atmospheric conditions. Error bars represent the standard deviation of three independent measurements.

Full cell potential (V)	**Current density (mA cm^{-2})**	**Faradaic efficiency (%)**							
		Acetate	**C_2H_4**	**EtOH**	**n-PrOH**	**Formate**	**CO**	**CH_4**	**H_2**
2.87	200	–	3.4	2.1	1.1	3.1	33.9	0.3	55.7
3.34	400	1.1	6.6	2.7	2.4	6.8	30.1	0.2	52.5
3.73	600	1.4	9.3	4.1	2.1	7.5	24.6	0.2	50.2
3.88	800	1.7	11.1	3.7	1.6	4.3	19.7	0.4	51.3
4.11	1000	1.5	9.2	2.8	–	2.8	14.1	0.6	63.9

J_{CO2RR} (mA cm^{-2})	**$SPCE_{CO2RR}$ (%)**	**EE_{CO2RR} (%)**	**J_{C2+} (mA cm^{-2})**	**$SPCE_{C2+}$ (%)**	**EE_{C2+} (%)**
87.8±3.7	16.6±3.7	19.9±1.9	13±1.2	0.9±0.4	2.6±0.8
199.6±5.9	35.0±4.5	18.9±1.8	52±2.5	3.8±1.1	4.4±0.9
295.2±11.9	48.2±3.9	16.5±2.0	101±4.8	7.4±1.7	5.2±1.1
340±13.8	51.4±3.4	13.6±1.8	145±6.2	10.7±2.1	5.4±1.0
310±16.8	46.0±4.2	9.4±1.9	135±6.9	10.0±1.9	3.9±0.8

Supplementary Table 50 | CCBH catalyst with 15 wt% COF loading. Operating conditions: anolyte flow rate: 20 mL min^{-1}; average CO_2 inlet flow rate: ~1 sccm cm^{-2}; and cell temperature and pressure: atmospheric conditions. Error bars represent the standard deviation of three independent measurements.

Full cell potential (V)	**Current density (mA cm^{-2})**	**Faradaic efficiency (%)**							
		Acetate	**C_2H_4**	**EtOH**	**n-PrOH**	**Formate**	**CO**	**CH_4**	**H_2**
2.71	100	1.7	19.2	5.8	4.5	6.1	16.2	0.2	39.9
2.92	200	2.3	23.4	8.3	4.9	7.3	12.5	0.1	34.8
3.09	300	3.1	28.9	9.1	3.2	5.7	8.6	0.1	31.9
3.34	400	3.7	33.8	8.2	2.7	4.6	7.7	0.2	30.2
3.63	500	2.9	30.4	5.7	1.9	3.1	4.1	0.3	38.8

J_{CO2RR} (mA cm^{-2})	**$SPCE_{CO2RR}$ (%)**	**EE_{CO2RR} (%)**	**J_{C2+} (mA cm^{-2})**	**$SPCE_{C2+}$ (%)**	**EE_{C2+} (%)**
54±3.9	20.9±4.4	24.0±1.9	31±2.5	6.8±1.2	13.2±1.3

118±8.6	42.0±3.8	24.2±2.0	78±4.6	16.9±1.8	15.3±1.4
176±9.3	56.3±4.1	22.7±1.8	133±6.9	29.0±2.6	16.6±1.4
244±14.6	73.7±4.3	21.6±1.7	194±8.9	42.4±3.8	16.9±1.2
242±17.8	67.8±3.8	15.7±1.9	205±10.1	44.7±4.8	13.1±1.3

Supplementary References

1. Ozden, A. et al. Cascade CO_2 electroreduction enables efficient carbonate-free production of ethylene. *Joule* **5,** 706-719 (2021).

2. Sisler, J. et al. Ethylene electrosynthesis: a comparative techno-economic analysis of alkaline vs membrane electrode assembly vs CO_2-CO-C_2H_4 Tandems. *ACS Energy Lett.* **6,** 997-1002 (2021).

3. Wang, X. *et al.* Efficient electrically powered CO_2-to-ethanol via suppression of deoxygenation. *Nat. Energy* **5**, 478–486 (2020).

4. Weisenberger, S. & Schumpe, A. Estimation of Gas Solubilities in Salt Solutions at Temperatures from 273 K to 363 K. *AIChE J.* **42**, 298–300 (1996).

5. Gabardo, C. M. *et al.* Continuous Carbon Dioxide Electroreduction to Concentrated Multi-carbon Products Using a Membrane Electrode Assembly. *Joule* **3**, 2777–2791 (2019).

6. Xu, Y. *et al.* A microchanneled solid electrolyte for carbon-efficient CO_2 electrolysis. *Joule* **6**, 1333–1343 (2022).

7. Li, S., Hu, C., Peng, Y. & Chen, Z. One-step scalable synthesis of honeycomb-like g-C_3N_4 with broad sub-bandgap absorption for superior visible-light-driven photocatalytic hydrogen evolution. *RSC Adv.* **9,** 32674–32682 (2019).

8. Zhao, Y. et al. Surface Reconstruction of Ultrathin Palladium Nanosheets during Electrocatalytic CO_2 Reduction. *Angew. Chem. Int. Ed.* **59,** 21493–21498 (2020).

9. Li, C. W., Ciston, J. & Kanan, M. W. Electroreduction of carbon monoxide to liquid fuel on oxide-derived nanocrystalline copper. *Nature* **508,** 504-507 (2014).

10. Dinh, C. T. et al. CO_2 electroreduction to ethylene via hydroxide-mediated copper catalysis at an abrupt interface. *Science* **360**, 783–787 (2018).

11. Ma, W. et al. Electrocatalytic reduction of CO_2 to ethylene and ethanol through hydrogen-assisted C−C coupling over fluorine-modified copper. *Nat. Catal.* **3,** 478-487 (2020).

12. O'Brien, C. P. et al. Single pass CO_2 conversion exceeding 85% in the electrosynthesis of multicarbon products via local CO_2 regeneration. *ACS Energy Lett.* **6**, 2952–2959 (2021).

13. Huang, J.E. et al. CO_2 electrolysis to multicarbon products in strong acid. *Science* **372**, 1074–1078 (2021).

14. Jouny, M., Luc, W. & Jiao, F. High-rate electroreduction of carbon monoxide to multi-carbon products. *Nat. Catal.* **1,** 748-755 (2018).

15. Ripatti, D. S., Veltman, T. R. & Kanan, M. W. Carbon monoxide gas diffusion electrolysis that produces concentrated C_2 products with high single-pass conversion. *Joule* **3**, 240–256 (2019).